# PhD Thesis

# Custom Power Active Transformer for Flexible Operation of Power Systems

*Mohamed Atef Abbas Elsaharty*

Barcelona, July 2018

# Custom power active transformer for flexible operation of power systems

## Mohamed Atef Abbas Elsaharty

# Custom Power Active Transformer for Flexible Operation of Power Systems

*Mohamed Atef Abbas Elsaharty*

Dissertation submitted to the Doctorate Office of the Universitat Politècnica de Catalunya in partial fulfillment of the requirements for the degree of Doctor of Philosophy by the

**UNIVERSIDAD DE MÁLAGA**

**UNIVERSIDAD DE SEVILLA**

**UNIVERSIDAD DEL PAÍS VASCO/EUSKAL ERRIKO UNIBERTSITATEA**

**UNIVERSITAT POLITÈCNICA DE CATALUNYA**

**Joint Doctoral Programme in Electric Energy Systems**



Barcelona, July 2018

Custom Power Active Transformer for Flexible Operation of Power Systems

# Acknowledgements

The academic and social experience I have gained living in Spain will always be an unforgettable moment of my life. I would like to thank my supervisor and mentor, Prof. Pedro Rodriguez Cortes for providing me this opportunity. I would like to express my humble gratitude towards him for his guidance and support during my PhD study. Through his influence, I have learned to balance my responsibilities to achieve the required goal and this thesis presents this challenging journey. It's an honor to work under your supervision and I will always be grateful to you.

I would like to express my sincere appreciation and gratitude towards Dr. Jose Ignacio Candela for his openness, guidance and support during this journey. The knowledge and experience I have gained from you will be the fuel for my future carrier and I am proud to have you as my teacher.

Dr. Alvaro Luna, there are no words to express my infinite respect and gratitude towards your personal and academic support throughout my journey here. I am very thankful for your advices and for facilitating me with the required devices in my PhD tasks. Your help and support will never be forgotten.

Special thanks to Dr. Joan Rocabert for his time and effort spent with me in the laboratory. I am very thankful for the laboratory skills and guidance you have provided me during my PhD study. Also, I would like to thank Dr. Raul Santiago for the support and experience he provided me during my stay.

Special thanks to Dr. Juan Ramon Hermoso, Khadija El Haddadi, Lidia Herrera and Elena Corbera for their academic guidance throughout the years. Your support in facilitating my academic process is highly appreciated.

I would also like to thank Borja Garcia, Victor Fauquet, Miguel Altes Martinez and Sergio Gimenez Arnal for the time and help they provided me in the laboratory. Special thanks to all the students who have followed me throughout this journey and provided me with support that I needed: Weiyi Zhang, Elyas Rakhshani, Daniel Remon, Antoni

*Mohamed Elsaharty*

Terrassa, Barcelona, Spain

July, 2018

# Abstract

As of July 2015, European Commission regulations have compelled transformer manufacturers to increase investment costs due to the requirement for higher efficiencies. Transformers form a core element in the power system and furthermore they are among the essential requirements for connection of active power system compensation systems.

One of the main challenges in the expansion of a power system is the issue of eliminating transmission and distribution system constraints and bottlenecks. With the increased peak customer demand, the distribution system suffers severe power quality and continuity of supply issues. There is general consensus that the future power grid will need to be smart, fault tolerant, self-healing, dynamically controllable, and energy efficient. Such requirements can be achieved through fast dynamic control provided through the installation of FACTS (Flexible AC Transmission Systems) and CPD (Custom Power Devices) which can cope with the trending changes in the power system. With such devices playing an important role in the power system, it is essential to develop flexible integration capability into the distribution and transmission system.

The Unified Power Flow Controller (UPFC) and Unified Power Quality Conditioner (UPQC) provide series and shunt compensation services to the transmission and distribution system. Such power compensation devices can be linked to the power system by using series and/or shunt transformers, which provide the flexibility of using off-the-shelf Voltage Source Converters (VSC) and satisfy required isolation requirements and winding connection options. However, the increased system cost and volume of such transformers entails a trade-off to more complex non-isolated connection approaches. All such drawbacks can by addressed by considering the benefits of utilizing the essential presence of coupling step-up and step-down transformers in the power system to facilitate isolated connection of FACTS devices and CPDs.

Integrated magnetics have been reported in literature as coupled inductors, integrated inductor, and integrated transformers (several transformers sharing a common core). Considering FACTS and CPD applications, integrated transformers have a reduced number of magnetic components, which in turn reduces the whole system volume. Moreover,

combination of several transformers into one would facilitate sub-transmission and distribution transformers with special functions, which would improve power system stability and quality. The most relevant applications of fully and partially active transformer have either required complex power electronics configuration, achieving one type of compensation or targeted for specific application.

This PhD dissertation proposes a new transformer, i.e., the Custom Power Active Transformer, characterized by a specific design of its magnetic circuit and auxiliary windings which allows shunt and series compensation to the power system in a single monolithic transformer. Such auxiliary windings are regulated using power converters based on power electronics. The power electronics converters are controlled based on the required added services to the power system which includes power flow control between different areas, power quality improvements, inertia emulation and several other services that are applicable through power electronics converters. The objective of the proposed transformer is to enable integration of power electronics to a transformer structure which empowers the transformer with added services aiding the transformer operation and power system flexibility.

Single-phase and three-phase structures are modelled based on their equivalent magnetic circuit and analyzed through simulations, real-time simulations and experimentation. The presented structures have been demonstrated to operate for UPFC and UPQC applications to reveal the applicability of the proposed transformer for general compensation systems. Furthermore, benefits of the combined structure, operating limits and selection consideration are revealed.

The CPAT equipped with a power converter can be utilized in distribution systems to control grid-current and load-voltage waveforms while operating as a step-up or step-down transformer between the grid and load. Moreover, it can provide other services that any typical shunt-series compensation arrangement provides. Design and analysis of a single-phase CPAT is presented showing the effect of coupling between windings and transformer parameters affecting CPAT operation. In this PhD dissertation, control of the CPAT in a UPQC application is investigated to attenuate grid-current and load-voltage harmonics as well as compensate for reactive power requirements and mitigate grid inrush current.

Moreover, the CPAT has been investigated to provide UPFC application services such as power flow control, reactive power compensation, voltage regulation and harmonics elimination. Simulations of the CPAT-UPFC with a stiff grid and a 5-bus power system demonstrates its functionality within an inter-bus coupling transformer while providing the required control objectives. Moreover, the impact of the CPAT-UPFC during load perturbations on the power system is investigated to further validate its transient and steady-state response.

Finally, this PhD dissertation presents the expected prospects of the CPAT and the possible research areas that would require development for the enhancement of the CPAT.

# Contents

# List of Tables

# Nomenclature

| | |
|---|---|
| FACTS | Flexible AC Transmission System |
| CPD | Custom Power Device |
| UPFC | Unified Power Flow Controller |
| UPQC | Unified Power Quality Conditioner |
| VSC | Voltage Source Converter |
| ST | Sen Transformer |
| STATCOM | STATic Synchronous COMpensator |
| SSSC | Static Series Synchronous Compensator |
| PCC | Point of Common Coupling |
| IEEE | Institute of Electrical and Electronics Engineers |
| IEC | International Electrotechnical Commission |
| DSTATCOM | Distribution STATCOM |
| DVR | Dynamic Voltage Regulator |
| DSOGI-FLL Frequency Locked | Double-Second Order Generalized Integrator |
| CSI | Current Source Inverter |
| PWM | Pulse Width Modulation |

| | |
|---|---|
| SVM | Space Vector Modulation |
| CIGRE | Conseil International des Grands Réseaux Électriques |
| MMF | Magneto-Motive Force |
| PR | Proportional Resonant |

# Introduction

*T*his chapter introduces the background of the thesis topic, brief review of related topics and objectives of this PhD study. The necessity for development of a power electronics integrated transformer are firstly revealed. Further on, the conventional configurations of FACTS are explained and compared to the required goal. Then the recent literature approaches into achieving the required goal are briefly discussed. Finally, the main objectives of this thesis are explained and organized along the forthcoming chapters.

## 1.1.    Background

In July 2015, the new European Commission regulations for manufacturing of power transformers was effective [1]. As the regulations states, "The availability of material to manufacture transformers with amorphous steel core needs further development, before such values of losses can be considered to become minimum requirements in the future." Therefore, such regulations compel manufacturers to increase material utilization and quality resulting in increased investment costs [2]. Considering a power system with a FACTS services such as a UPFC or a UPQC shown in Fig. 1.1, the number of isolating transformers required significantly increases. Alongside, the growing demand of electricity by customers, high proliferation of non-linear loads and increased line congestion all have exhibited serious power quality, reliability, stability and energy price issues [3]. Consequently, transformer-less power converters have shown growing interest in literature to aid the power system as well as eliminate the requirement of an isolating transformer [4] [5] [6]. However, the complexity of such systems increases as the power and voltage level increases as presented in Fig. 1.2.

FACTS devices propose a fast dynamic and efficient solution to maintain a reliable, sustainable and intelligent electric network. To overcome the complexity of transformer-

less power electronics configurations and number of isolating transformers, an integrated transformer design would resolve such bottle-necks. The goal of this thesis is to determine a transformer design that would facilitate connection of shunt and series power converters while achieving the required voltage matching between both electrical networks.
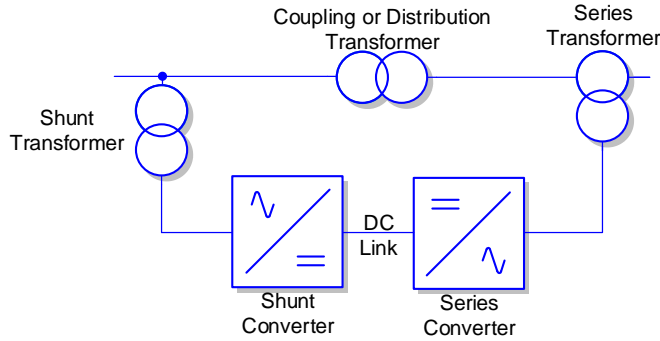


**Fig. 1.1.** Configuration of a UPFC/UPQC in a power system.
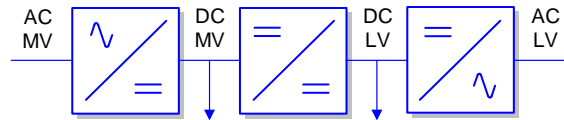


**Fig. 1.2.** Configuration of a transformer-less compensation system.

## 1.2.    Summary of Integrated Compensation Systems

The concept of integrating power converters into transformers was originally introduced in [7]. Recently, this concept has been further developed and improved under the name of "Smart Transformer" [8] [9]. This is considered among the most effective approaches [10] [11]. The Smart Transformer, a back-to-back converter configuration shown in Fig. 1.3, provides robust dynamic control over power flow as well as auxiliary services to the grid [12].   However, this configuration requires complex power electronics structures and topologies, as well as power devices capable of supporting full load rated power [13]. The number of conversion stages and number of power electronic units connected in shunt/series as presented in Fig. 1.3 creates a concern in regard to cost and reliability.

Several approaches have been presented in literature to integrate power processing functionalities into a transformer which allow series voltage compensation [14] [15] [16], shunt reactive power compensation [17], series harmonic passive filtering [18], series power flow control [19], transformer core sharing by multi-shunt power converters [20], power converter filter inductance integration [21], controllable reactor transformer [22], series fractional power converter integration [23], series harmonic passive filtering [24], wound rotor induction machine based power flow control [25], converter passive filter integration [26] and shunt magnetic path integration [27]. However, such compensation devices have explored a single type of compensation (series or shunt) and/or operate for a specific

application. The most remarkable approach to achieve the required goal of this thesis was presented in the Sen Transformer (ST) [28].
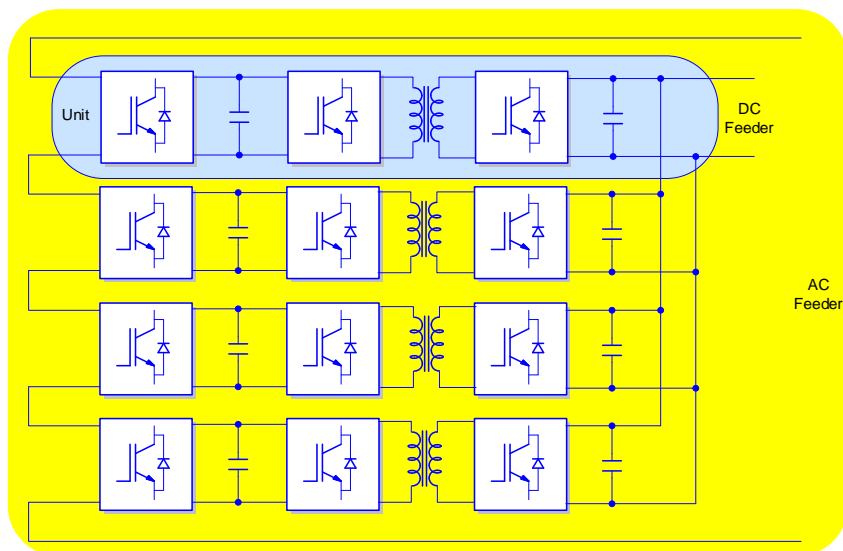


**Fig. 1.3.** Single-phase Smart Transformer architecture of one conversion stage.

The method for modeling the interface between an electric circuit and a magnetic component has been already discussed in the literature. For example, a method for developing the electrical equivalent circuit of any complex integrated magnetic component based on a z-parameter two-port network model was presented in [29]. However, such analyses have not been ever used to develop a series-parallel compensation system integrated in the transformer magnetic core. The structures in [15], [17], [20], [27] and [28] are of particular interest in this thesis due to their capability of integrating several magnetic structures into a single unit while facilitating power electronics converters connection. The following sections explain the basic concept discussed in these reference for the integration of several series/shunt transformers. Further details into the operation principle of those integration concepts will be discussed in Chapter 2.

### 1.2.1.      Integrated Series Transformer

The configuration discussed in [15], utilizes multiple series transformers with multi-secondary windings as shown in Fig. 1.4. In such a configuration, series compensation of each phase is distributed over several converters connected through a single series transformer. Multiple power electronics converters inject the corresponding secondary winding currents to achieve the required fundamental reference current. Therefore, the configuration explores the possibility of multiple series power electronics converters to be conjoined in a monolithic structure. The equivalent circuit of each transformer shown in Fig. 1.4 can be represented as multiple shunt converters connected in series with the power circuit [29].
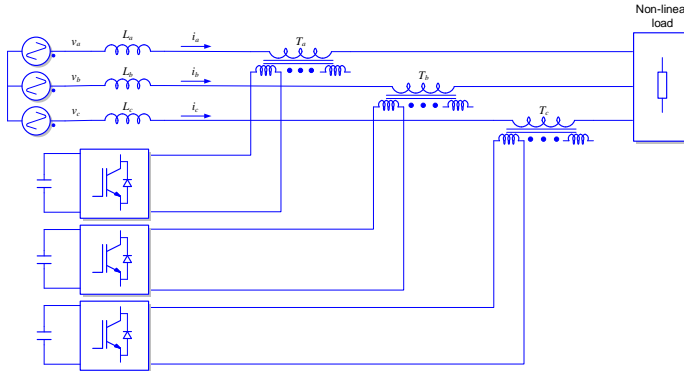
**Fig. 1.4.** Integrated series transformer with multiple secondary windings for active filter application.

Integration of a series controller in a power transformer has been discussed in [27]. This approach utilizes a shunt magnetic path as shown in Fig. 1.5 accompanied with an air gap that is designed in conjunction with the physical dimensions of magnetic core to determine the minimum and maximum output current of the transformer. In such an approach the output voltage ($v_{sec}$) of the transformer is controlled through the AC voltage induced in the shunt magnetic path ($v_{ser}$). However, this integrated configuration has not been discussed in literature for power system applications.
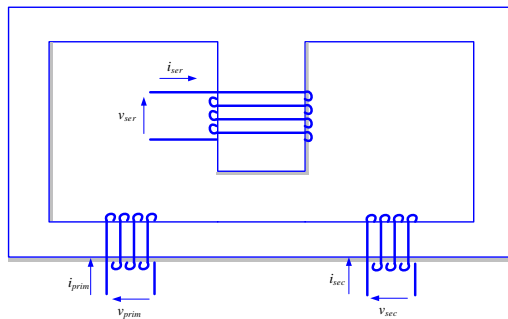


**Fig. 1.5.** Configuration of a shunt magnetic path between primary and secondary windings in a single-phase transformer.

### 1.2.2. Integrated Shunt Transformer

The configuration proposed in [17] introduce the changes in the core windings of a transformer to integrate a shunt power converter as illustrated in Fig. 1.6. By using the surplus capacity of the transformer, the Static Synchronous Compensator (STATCOM) is capable of compensating reactive power for the transformer and its loads while minimizing the cost and volume of the whole system. The application of such compensation has been presented for low-capacity intelligent box-type substation. As stated in [17], the connection method can save some materials, reduce cost and volume of the substation, and reduce the difficulty of heat dissipation design. This configuration is of particular interest due to its

ability to combine a shunt transformer with a distribution transformer in a single structure which is among the goals of this thesis.
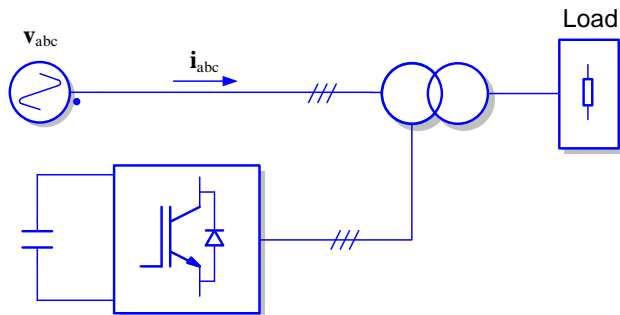


**Fig. 1.6.** Schematic of STATCOM integrated transformer (a) power line diagram and (b) winding configuration of shunt compensation.

Another approach into integrating multiple converters is discussed in [20]. The configuration shown in Fig. 1.7 illustrates the possibility of combining multiple transformer cores into a monolithic structure. However, shunt and series connection of each element to a common point has not been investigated with such a design.
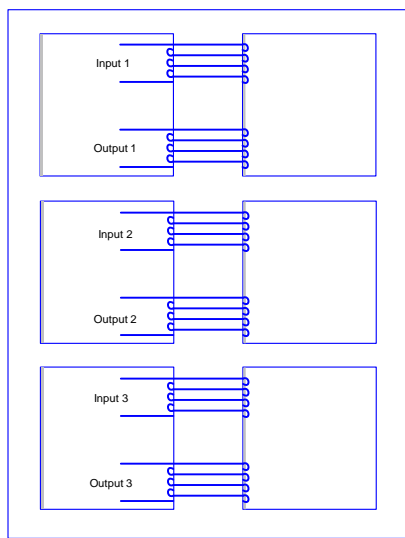


**Fig. 1.7.** Multiphase power converter connection to shared magnetic core transformers.

### 1.2.3.      Integrated Series-Shunt Transformer

A unified transformer structure incorporating shunt and series winding configuration was discussed in [28] and [30] [31]. The configuration shown in Fig. 1.8 reveals the winding

arrangement of an ST which is based on a single-core, three-phase transformer and tap changers. The ST provides voltage regulation at the point in the transmission line as well as power flow control through the line. The Exciter Unit is connected in shunt to the sending end voltage ($v_{sa}$, $v_{sb}$, $v_{sc}$) to induce a bipolar voltage in the secondary winding. Through the Voltage & Impedance Regulating Unit, a compensating voltage with variable magnitude and in quadrature with the line voltage is generated from the phase-to-phase voltage of the induced voltage of the regulating transformer. This regulating voltage is provided through the tap-changers provided in the ST. The resulting structure enables power flow control between sending end voltage and receiving end voltage ($v_{ra}$, $v_{rb}$, $v_{rc}$) as well as voltage regulation at the sending end. Therefore, the ST can operate as a UPFC through the step-changes applied in the Voltage & Impedance Regulating Unit. However, the ST presents several limitations including use of tap changers which introduces limitations in the degrees of freedom as well as its inability to provide extra services to the grid such as power quality enhancement. Moreover, ST is not adequate for fast dynamic control over power flow since control is provided through step changes. Faster dynamic response can be incorporated through the use of thyristor units at each tap. Nevertheless, the possible controllability in such case is dictated by the number of available taps.
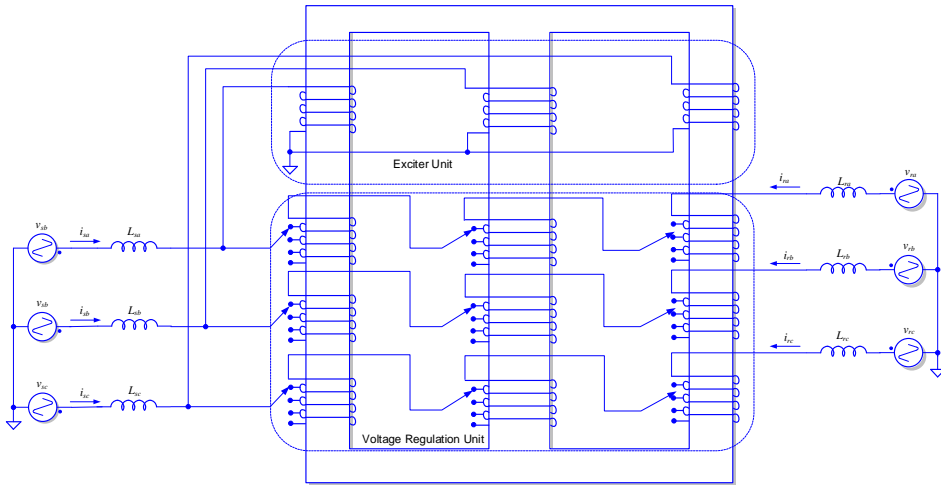


**Fig. 1.8.** Configuration of a ST shunt-series combining transformer.

## 1.3.   Objectives of This PhD Dissertation

The research activity of this PhD dissertation was aimed towards the goal of designing shunt-series combining transformer within a distribution and transmission transformer. The combined structure would provide access to incorporate power electronics converters through the available shunt and series windings in the proposed structure to enable a wide range of compensation requirements. Several objectives were stated to guide the PhD research which are summarized as follows:

1- Propose a power electronics integrated transformer design that utilizes auxiliary windings and a custom core design in order to provide series and shunt compensation configurations.

2- Select suitable power electronics configurations to be utilized with the integrated transformer for single-phase and multi-phase systems.

3- Present and evaluate control strategies for the proposed transformer that provide distribution and transmission system services including mitigation of transients, waveform distortions, inrush current as well as voltage regulation and power flow control.

4- To evaluate the merits of the proposed system in regard to operation limits as well as minimization of cost and overall volume.

The results in this PhD dissertation aim to report the investigation of the operation of the proposed design in single-phase and three-phase systems for power quality improvement and power flow control applications. These objectives contribute in realizing the required transformer design to achieve the required goal.

A. Integrated transformer design

Based on the concepts presented in [15], [17], [20], [27] and [28] ,the principle of operation and structure can be combined into a monolithic structure that facilitates the discussed compensation approaches. In such a case the resulting structure would in theory have auxiliary windings and a specific core structure. The concept presented in [15], [27] and [28] have revealed that it is possible to integrate an equivalent series circuit in a transformer through a shunt magnetic path. Therefore, this can be the basic theory for integration of a series power electronics converter in a transformer. Similarly, [17] and [20] have revealed the possibility of combining several independent shunt transformers into a monolithic structure. Thus, using these approaches the first objective of this PhD dissertation can be achieved. Finally, the resulting structure can be analyzed and validated theoretically based on the transformer and power electronics integration method discussed in [29].

B. Power electronics configuration

Based on the proposed design, typical power electronics compensation configurations can be utilized to achieve the required services. Since the objective is to combine several transformers into one monolithic structure, the provided auxiliary windings of the transformer can be connected with any power electronics topology that can operate as a controlled voltage source or controlled current source. This includes the typical back-to-back configuration illustrated in Fig. 1.1 for multi-phase systems as well as single-phase configuration shown in Fig. 1.4.

C.   Control architecture

The resulting transformer accompanied with power electronics topology would form a generalized shunt-series compensation system which exploits several applications and services provided to the grid. This PhD dissertation will focus on resolving power quality issues in distribution systems and power flow control in transmission systems. Therefore, due to the generalization of the proposed transformer structure, any classical control architecture utilized in literature for these control objectives would be feasible. This thesis will focus on the operation of the proposed transformer as a UPQC in distribution applications and UPFC for transmission applications. Further enhancements of the control architecture would be exploited as well to investigate any possible limitations of the proposed structure and control architecture. Mainly, these enhancements resolve technical aspects of the presented structure which includes harmonics elimination and inrush current mitigation.

D.   Evaluation methods

The proposed transformer is to be evaluated based on its equivalent model and construction. A transformer modelling approach is selected based on the required frequency response analysis. Since slow transients (up to 1kHz) [32] are of primary concern in the investigated applications for the proposed transformer, the magnetic circuit modelling approach discussed in [33] would be adopted. Through this modelling approach, accurate simulations of the proposed transformer with the required control architecture would be executed. The proposed transformer operating as a UPQC would be evaluated operating with a non-linear load and distorted grid in order to validate the capability of the transformer to achieve shunt current and series voltage harmonics injection. In a UPFC application, the proposed transformer would be evaluated operating under stiff grid connection and a multi-bus power system to investigate its impact on different areas of the power system. Final evaluation of this PhD dissertation proposal is acquired through experimentation to investigate its practicality.

## 1.4.   PhD Dissertation Organization

This PhD dissertation is organized into 6 chapters in the following order:

Chapter 2 reviews the classical power electronics based transmission and distribution compensation devices accompanied with their control, topologies and modelling methods.

Chapter 3 presents the Custom Power Active Transformer, a power electronics integrated transformer for the required objectives. Single-phase and multi-phase configurations are revealed and the principle of operation for the required objectives is discussed.

Chapter 4 analyzes the single-phase structure of the CPAT for UPQC applications through modeling, simulations and experimental prototype.

Chapter 5 analyzes the three-phase structure of the CPAT for UPFC applications through modeling, simulations and experimental prototype.

Chapter 6 discusses the concluded results of the proposal as well its future perspective research.

## 1.5. Publications During This PhD Project

Some of the analysis and results of this PhD project were published or accepted for publication in journals and conference proceedings. These publications are listed below:

1- M. A. Elsaharty, J. I. Candela and P. Rodriguez, "Custom Power Active Transformer for Flexible Operation of Power Systems," in IEEE Transactions on Power Electronics, vol. 33, no. 7, pp. 5773-5783, July 2018.

2- M. A. Elsaharty, J. I. Candela and P. Rodriguez, "Power System Compensation Using a Power Electronics Integrated Transformer," in IEEE Transactions on Power Delivery, vol. 33, no. 4, pp. 1744-1754, Aug. 2018.

3- M.A. Elsaharty, J. Rocabert, J.I. Candela and P.Rodriguez, "Three-Phase Custom Power Active Transformer for Power Flow Control Applications," in IEEE Transactions on Power Electronics,(Under Review)

4- M. A. Elsaharty, A. Luna, J. I. Candela and P. Rodriguez, "A Unified Power Flow Controller Using a Power Electronics Integrated Transformer" in IEEE Transactions on Power Delivery, (Under Review)

5- M. A. Elsaharty, J. I. Candela and P. Rodriguez, "Power System Compensation Using a Power Electronics Integrated Transformer," in 2018 IEEE Power and Energy Society General Meeting (PESGM), Portland, OR, 2018, (On Already Accepted PES Transactions Paper Abstract).

6- Cristian Verdugo, Mohamed A. Elsaharty and Pedro Rodriguez, "Integrated Series Transformer in Cascade Converters for Photovoltaic Energy Systems," 2018 IEEE Energy Conversion Congress and Exposition (ECCE), (Accepted)

7- D. Remon, A. M. Cantarellas, M. A. A. Elsaharty, C. Koch-Ciobotaru and P. Rodriguez, "Equivalent model of a synchronous PV power plant," 2015 IEEE Energy Conversion Congress and Exposition (ECCE), Montreal, QC, 2015, pp. 47-53.

8- D. Remon, A. M. Cantarellas, M. A. A. Elsaharty, C. Koch-Ciobotaru and P. Rodriguez, "Synchronous PV support to an isolated power system," 2015 IEEE Energy Conversion Congress and Exposition (ECCE), Montreal, QC, 2015, pp. 1982-1987.

# Review on Modern FACTS

*T*his chapter introduces the most relevant modern power electronics-based compensation systems for transmission and distribution networks. In the following sections, different power quality and power flow management strategies are discussed along with their modelling and control approaches. Through this literature review, a summary of the required compensation configurations and control architectures are revealed. This information is relevant for the development of the proposed transformer , which is explain in the next chapter.

## 2.1. Introduction

The transmission and distribution systems may experience power quality and stability issues, such as poor voltage regulation, increased harmonic currents, and load unbalance. Traditional methods for mitigating such disturbances may not result totally effective in the incoming network scenario, especially with successive load changes, non-linear loads and the increasing DG penetration. Due to this several power electronics based FACTS have been proposed and implemented to support the transmission grid. However, power electronics based compensation located at the distribution side can be also a feasible alternative to support the grid. This is due to the fact that lower cost components can be used as, even though currents are higher, the operation at a lower voltage compared to the transmission side requires expensive devices.

.

## 2.2.   Transmission System

The modern power system has evolved through several decades becoming one of the most complex man-made systems. The path through the de-carbonization of energy supply is also impacting on the distribution and transmission network, giving rise to challenges in the operation, management and control of electrical networks [34]. One of the most relevant challenges is the management of the penetration of distributed generation, the increasing peak customer demand and the use of non-linear loads drawing excessive harmonic currents [35]. Possibly the most significant issue in terms of grid utilization is that of active power flow control. Utility customers purchase real power, megawatts and MW-Hrs, and not voltage or reactive power. Thus, controlling how and where real power flows on the network is of critical importance and is the underlying premise behind the realization of an electricity market [36].

Transmission system possess several limitations and operating conditions that can affect the security, stability and reliability of power system. These limitations can be categorized into thermal, voltage and stability limits as shown in Fig. 2.1 [37].
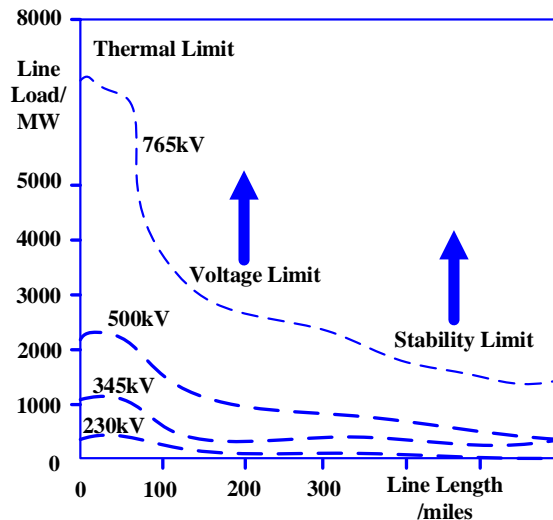


**Fig. 2.1.** Operation limits of transmission lines at different voltage levels.

Contingencies, that may arise due to the protection trip of a line or a generator, can give rise to the overload of some lines, what finally can threaten the overall system security. Moreover, increased loading of the transmission lines can cause voltage collapses due to insufficient reactive power delivery [38]. Steady-state and transient stability limits the maximum electric power transfer over a transmission system. Such limits define the maximum electric power that can be transmitted without damaging either the transmission lines, the utility or the equipments of the customers. Angle stability limit can be altered by modifying the natural inductive reactance of the transmission line through the utilization of series compensation or modifying the relative phase angle difference using a phase shifting

transformer [39]. An excessive current flow can drive the transmission line to reach the thermal limits, causing the overheating of the line or other electric equipments, which may suffer finally permanent damages. By means of performing a network topology reconfiguration, it is possible to bring current flows back to safe limits. Voltage swells and sags apply a limiting factor since network reconfiguration can give rise to unacceptably high or low voltage conditions which can evidently reach or exceed thermal limits. Such issue is addressed by supplying reactive power so as to improve load power factor and reduce reactive losses in transmission lines and transformers. Active power flow control requires cost-effective solutions that can alter the impedance of the power lines or change the angle of the voltage applied across the line, thus controlling power flow. Series reactive compensation is applied normally in long transmission lines, but is not likely to be used in other applications, mainly because of the associated high cost and the complexity of achieving voltage isolation, as well as the issues related to fault management [40].

There is general consensus that the future power grid will need to be smart and aware, fault tolerant, self-healing, dynamically & statically controllable and energy efficient at a time. Such requirements can be achieved by means of using fast dynamic control over reactive and active power. Therefore, it is necessary to count on high power electronic controllers which makes the AC transmission network more flexible and able to get adapted to the effects of contingencies and load variations [41].

## 2.2.1   Flexible AC Transmission Systems

FACTS was first introduced and defined as "Alternating current transmission systems incorporating power electronic-based and other static controllers to enhance controllability and increase power transfer capability" [41]. The FACTS controller is defined as "a power electronic based system and other static equipment that provide control of one or more AC transmission system parameters". The main objective of FACTS can be summarized as:

- Increase power transfer capability in the electrical network

- Improve the stability of the network

- Damp low and sub synchronous frequency oscillations

- Control dynamic voltage variations

Depending on the compensation objectives, the compensation device can be connected as shown in Fig. 2.2 giving rise to different kind of FACTS, as stated in [39] [41], which are normally categorized as:

- Shunt compensation controllers

- Series compensation controllers

- Combined compensation devices
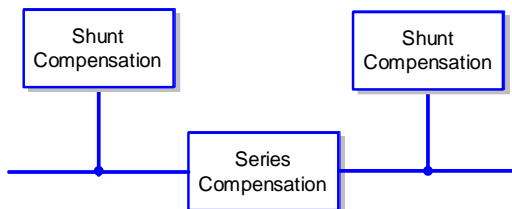
**Fig. 2.2.** Possible compensation connection methods.

In shunt compensation applications the main objective of using FACTS in transmission systems are:

- Reducing the undesired reactive power flows and the associated power losses in the network.

- Keeping the contractual power exchanges with balanced reactive power.

- Compensating the effect of thyristor converters e.g. in conventional HVDC lines.

- Improvement of static or transient stability.

On the other hand, series devices are able to provide other functionalities in transmission systems, such as:

- Improvement of the damping of power oscillations.

- Limiting short circuit currents in networks or substations,

- Avoiding loop flow response and power flow adjustments.

FACTS were primarily designed based on variable impedance type controllers technology, which utilizes thyristor switches such as: Static Var Compensators, Thyristor Controlled Series Compensators or Thyrsitor Controlled Phase Shifting Transformers [42].

However, with the evolution of power electronics technology, the utilization of self-commutating power semiconductors increased due to its flexibility and controllability advantages over natural-commutated power semiconductors. Typical modern FACTS are based on VSC power electronic devices due to its advantages of compactness, capability to provide active power from energy source and capability to supply reactive power. In this regard, typical VSC based FACTS controllers are:

- STATic synchronous COMpensator (shunt connected)

- Static Synchronous Series Compensator (SSSC) (series connected)

- Unified Power Flow Controller (combined shunt-series)

Each type of compensator affects the power flow in different ways. The STATCOM affects the bus voltage, the SSSC affects the line impedance and the UPFC adjusts both parameters as shown in Fig. 2.3.



$$P = V_1 V_2 \frac{1}{X_L} \sin(\delta_1 - \delta_2)$$
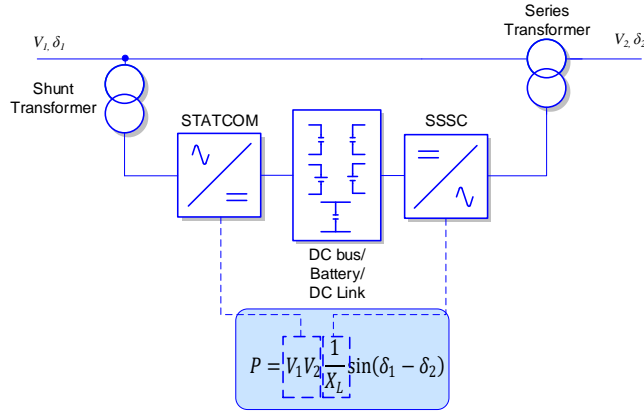
**Fig. 2.3.** Types of VSC based power flow controllers.

Other combinations have been introduced in the literature, such as the Generalized UPFC or the Interline UPFC. They all utilize a combination of series and/or parallel connected VSCs in order to provide power flow controllability in more than one line starting from the same substation [43] [44]. Moreover, Back-to-Back systems, such as in HVDC, allow power flow controllability while additionally frequency decoupling of both sides. FACTS have also been introduced in the literature in distributed form as Distributed FACTS where the VSCs are compacted and distributed among several areas and the control is linked by communication [36] [45].

## 2.2.2 STATCOM

The ideal objective of a STATCOM is to obtain a controllable three-phase AC voltage at the point of common coupling (PCC), in order to regulate reactive current flow by generation or absorption of reactive power through a VSC. A simplified structure and the operational characteristic are shown in Fig. 2.4 A STATCOM is able to supply variable reactive power, what indeed permits to regulate the PCC bus voltage. In some applications, the introduction of a STATCOM permits to increase the power transfer capacity of the network. Moreover, a STATCOM-based damping stabilizer extend the critical clearing time and enhance greatly the power system transient stability [45]. If a proper energy storage system is integrated at the DC bus, a STATCOM would be able to handle active power, permitting thus this device to operate in all four quadrants of the P-Q plane. In this application the active power flow is adjusted by varying the phase angle between bus voltage and the VSC fundamental output AC voltage, while the reactive power flow is greatly varied with the difference in magnitude between both voltages. A lagging phase difference allows active power flow to the bus and vice versa. Whereas for a zero-angle

difference, if the VSC output voltage is greater than bus voltage, the STATCOM is considered to be operating in capacitive mode i.e. delivering reactive power to the bus.
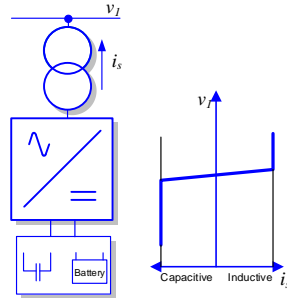


**Fig. 2.4.** STATCOM configuration and characteristics.

### 2.2.3    SSSC

The SSSC is a series connected device in which a VSC injects fundamental voltage in series with the transmission line, as shown in Fig. 2.5. Ideally the VSC operates in quadrate with the lines current such that it behaves like an inductor or a capacitor. Therefore the inverter does not consume or generate active power [46]. If the VSC output lags the line current 90º, the operating mode is capacitive and the line current magnitude is increased which leads to an increase in the power flow. Meanwhile, if the VSC output voltage leads the line current 90º, the operating mode is inductive and the line current magnitude is decreased. One of the advantages of SSSC lays on its capability to handle transient line power reversals. This feature allows using the full dynamic range of SSSC under contingency conditions in order to improve the overall stability [41]. The duration of this transient compensation is limited by the energy stored in the DC capacitor. However, if a charging mechanism or battery is integrated at the DC side, the device could work as an uninterruptible power supply.
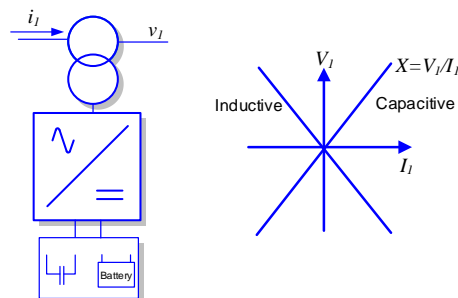


**Fig. 2.5.** SSSC power line configuration and characteristics.

### 2.2.4 UPFC

The UPFC shown in Fig. 2.6, is a complete controller in which the benefits of a STATCOM and a SSSC are combined. The main principle of the UPFC, as the combination of STATCOM and a SSSC, was first introduced in 1991 by Gyugi [47]. UPFC is considered to be the most versatile FACTS controller for regulating voltage and power flow in a transmission line. When the converters of the STATCOM and the SSSC do not share a common DC link, each converter will act based on its primary function. Sharing a common DC link enables the two converters to exchange active power. The inclusion of a power source at the DC side of the SSSC permits to control active and reactive power flow in the line, while the STATCOM not only provides this required power, but also regulates the reactive power injected to the PCC. Thus, a UPFC provides three degrees of freedom in the compensation if compared with other FACTS, which have only one degree of freedom [48].
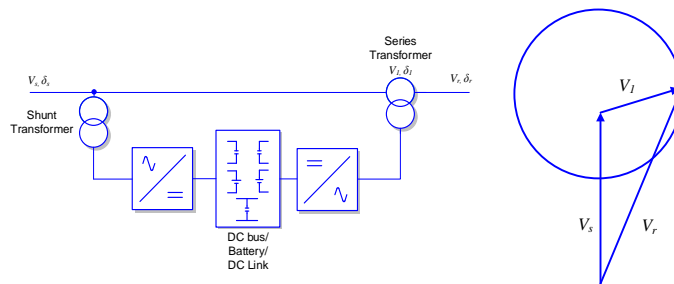


**Fig. 2.6.** UPFC power line configuration and characteristics.

## 2.3. Distribution Systems

Distribution systems suffer severe power quality issues such as poor voltage regulation, increased harmonic currents, reactive power burden or load unbalance among others. Such problems can be minimized if sufficient margins in the power transfer capability are maintained. However, these margins creates difficulties in the expansion of the transmission network. With the deregulation of the electric power energy market, the awareness regarding power quality, specially voltage performance, has increased among different categories of customers [49]. [50] [51].

### 2.3.1 Power Quality Classification

The Institute of Electrical and Electronics Engineers (IEEE), standard IEEE 1100 defines power quality as "the concept of powering and grounding sensitive electronic equipment in a manner suitable for the equipment." In practical terms, it refers to maintaining a near sinusoidal power distribution bus voltage at rated magnitude and frequency while providing an uninterrupted service. A summary and classification of different power quality problems are presented in Table 2.1 [34] [50] [51] [52].

**Table 2.1.** Summary of classification of power quality problems.

| Categories | Specific Categories | Cause | Characterization |
|---|---|---|---|
| Short-duration interruptions | Sag | Ferromagnetic transformers, single line to ground faults, induction motor start-up | Type (instantaneous, momentary, temporary), time duration (cycles, seconds) and amplitude change. |
| | Swell | Circuit Capacitance, Switching out large loads, Load rejection, Phase fault. | |
| | Interruptions | Temporary (self-clearing) faults | |
| Long-duration interruptions | Undervoltage | Switching on loads, capacitor de-energization | Time duration (minutes), amplitude change |
| | Overvoltage | Switching on loads, capacitor de-energization | |
| | Interruption | Faults | |
| Waveform distortions | DC Offset | Geo-magnetic disturbance, half-wave rectification | Voltage, Amps |
| | Notching | Power electronic converters | THD, Harmonic spectrum |
| | Harmonics | Adjustable speed drives and other non-linear loads | THD, Harmonic spectrum |
| Transients | Impulsive | Lightning strike, transformer energization, capacitor switching | Peak magnitude, rise time and duration |

| | Oscillatory | Line or capacitor or load switching | Peak magnitude, frequency component and duration |
|---|---|---|---|
| Imbalance | Multi-phase systems | Single-phase loads, single phase conditions | Symmetrical components |
| Flicker | Sag/swell | Arc furnace, arc lamps | Frequency of occurrence, modulating frequency |
| Power Frequency Variation | | Rapid change to connected load | ±0.5Hz |

### 2.3.2 Power Quality Standards

Geneva based International Electrotechnical Commission (IEC) and the Institute of Electrical and Electronic Engineers (IEEE) have proposed various power quality standards. The following Table 2.2 lists some of these standards.

**Table 2.2.** Power quality standards.

| Phenomena | Standards |
|---|---|
| Classification of power quality | IEC 61000-2-5: 1995, IEC 61000-2-1: 1990, IEEE 1159:1995 |
| Transients | IEC 61000-2-1: 1990, IEEE c62.41: (1991), IEEE 1159:1995, IEC 816: 1984 |
| Voltage sag/swell and interruption | IEC 61009-2-1: 1990, IEEE 1159: 1995 |
| Harmonics | IEC 61000-2-1: 1990, IEEE 519:1992, IEC 61000-4-7: 1991 |
| Voltage flicker | IEC 61000-4-15: 1997 |

The distribution system has to tackle PQ in order to provide customers an acceptable power quality in terms of:

- Balanced three-phase AC supply.

- Improved power factor.

- Steady-state voltage with permissible limits of variations.

- Pure sinusoidal voltage waveform.

- Minimum interruptions in power supply.

- Voltage sags and swells within permissible limits.

### 2.3.3    Custom Power Devices

FACTS where was originally conceived for transmission network applications. However, it has been also extended for power quality improvements at the distribution level, operating at low or medium voltages [53]. Hence, topologies used in FACTS can be applied to the power distribution systems to increase the reliability and the power quality supplied to the customers. These devices, initially known as CPD, take advantage of power electronic or static controllers installed in medium and low voltage distribution systems for enhancing the level of reliability and/or power quality that is required by customers which are sensitive to power quality indexes. CPDs benefits the industrial, commercial and domestic customers, as they offer solutions to problems faced by utilities and power distributors [54]. As mentioned earlier power quality issues are classified into several categories shown in Table 2.1. Generally, power quality issues are either related to the quality of the voltage supply and/or quality of the current drawn by the load.

CPDs can be categorized in to two types: network reconfiguration type and compensation type. Network reconfiguration type CPDs involve the utilization of power electronic switches for fast action current limitation, fault breaking and fast load transfer between different feeders during contingencies. Whereas compensating type CPDs deal with power quality related issues including active filtering, load balancing, power factor correction and voltage regulation [49]. Moreover, Distributed Generation (DG) sources can include added control functions of CPDs in order to preform compensation objectives during operation such as Flexible Distributed Generation [55].

Configurations of compensation CPDs are similar to that of FACTS since compensation can be applied in series, shunt or a combination. However, the controller function in this scenario is specifically oriented to achieve a certain power quality requirement. [56]

### 2.3.4    Distribution STATCOM

Shunt connected CPDs in distribution system are called Distribution STATCOM (DSTATCOM). A DSTATCOM is similar to the transmission system STATCOM in its configuration. It can perform load compensation, i.e., power factor correction, harmonic filtering and load balancing when connected at the load terminals. It can also perform reactive-power compensation of rapidly changing industrial loads and for stability improvements such as wind turbine systems [57], thus holding the bus voltage constant against any unbalance or distortion in the distribution system. A Shunt Active Filter configuration shown in Fig. 2.7, is similar to that of a DSTATCOM. However, it should be noted that there is a substantial difference in the operation characteristics if compared to a STATCOM. In the distribution case, the goal is to inject compensating currents so that the source current is free of all possible power quality issues mentioned earlier. [58]. Shunt CPDs have the advantage of carrying only the compensation current, plus a small amount

of active fundamental current supplied to compensate the system losses. It is possible to connected several shunt devices in order to achieve higher currents, which makes this type of circuit suitable for a wide range of power ratings.
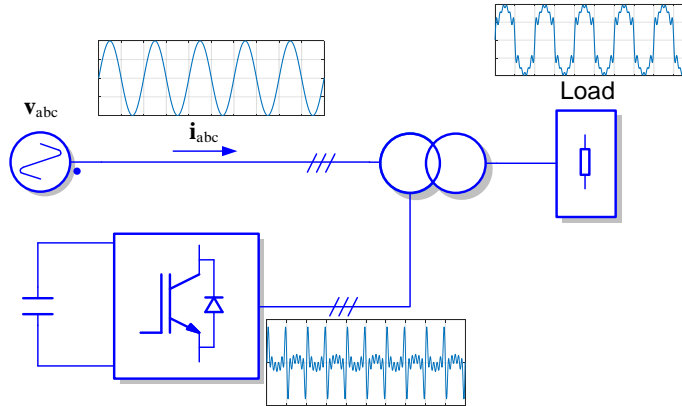


**Fig. 2.7.** DSTATCOM operating as a Shunt Active Filter.

### 2.3.5 Dynamic Voltage Regulator

A Dynamic Voltage Regulator (DVR), shown in Fig. 2.8, is a series compensator, analogous to a SSSC, used to protect sensitive loads from voltage sag/swell. Moreover, it can be utilized as a series active filter to isolate the load from voltage harmonics at the source side. In the scenario of voltage sag mitigation, the inverter generates a compensating voltage, which is inserted into the distribution system through series matching transformer. An energy storage element is required to provide part of the active power drawn by the load during a voltage sag.
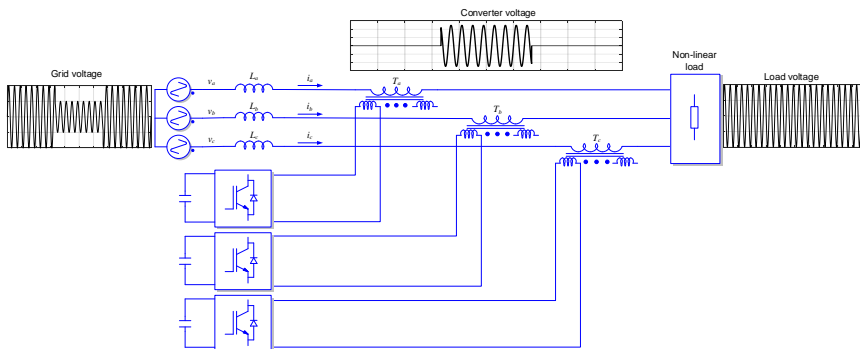


**Fig. 2.8.** DVR configuration for voltage regulation.

However, this energy is only required during the sag interval. During voltage swells, the excess of energy flows to the DC side of the inverter. The stored energy has to be dissipated using resistors, otherwise the DC capacitor can be charged to high voltage levels, causing an avalanche breakdown of the valves [59]. Operating as a series active filter, it forces the source current to become sinusoidal. The approach is based on a harmonic isolation principle, by controlling the output voltage of the series active filter. In other words, the series active filter presents a high impedance to harmonic currents, blocking the harmonic current flow from the load to the ac source and from the ac source to the load side. The main advantage of series filters over parallel ones lays on the fact that they are ideal for eliminating voltage-waveform harmonics as well as for balancing three-phase voltages. This, in fact, means that this category of filter is used to improve the quality of the system voltage for the benefit of the load. It provides the load pure sinusoidal electrical waveform, which is important for voltage-sensitive devices.

### 2.3.6   UPQC

UPQC is a very versatile device that is able to inject current in shunt and voltage in series simultaneously in a dual control mode. Therefore, it can perform both the functions of load compensation and voltage control at the same time. A UPQC is able to provide several functionalities, including [60]:

- Compensation for supply voltage flicker/imbalance and harmonics.

- Providing VAR requirement of the load reducing the requirement for power factor correction equipment.

- Maintaining load end voltage at rated value at presence of voltage sags. Moreover, injected voltage is provided through the DC link. Thus, no energy storage element is required.

### 2.3.7   Custom Power Park

By means of using Custom Power Devices, achieving higher power quality levels as well as to satisfy the needs of sensitive loads has become possible. A Custom Power Park [51] integrates power quality devices within a utility's distribution system, which are able to provide tenants controlled, cost-effective and nearly undisturbed energy. Fig. 2.9 represents a Custom Power Park concept where the Park operations center receives power from multiple distribution feeders, being even able to combine it with distribution sources or energy storage systems, and then distribute power to its tenants in the park. Another possible Custom Power Park design includes a utility corridor with multiple electric circuits. Electric power with different power quality specifications could be provided to tenants with different needs.
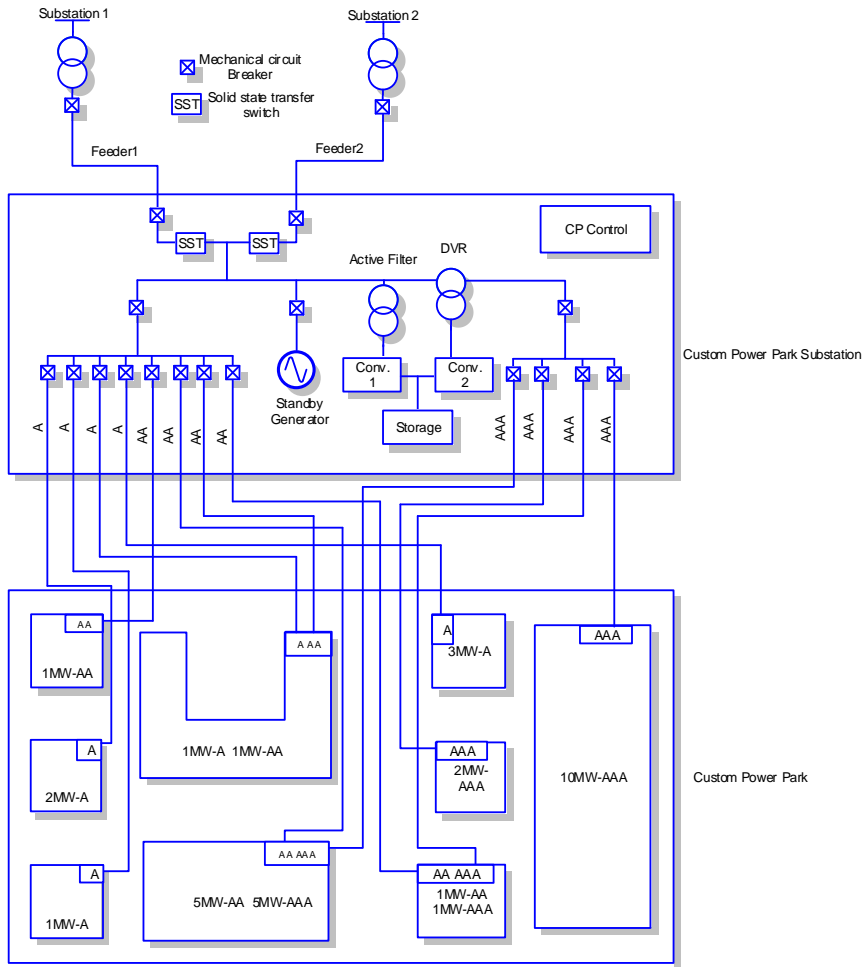
**Fig. 2.9.** Custom Power Park concept.

## 2.4. Control of compensation devices

The control system is the heart of the state-of-the-art of compensation devices for dynamic control of power flow and power quality. Based on the application, the requirements and system configuration, control parameters are controlled in order to achieve the required performance. Control techniques play a vital role in the overall performance of the power conditioner. The rapid detection of the disturbance signal with high accuracy, fast processing of the reference signal, and high dynamic response of the controller are the prime requirements for achieving the desired compensation [61].

### 2.4.1   Shunt Compensation Controllers

As mentioned earlier, a shunt compensation device can be used for voltage regulation or load current compensation purposes. Considering a shunt compensation device, the active and the reactive current are regulated in such way that active current maintains a constant DC voltage across the storage element terminals, while reactive has three possible operating modes: VAR control mode, automatic voltage control mode and active filter control mode, as shown in Fig. 2.10 [62]. In VAR control mode, the reactive current is set according to the required inductive or capacitive VAR command. Among the approaches of generating the reference current is the Instantaneous Reactive Power Theory [50] shown in Fig. 2.11 [60].Whereas in RMS voltage control mode, the reference reactive current is determined by the AC bus voltage controller which incorporates droop characteristics [63].
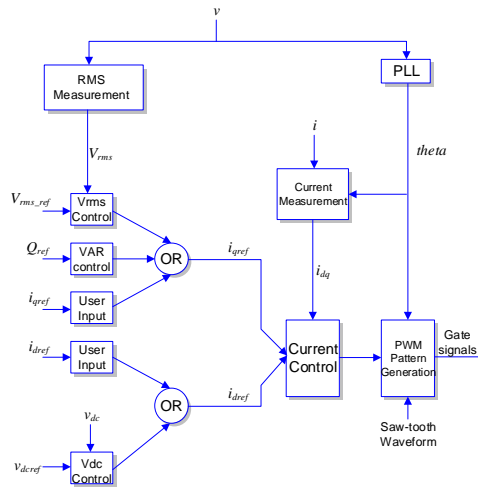


**Fig. 2.10.** Control structure of a shunt compensation controller.
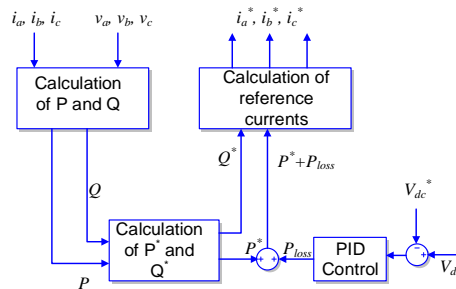


**Fig. 2.11.** Reference current generation using Instantaneous Reactive Power Theory.

When operating as a shunt active filter, the fundamental component of line current is extracted and subtracted from the line current to provide the reference harmonic components current as shown in Fig. 2.12.
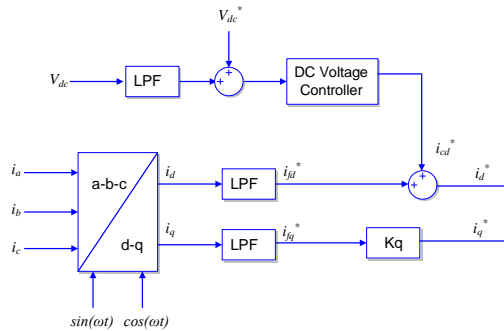
**Fig. 2.12.** Control structure of shunt active power filter.

## 2.4.2    Series Compensation Controllers

A series compensator is utilized to inject a series voltage of a required magnitude and angle, with respect to the bus voltage. There are several control methods for the injected series voltage which includes: SSSC, DVR and Series Active Power Filter [64] [65] [66].

The operation as a SSSC presented in Fig. 2.13 is achieved by controlling the magnitude and phase angle (with respect to bus voltage) of the series injected voltage. The magnitude and phase angle are determined based upon the required active and reactive power flow through the line.
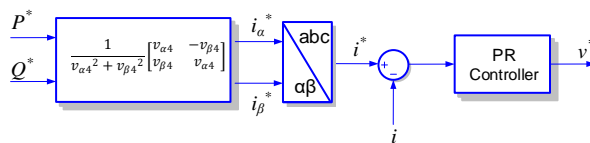


**Fig. 2.13.** Control of series compensator operated as SSSC.

On the other hand, a DVR controller, which is shown in Fig. 2.14 , consists of a combined feed-forward/feed-back medium voltage controller. The control structure of the DVR shows that the d-q technique is used for the detection of the sag. However, in this technique, the selection of the parameters and the order of the low pass filter play a vital role in the filter's performance. Hence, the effect of the filter increases with the filter's order, but the response time gets worse and the phase-shift of the output signal becomes bigger. Also, the d-q technique takes at least one-cycle time to track the voltage sag.

The harmonic compensation is obtained by using resonant controllers instead of synchronous frame d−q integral controllers at each frequency, due to the significant computational advantages achieved when stacking multiple controllers, their single-phase usage options, and also due to their combined positive and negative sequence compensation [67].
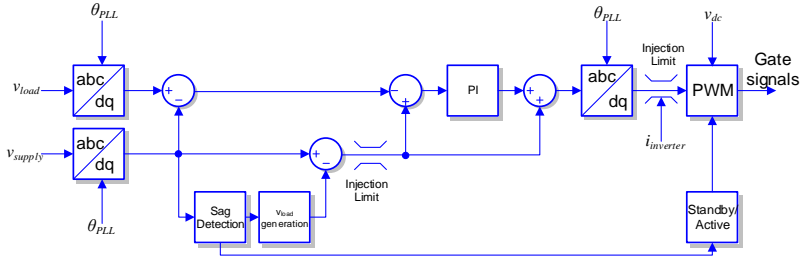
**Fig. 2.14.** Control of series compensator operated as DVR.

### 2.4.3    Series - Shunt Compensation Controllers

Combining both controllers (series and shunt) mentioned earlier it is possible to achieve the operation of a UPFC or UPQC. The shunt controller regulates the DC bus voltage and injects the required current while series the controller injects the required voltage according to the control objective. A simplified active power filter control of a UPQC is shown in Fig. 2.15 [68] where the parallel and series converter injects the harmonic currents determined by subtracting the filtered components from the measured components. Thus, the parallel converter establishes a sinusoidal source current and the series converter establishes a sinusoidal load voltage.
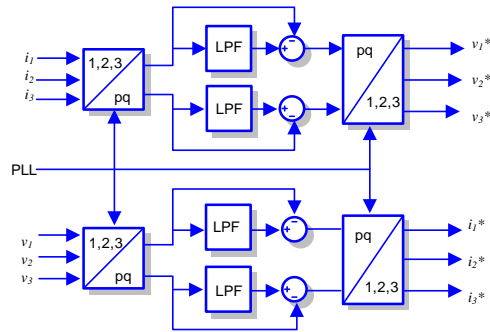


**Fig. 2.15.**  Block diagram of the UPQC control operating as an active power filter.

The control strategy plays a crucial role in deciding the behavior, the desired operation and the effectiveness of the UPQC system. Based on the reference signals (current and voltage) the control strategy determines the switching instants of inverter switches to achieve the required performance. Frequency domain-based control methods, such as those based of Fast Fourier Transform are not popular due to the large computation burden and delay that they require.

As mentioned earlier, the reference signals can be generated using instantaneous power theory [69], instantaneous reactive power theory in a rotating reference frame which is used to eliminate harmonics and to correct the power factor [70] and synchronous reference

frame method or three-phase dq theory [71]. These methods convert the signals from ABC frame to stationary or rotating reference frame to separate the fundamental and harmonic quantities.

### 2.4.4 Synchronization

The synchronization with the injected shunt current, as well as with the series voltage can be achieved by using a Double-Second Order Generalized Integrator Frequency Locked Loop (DSOGI-FLL) shown in Fig. 2.16 [97] which determines the filtered positive sequence $\alpha\beta$ components ($v_{\alpha\beta}{}^{+'}$) of the input voltage ($v$) and its equivalent frequency ($\omega$). The magnitude of the signal is determined by applying $\sqrt{(v_\alpha{}^{+'})^2 + \left(v_\beta{}^{+'}\right)^2}$ and dividing the magnitude by $v_{\alpha\beta}{}^{+'}$ to derive the equivalent synchronizing signals ($sin(\omega t),\ cos(\omega t)$). The DSOGI consists of two Second Order Generalized Integrator Quadrature Signal Generators with gain $K_{DSOGI}$ that are used to generate the direct and in-quadrature signals ($v_{\alpha\beta}{}',qv_{\alpha\beta}{}'$) from the $\alpha$ and $\beta$ components of the input voltage ($v_{\alpha\beta}$). A Positive/Negative Sequence Calculation block is used to determine $v_{\alpha\beta}{}^{+'}$ from $v_{\alpha\beta}{}'$ and $qv_{\alpha\beta}{}'$. Using the SOGI-QSG error ($\varepsilon_{\alpha\beta}$) and $qv_{\alpha\beta}{}'$, the FLL derives the frequency ($\omega_k$) through its FLL gain ($K_{FLL}$) and an initial frequency ($\omega_0$).
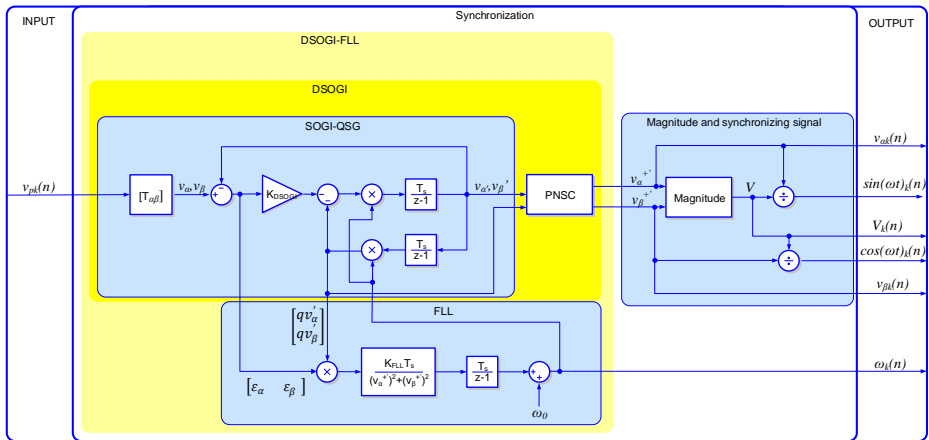


**Fig. 2.16.** Synchronization block structure.

## 2.5.  Compensation System Topology

Considering UPFC/UPQC as the generalized compensator, several topologies and configurations have been presented in the literature. These configurations can be categorized based on the type of converter (current or voltage source), the connection configuration (single-phase two-wire, three-phase three-wire and four-wire, isolated and non-isolated connection).

### 2.5.1    Converter Topology

In a series-shunt converter structure, both shunt and series converters share a common dc-link. The shunt converter regulates the dc-link at a set reference value. Typical VSC converters, shown in Fig. 2.17, consists of several IGBT switches connected in series to deliver a high blocking voltage capability for the converter, and therefore increase the dc bus voltage level. Antiparallel diodes are also required to enable four-quadrant operation of the converter. The DC bus capacitor provides the required energy storage to fulfill power flow control and provide filtering of dc bus harmonics. The converter is typically controlled through a Pulse Width Modulation (PWM) technique and the harmonics are directly associated with the switching frequency. [72]. The advantages offered by a VSI topology over a CSI one include lower weight, no need of blocking diodes, cheaper, capability of multilevel operation, and flexible overall control.
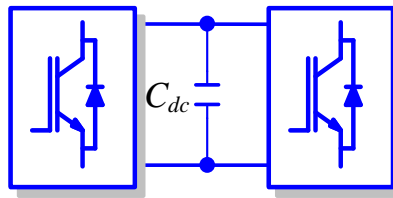


**Fig. 2.17.** UPQC configuration with VSI.

Several VSC topologies have been proposed in the literature to increase the number of output voltage levels, reduce switching frequency and improve output voltage quality [73] [74]. The typical VSC, shown in Fig. 2.17, has two output voltage levels as shown in Fig. 2.18. By increasing the number of output voltage levels, the output voltage have more steps generating a staircase waveform which has reduced harmonic distortion compared to the two level output voltage. However, increasing the number of levels yields an increased control complexity and voltage balancing issues which will be discussed later.
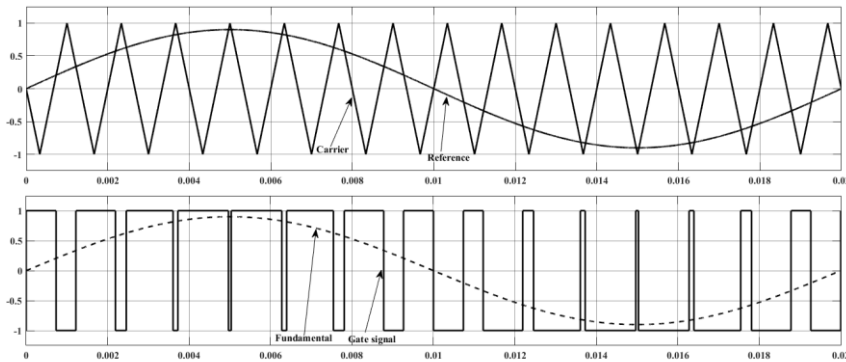


**Fig. 2.18.** Output voltage waveform of a SPWM two-level VSC.

Four main topologies are applicable in FACTS applications due to their modularity and capability to store energy [75] [76] :

- Neutral Point Clamped.

- Flying Capacitor.

- Cascaded H Bridge.

- Multipulse converter.

- Modular Multilevel Converter.

Multilevel inverters are attractive due to its advantages over two level inverters such as [77]:

- Low distortion output voltage with lower dv/dt.

- Input current withdrawn contains low distortions.

- They operate with lower switching frequency.

When comparing different types of multilevel converters, several factors are taken into considerations:

- Number of components.

- Modularity.

- Control complexity.

- Fault tolerance.

## 2.5.2   Connection Configurations

The connection of the compensator to the power system depend on the wiring of the supply, the connection configuration and the topology of the converter. Single phase connection are more eminent in UPQC for power quality related issues regarding voltage, reactive current and current harmonics. Fig. 2.19(a) shows the most popular configuration in single phase systems based on two VSI H bridge topology [78]. Similarly a CSI based topology can be utilized for a single phase two wire system [79] For low-cost and low power applications, minimizing the number of switches is possible as shown in Fig. 2.19 (b) and Fig. 2.19 (c). [80] [81]. In Fig. 2.19 (b), one leg controls a series compensation and another controls the shunt compensation while the third leg is a common element to both compensators. The decoupling of each converter leg with respect to the common leg can be achieved if Space Vector Modulation (SVM)[97] is implemented. The operation sector ($n$) and the respective time weights for that sector ($t_n, t_{n+1}$) are calculated with the two zero

vectors ($t_0,t_7$) based on the apportioning factor ($\lambda$). The time weights of each vector are then used to determine the pulse width of each leg over the sampling period which is used to determine the duty ratio of each leg for the PWM of each leg. The half-bridge topology in Fig. 2.19(c) consists of one leg per compensation type and a split capacitor with neutral point connected. Although there is a reduction in the number of switching devices, it has to be noted that the compensation performance may be compromised in such a connection.



(a)                                                    (b)                                                    (c)
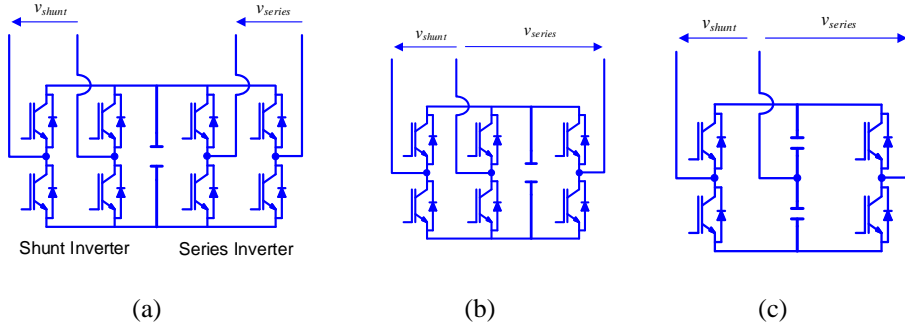
**Fig. 2.19.** Single phase series-shunt compensator connection with (a) 8 switches, (b) 6 switches and (c) 4 switches configurations.

The most widely studied configuration of three phase series-shunt compensator is shown in Fig. 2.20(a) [82]. Since not all industrial and commercial loads are three-phase loads, a variety of single-phase loads and three phase loads are supplied with three phase four wire system. The presence of a neutral wire causes excessive neutral current flow and requires additional compensation. Split-capacitor, four-leg and Three H Bridge topologies are among the most common configurations with neutral point connection, as shown in Fig. 2.20(b), Fig. 2.20(c) and Fig. 2.20(d). The trade-off in a split-capacitor configuration is the requirement of an additional control loop to regulate the voltage across both capacitors in order to maintain the common point at zero potential. According to [83], for high-voltage applications the three H bridge topology may be considered as the most advantageous one if compared to the others. However, there is an increase in the total number of switches, losses, size and cost.

An approach to minimize the number of switches has been discussed in [84] by using a nine-switch inverter as shown in Fig. 2.21 where the upper six switches control the series compensator output voltage and the lower three switches control the capacitor voltage through the shunt transformer.
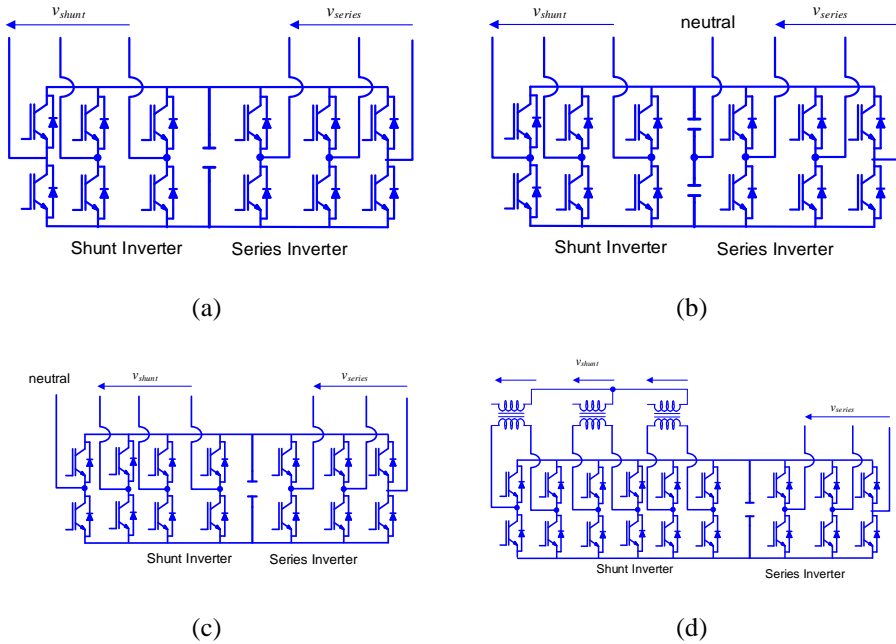
**Fig. 2.20.** Three phase series-shunt compensator connection with (a) three-wire, (b) four-wire and split capacitor, (c) four-wire non-isolated and (d) four-wire isolated configurations.
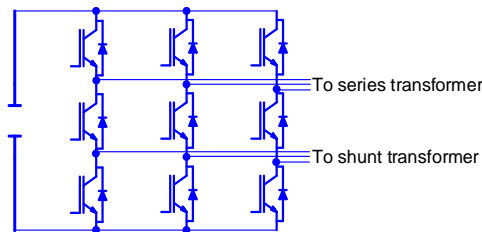


**Fig. 2.21.** Three phase series-shunt compensator a with nine switch converter.

## 2.6.   Isolating Transformers

Power transformers represent the largest portion of capital investment in transmission and distribution substations. In addition, power transformer outages have a considerable economic impact on the operation of an electrical network. A transformer is a static electrical device that uses electromagnetic induction to transfer power from one circuit to another [85]. Often, the leakage impedance of the interconnecting transformer used in FACTS and CPDs serves as the inductive impedance that has to separate the sinusoidal bus voltage and the voltage injected by the VSC (which contains harmonics).

A typical transformer consists of core, coils, tank, insulation and other accessories. Transformers create a high magnetic-flux density within a high magnetic-permeability iron core with the minimal magneto-motive force possible. The limitation to the minimum and maximum size of the core depends on shipping limitation and flux density limitation to about 1.7 Tesla. The iron core is typically made of thin laminations of silicon alloy, to reduce eddy current losses and to improve the magnetization characteristics.

The coils can be concentric, interleaved or "Pancake" wound. In certain applications, one or the other type may be more efficient. However, in general they can both be designed to function well in terms of cooling features, capability to withstand high voltage surges, and mechanical strength under short circuit conditions [86].

Several core designs have been discussed in literature. The most representative ones are shown in Fig. 2.22.The most widely used three phase transformer core design is the stacked core design shown in Fig. 2.22 (b) due to economic reasons. In shell-type transformers shown in Fig. 2.22 (c), the flux-return-paths of the core are external and enclose the windings, providing thus a better magnetic shield which is suitable for supplying power at low voltage and high currents. Whereas core-type transformers shown in Fig. 2.22(b),(d) and (e),  have their limbs surrounded concentrically by the main windings. Having the top and bottom yokes equal in cross section to the wound limbs, no separate flux-return path is necessary. Shell type transformers present a better short circuit and transient voltage response relative to core form. [85]

The core-design defines an important distinction in the effective reluctance of the transformer. In triplex core, shell core, five-legged stacked and wound core, the zero-sequence flux flows in the core material through the provided extra limb. Therefore, such core designs are low reluctance transformers, requiring thus a low excitation current and reduced excitation losses. Whereas in three-legged stacked core designs, the zero-sequence flux flows through the air and tank of the transformer, which is a high reluctance path. In such design, the  excitation current and losses cannot be neglected. [87].



|     |     |     |
|:---:|:---:|:---:|
| (a) | (b) | (c) |

|           |           |
|:---------:|:---------:|
|    (d)    |    (e)    |
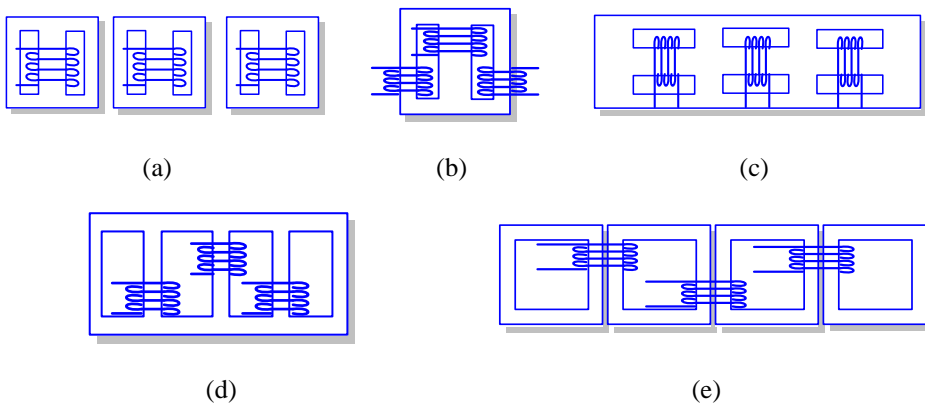
**Fig. 2.22.**  Three-phase transformer core designs: (a) Triplex core, (b) three-legged stacked core, (c) shell core, (d) five-legged stacked core and (e) five-legged wound core.

### 2.6.1   Modelling

Transformer modelling is a complex topic, as it is necessary to consider every transient phenomena, requiring a model valid for a frequency range from dc to several MHz. Such model is very difficult to achieve and in most cases is not feasible. This complexity is due to the large number of core designs the nonlinear nature of the parameters and frequency dependency. Frequency dependent attributes that may be required in a transformer model representation are core and coil configuration, self-mutual inductance, leakage flux, skin effect, proximity effect magnetic core saturation, hysteresis and eddy current losses, and capacitive effect [88]. The development of a model that includes all these effects, being able to work in any kind of transient conditions and frequencies, is not a simple task. At the present time, the most complete model available was developed by De León and Semlyen [89].

A classification of frequency ranges of transients has been proposed in [90] in accordance with Conseil International des Grands Réseaux Électriques (CIGRE) WG 33.02 which are: slow transients (5Hz to 1kHz), switching transients (fundamental frequency to 10kHz), fast front transients (10kHz to 1MHz) and very fast front transients (100kHz to 50MHz). According to CIGRE WG 33.02 [91], model requirements based on these frequency ranges is presented in Table 2.3. Transformer models are based on a linear part (winding arrangement) and a non-linear part (core configuration). Both parts are frequency dependent and play a different role depending on the study for which the transformer model is required.

Considering low-frequency transients as the primary concern in the development of FACTS, three modeling approaches have been discussed in the literature [85] [87] [89] [90] [91]. The models are characterized as: Matrix, saturable component and topology representations. Each type of model have certain limitations regarding core design representation and parameter determination.

The basic quantitative representation of a coil wound magnetic circuit are given in Equations (2.1) through (2.6) with the following variables: $\mathfrak{R}$: reluctance, $i$: current, $\mu$: permeability, $A$: Area of core, $\varphi$: flux, $F$: magnetomotive force, $N$: number of turns, $H$: magnetic field intensity, $B$: flux density, $l$: length of core, $L$: inductance, $\lambda$: flux linkage, $e$: induced electromotive force.

**Table 2.3.** CIGRE modeling recommendation of power transformer.

| Parameter/Effect | Low frequency transients | Slow front transients | Fast front transients | Very fast front transients |
|---|---|---|---|---|
| Short-circuit impedance | Very important | Very important | Important | Negligible |
| Saturation | Very Important | Very Important for transformer energization phenomena, otherwise it is just important | Negligible | Negligible |
| Iron losses | Important only for resonance phenomena | Important | Negligible | Negligible |
| Eddy Current | Very important | Important | Negligible | Negligible |
| Capacitive coupling | Negligible | Important | Very Important | Very important |

$$\Re = \frac{l}{\mu A} \tag{2.1}$$

$$F = N.i = \varphi.\Re = H.l \tag{2.2}$$

$$B = \frac{\varphi}{A} = \mu.H \tag{2.3}$$

$$\lambda = N.\varphi = L.i \tag{2.4}$$

$$L = \frac{N^2}{\Re} \tag{2.5}$$

$$e = \frac{d\lambda}{dt} \tag{2.6}$$

### 2.6.2 Matrix representation model

The transformers modeled in Electromagnetic Transient Programs utilize the subroutine BCTRAN which creates an impedance or admittance matrix representation of the transformer [92]. In such approach, transformers are represented as coupled [R]-[L], as presented in Equation (2.7).

$$[v] = [R][i] + [L][\frac{di}{dt}] \qquad (2.7)$$

This approach includes coupling between phases but does not consider differences in the core and winding topology. Thus, all core designs receive the same mathematical equation. Complications arise when the impedance matrix [Z] is ill-conditioned due to very small excitation currents or when these currents seize to exist. One of the approaches to address such issue is the use of admittance matrix in (2.8). Where [Y] is the admittance matrix and its elements always exist and obtained directly from short-circuit tests. For transient studies, the admittance matrix is splitted into real and imaginary parts as in (2.9). Such approach is not topologically correct. However, such models are linear and theoretically valid for fundamental frequency, and reasonably accurate for frequencies below 1kHz. The excitation may be omitted from the matrix representation and attached externally at the model terminals in the form of non-linear element [82] [85] [91].

$$[I] = [Y][V] \qquad (2.8)$$

$$\left[\frac{di}{dt}\right] = [L]^{-1}[v] - [L]^{-1}[R][i] \qquad (2.9)$$

The data that are usually available for any power transformer are: ratings, excitation, and short-circuit test data for direct and homopolar sequences, saturation curve, and capacitances between terminals and between windings. The determination of the transformer parameters are based on the theory presented in [92] and [93] using positive sequence, zero sequence excitation and short circuit test to obtain the inductance matrix [L] parameters. While copper losses are represented by the [R] diagonal matrix. The core losses are modeled by additional shunt resistances connected to the terminals of one of the three-phase windings as shown in Fig. 2.23.
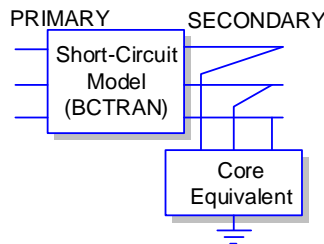


**Fig. 2.23.** BCTRAN model for two winding three phase transformer.

### 2.6.3    Saturable Transformer Component Model

This model is based on single-phase multi-winding transformer model used in a star-circuit representation shown in Fig. 2.24.  The equation of a single-phase N-winding transformer, without including the core, has the same form of (2.9). However, the matrix product is symmetric, which is not true in the general case. The effect of saturation and hysteresis are modeled by adding an extra nonlinear inductor at the star point. The model can be extended to a three-phase case by means of adding a zero-sequence reluctance parameter. However, this model is of limited application, since the representation is not topologically correct. Moreover, it cannot be used for more than three windings.
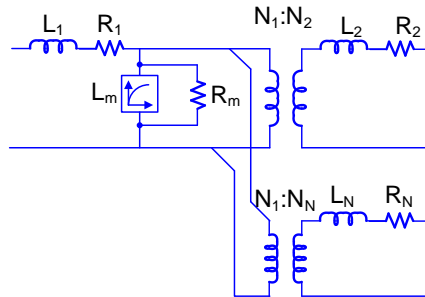


**Fig. 2.24.**  Star-circuit representation of single-phase N winding transformer.

### 2.6.4    Topology Model

The topology based models can accurately represent any type of core design. Such models can be achieved either through the principle of duality or geometry. Geometric models or magnetic circuit based models are topologically correct models utilizing coupling between magnetic and electric equations as in (2.1) through (2.6) and represented in Fig. 2.25. The electromagnetic structure of a transformer can be directly represented using reactance. Relatively complex structures can be examined as a magnetic model. In this regard, the accuracy of the magnetic circuit is highly related to the assumptions made to discretize the magnetic structure in a lumped parameter magnetic circuit. Nonlinear reactance is used to represent iron limbs and linear reactance to represent the air paths. [94] [95]. The core and winding losses cannot be directly included in the magnetic model and are connected at the winding terminals. Eddy current losses in the core are represented by using voltage-dependent resistances while high order polynomial function are used to model non-linearity and hysteresis effect.
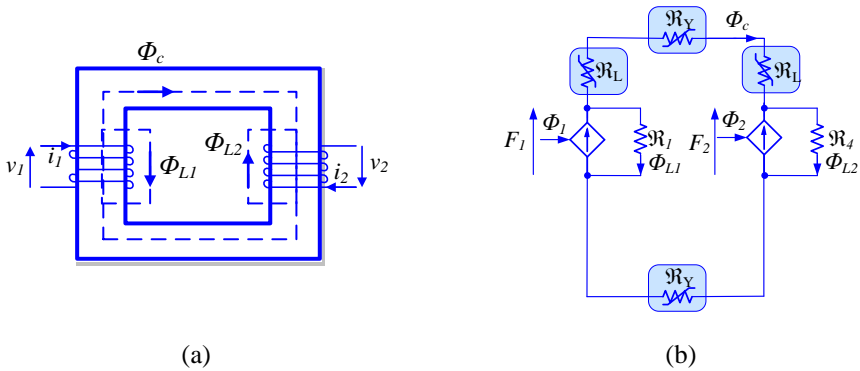
**Fig. 2.25.** Topology based model based on core geometry where (a) is core structure and (b) represents equivalent magnetic circuit.

Based on the approach in [96], topologically-correct equivalent electric circuit model can be derived from the previous magnetic circuit model using the principle of duality. Such models include the effects of saturation in each individual leg of the core, interphase magnetic coupling and leakage effects. In the equivalent magnetic circuit, windings appear as magnetomotive-force (MMF) sources, leakage paths appear as linear reluctances, and magnetic cores appear as saturable reluctances. The mesh and node equations of the magnetic circuit are duals of the electrical equivalent node and mesh equations, respectively. The winding resistances, core losses, and capacitive coupling effects are not obtained directly from the transformation, but can be added to the equivalent circuit. An example of duality transformation approach is shown in Fig. 2.26.
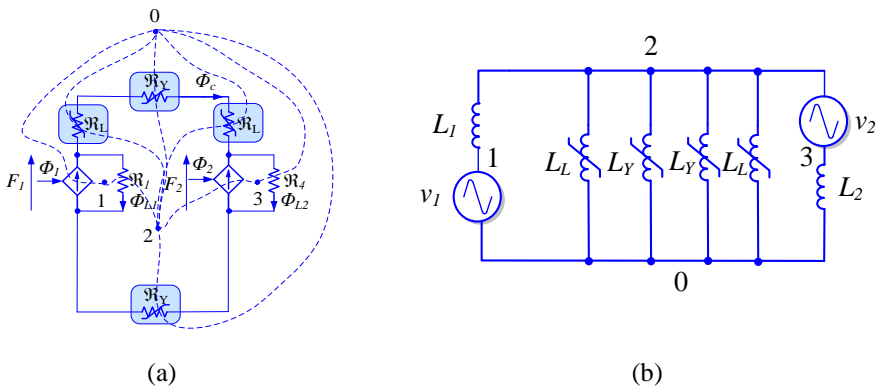


**Fig. 2.26.** Duality based equivalent circuit of a single phase transformer (a) magnetic circuit and (b) equivalent duality circuit.

# The Custom Power Active Transformer

*T*his chapter introduces an invention, which is proposed based on the objectives *discussed in Chapter 1. This invention entails a new transformer, namely "Custom Power Active Transformer" (CPAT), which is characterized by the design of its magnetic circuit and auxiliary windings. The proposed design permits to provide shunt and series compensation in an electrical system using a single transformer. These auxiliary windings are regulated using power converters based on power electronics. In turn, these converters are controlled based on the services to be provided to the network where the CPAT is connected. In a nutshell, the proposed invention enables the integration of power electronics in a transformer, which would empower the transformer with added services improving finally the power system's flexibility.*

## 3.1    Construction

The construction of a single-phase transformer with auxiliary windings, which are equivalent to shunt and series circuits is presented in Fig. 3.1. The diagram shows the basic concept of a single-phase CPAT, where $v_{prim}$, $v_{sec}$, $v_{sh}$ and $v_{ser}$ represent the primary voltage, the secondary voltage, the shunt voltage and the series voltage, respectively. Using the simple analogy between the magnetic flux through a winding in a magnetic circuit ($\Phi$) and the electric voltage across such a winding; windings wound on a common core are equivalent to parallel-connected voltage sources, while windings wound over parallel shunt cores are equivalent to series-connected voltage sources [29]. This analogy also entails the MMF in the magnetic circuit ($F$ in Fig. 3.1(a)) being equivalent to currents in the electric circuit ($i$) [15]. By assuming an ideal transformer with no leakage inductance and a coupling factor $k = 1$ (i.e. with $\Phi_0 = 0$ and $\Phi_{prim} + \Phi_{ser} + \Phi_{sec} = 0$), the equivalent electric circuit, shown in Fig. 3.1(b), can be deduced from Fig. 3.1(a).

(a)



(b)
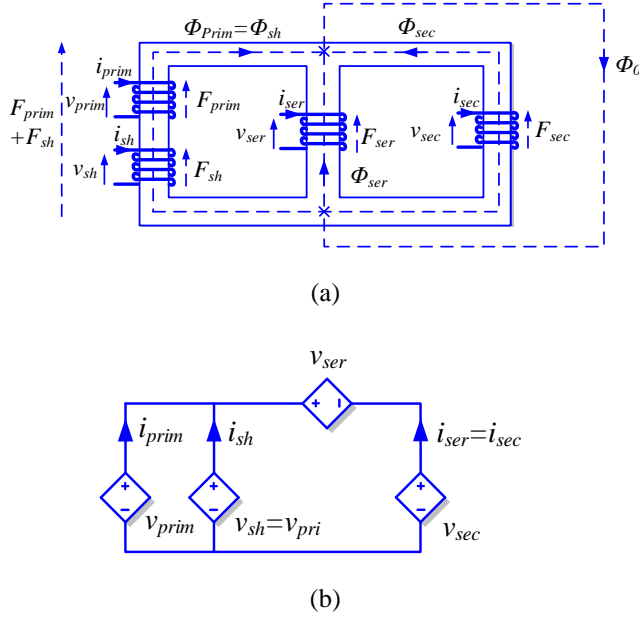
**Fig. 3.1.** Configuration of a single-phase CPAT. (a) Magnetic circuit and (b) Ideal equivalent electric circuit.

According to Ampere's law, the MMF in the primary limb of the magnetic circuit in Fig. 3.1(a), or its equivalent electric current in the circuit in Fig. 3.1(b), is equal to the MMF in any other limb. This concept is mathematically expressed through equations (3.1) and (3.2), where F and N represent the MMF and the number of turns of windings, respectively [17]. According to (3.2), for a given current circulating through the secondary winding ($i_{sec}$), the current circulating through the primary winding ($i_{prim}$) can be actively regulated by controlling the current flowing through the shunt winding ($i_{sh}$). Likewise, according to Gauss's law, the sum of magnetic flux from the three limbs in Fig. 3.1(a) should equal zero. This is mathematically expressed in (3.3) and (3.4), where $v$ is the induced voltage across a winding and $\Phi$ is the flux through its core. Therefore, according to (3.4), for a given $v_{prim}$, the output $v_{sec}$ can be actively regulated by controlling the voltage across $v_{ser}$ [27]. The control over the series winding's voltage and the current at the shunt winding can be implemented through power converters and an appropriate controller.

$$F_{prim} + F_{sh} = F_{ser} = F_{sec} \tag{3.1}$$

$$N_{prim} i_{prim} + N_{sh} i_{sh} = N_{ser} i_{ser} = N_{sec} i_{sec} \tag{3.2}$$

$$\Phi_{prim} + \Phi_{sec} + \Phi_{ser} = 0 \quad ; \quad \Phi_{prim} = \Phi_{sh} \tag{3.3}$$

$$\frac{v_{prim}}{N_{prim}} + \frac{v_{sec}}{N_{sec}} + \frac{v_{ser}}{N_{ser}} = 0 \quad ; \quad \frac{v_{prim}}{N_{prim}} = \frac{v_{sh}}{N_{sh}} \tag{3.4}$$

The CPAT of Fig. 3.1(a) can be extended to multi-phase systems by interconnecting multiple single-phase transformers. However, a more effective approach is shown in Fig. 3.2(a). This diagram, represents a generalized layout of a multi-phase CPAT for multi-compensation purposes [20]. In this case, windings are named $tp^r_k$ and $np^r_k$, where $t$ corresponds to the positive terminal of the winding, $n$ corresponds to the winding's return terminal, $p$ indicates the phase number, $r$ the series winding number, and $k$ the shunt winding's number (Fig. 3.2(a)). Likewise, each phase consists of several shunt-connected limbs. In Fig. 3.2(b), these limbs, act as several series-connected voltage sources in the equivalent magnetic circuit, and $L_0$ is the equivalent zero sequence return path. In such a configuration, many CPATs can be stacked on top of each other, each having many series limbs and many shunt windings per limb. This generalized structure illustrates the possibility of having several shunt compensators at the primary winding to enable a multi-converter system connection. This would allow power exchange between different compensation windings and the use of low-power independent converters for each compensation objective. Moreover, series windings may have many shunt windings with power exchange capacity. This power conditioning configuration, with multi-shunt multi-series windings through a single core, is very flexible because it allows the connection of multiple distributed power converters to a common multi-port transformer.



(a)                                           (b)
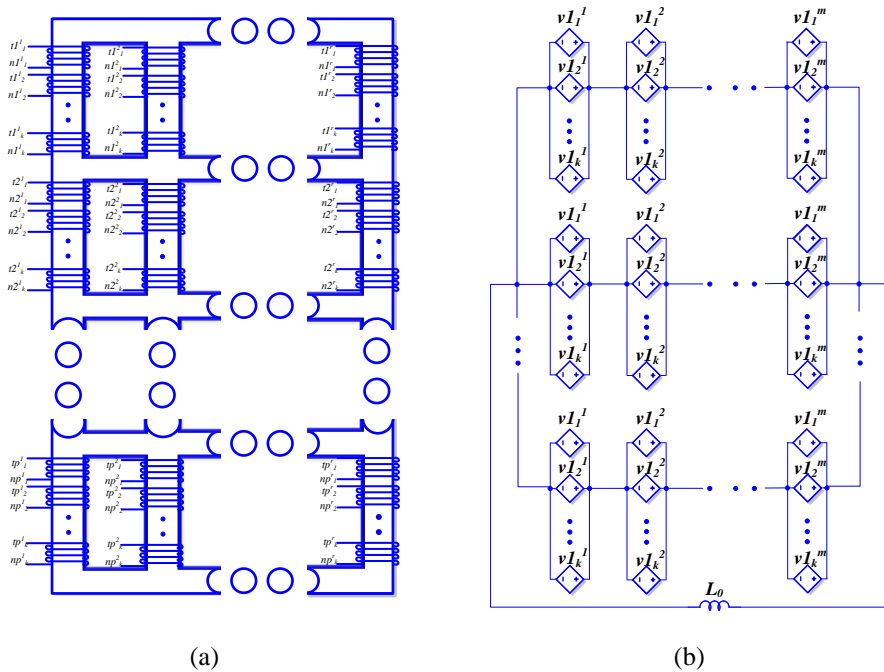
**Fig. 3.2.** Generalized layout of multi-phase multi-series/shunt auxiliary winding transformer. (a) Magnetic and winding layout and (b) Equivalent electric circuit.

The term $Np^r_k$ represents any winding in the configuration; these windings can take any winding architecture. Assuming that the transformer has no losses and if it is connected to

a balanced system, the equivalent electric circuit in Fig. 3.2(b) shows that the induced $F$ in a limb is equal to the sum of all MMFs induced by each winding in that limb. This is presented in equation (3.5). The overall total flux from all limbs in a phase would be zero (3.6). This shows the possibility of adjusting the voltage induced at any limb, by adjusting the adjacent limb flux through any of its windings. The MMF in all limbs are equal and can be expressed as in (3.7). Thus, the current in any winding on a limb can be adjusted by varying the MMF induced in that limb by other windings.

$$Fp^n = \sum_{x=1}^{x=k} Fp_x^n \qquad\qquad (3.5)$$

$$\sum_{x=1}^{x=n} \varphi p_k^x = 0 \qquad\qquad (3.6)$$

$$\sum_{x=1}^{x=n} Fp_x^1 = \sum_{x=1}^{x=n} Fp_x^2 = \cdots = \sum_{x=1}^{x=n} Fp_x^m \qquad\qquad (3.7)$$

In the conventional multi-transformer approach, the series and shunt compensators are connected to the grid by means of separated insolation transformers. The main characteristics and advantages of the proposed combined construction can be summarized as follows:

- It permits having fewer windings and smaller core size as compared with the conventional approach (in which each type of converter is connected through its own isolation transformer).

- It provides magnetic coupling of series and shunt converters' circuits to the primary and secondary winding of a transformer.

- It allows using a single transformer with controlled flux and reduced inrush currents, as the pre-energization of the transformer core is partially provided through the available converters.

- It eliminates the need of high-voltage or current handling windings (which are usually present on the primary side of series and shunt isolation transformers).

## 3.2    Proposed Configurations

In a distribution system, the single phase CPAT in Fig. 3.1(a) can be combined with a three-phase converter adopted from [97]. The aim is to meet UPQC application purposes, as shown in Fig. 3.3 [82]. The objectives of the shunt winding in the proposed UPQC are as follows:

- To achieve sinusoidal grid current

- To damp grid current during transients

- To compensate for reactive power requirements

- To maintain a constant DC bus voltage.

The series winding is required to achieve sinusoidal load voltage and to regulate the voltage magnitude at the load side.
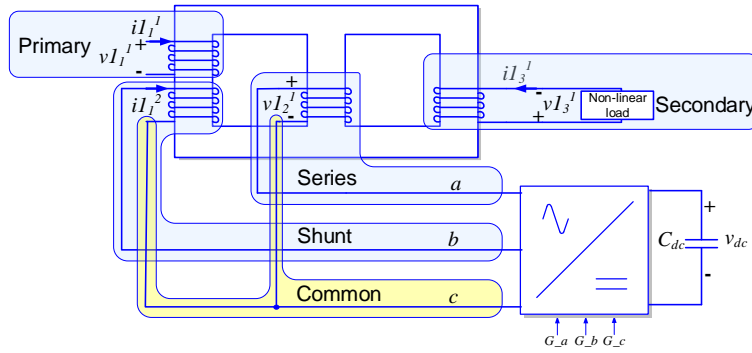


**Fig. 3.3.** Single-phase configuration of a CPAT for UPQC applications.

Taking these principles into account, the configuration in Fig. 3.4 represents a three-phase CPAT for transmission applications. As shown in the figure, the configuration consists of three single-phase CPATs equipped with a three-phase back-to-back converter. Each CPAT is labelled *CPAT$_p$*, where p represents the phase number. The winding voltages and currents of each CPAT are represented by $v_{pk}$ and $i_{pk}$, respectively where *k* represents the winding number. The primary and secondary windings of a CPAT (*k=1, k=4*) are connected to the grid as in a typical transformer. A three-phase back-to-back converter is connected to the shunt and series windings (*k=2, k=3*) to control the shunt winding current and series winding voltage. The shunt converter provides services to the primary winding such as harmonic elimination and reactive power compensation; it also regulates the DC bus voltage. Likewise, the series converter controls active and reactive power through the secondary winding to operate as a UPFC.
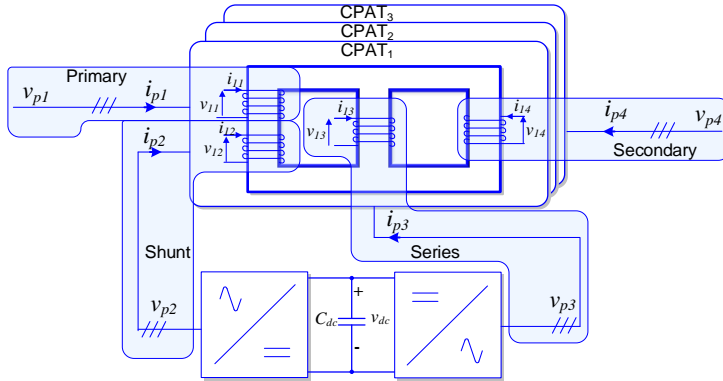
**Fig. 3.4.** Three single-phase CPAT configuration for UPFC applications.

To further integrate the configuration, the structure proposed in Fig. 3.5 stacks the three CPATs on top of each other in a three-phase shell-type monolithic structure. This integration of cores shares transformer yokes between each phase and reduces the setup footprint, tanks, bushings and protection equipment.
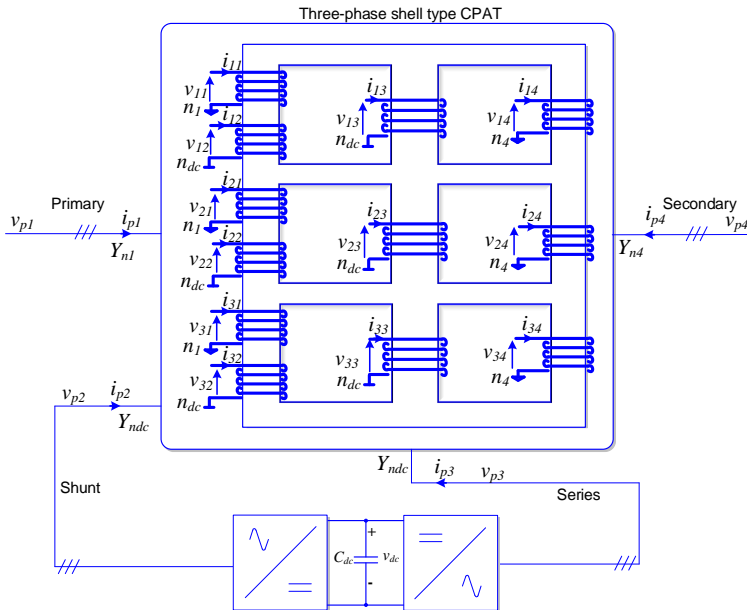


**Fig. 3.5.** Three-phase shell type CPAT for UPFC applications.

## 3.3    Single-phase Structure Analysis

The CPAT combines a shunt, a series and an isolation transformer into a single transformer. The main advantage of the CPAT over a conventional multi-transformer

solution lays mainly on the fact that permits to achieve overall reduction of core material, winding and manufacturing cost.

### 3.3.1 Core Material Reduction

The CPAT core-material saving was assessed by comparing the proposed solution with a conventional one. The comparison was based on three independent transformers, one devoted to voltage level transformation, another one for performing series compensation and the last one to conduct shunt compensation. In single-phase applications, the shell type construction shown in Fig. 3.6 is typically utilized. It consists of a type *c* limb, two type *a* limbs and four type *b* yokes. In a conventional compensation system, three shell type transformers would be necessary. One of them would be used as a power transformer; the other two would act as compensation transformers.
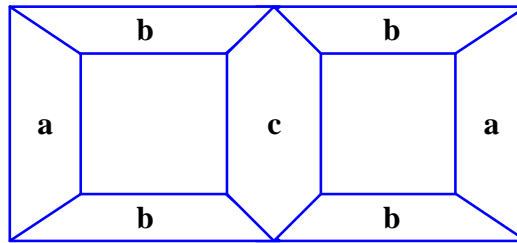


**Fig. 3.6.** Core structure of single-phase CPAT and single-phase shell type transformer.

In the power transformer, the type *c* limb would be larger than the other two limbs. The compensation transformer's size would depend on a core size reduction factor. In this assessment, the relationship between the core size of the power transformer ($Q_p$) and each compensation transformer ($Q_c$) is assumed to be linear for all the core elements as indicated in (3.8), where *m* is the core size reduction factor. The size of the type *c* limb is assumed to be twice the size of other limbs, due to its required power handling capability, whereas the type *a* limb and the type *b* yoke are roughly equal in size. Given these assumptions, the system's total core size ($Q_s$) can be calculated as in (3.9).

$$Q_c = mQ_p \tag{3.8}$$

$$Q_s = Q_p + 2Q_c = (8 + 16m)a \tag{3.9}$$

A single-phase CPAT having the configuration shown in Fig. 3.3, would entail equal sizes for the *a* limb and the *b* yokes. Both would larger than the *c* limb, as they handle more power. Moreover, the *c* limb is designed to have the same size as a series compensation transformer limb. Therefore, the total core size $Q_T$ of a CPAT can be calculated as presented in (3.10).

$$Q_T = 2a + 4b + ma = (6 + m)a \tag{3.10}$$

Due to the fact that the limb $a$ in (3.10) is a power-handling limb, its size would be twice than the one in (3.9). Taking this into account, equating (3.9) and (3.10), would reveal that at $m = 0.286$ the CPAT would require the same material size as in a conventional approach. Therefore, the CPAT would incur lower material costs if the compensation transformers are larger than 28.6% of the size of the power transformer.

### 3.3.2   Winding Reduction

Shunt and series compensation transformers in conventional applications consist of high-voltage and high-current windings at the grid side. However, the CPAT does not need such windings because the shunt and series compensation devices are directly coupled to the grid through the transformer core.

In a multi-transformer configuration, two windings per phase and per transformer are required. Hence, as each compensation connection requires two windings per phase, the total windings in a shunt-series compensation system with a power transformer would be $6p$, where $p$ is the number of phases. On the other hand, a CPAT consists of four windings per phase; hence, in a CPAT the number of windings with shunt-series compensation is $4p$.

### 3.3.3   Manufacturing Cost Reduction

Combining several transformers into a single transformer reduces the manufacturing costs related to tanks, bushings, and protection equipment, as well as the overall footprint. This is due to the fact that a solution based on several transformers would require an independent tank for each transformer, whereas the CPAT eliminates the cost of compensation transformers' tank and other auxiliary equipment.

### 3.3.4   Comparison

The most relevant device to incorporate both series and shunt control in a single magnetic element is shown in the ST presented in  [31]. Other approaches of magnetic integration have discussed either shunt or series integration independently. It is worth noting that the CPAT finds a perfect application in transmission systems, because the shunt and series windings allow the provision of series power flow regulation and shunt reactive power compensation, as in a typical three-phase UPFC application.

Comparing a three-phase CPAT, ST and a multi-transformer compensation configuration it is possible to conclude that, the major advantages that a CPAT over the other configurations would be the wide control bandwidth, linear response, increased number of integrated transformers, ability to provide reactive power, ability to operate for harmonics compensation and the need of a reduced number of windings.

Though the multi-transformer approach leads to a simple design, CPAT and ST yield better cost effectiveness and provide a more compact solution.

## 3.4 Three-phase Structure Analysis

### 3.4.1 Windings

Certain design aspects must be considered when selecting appropriate shunt and series converters for a CPAT. As discussed earlier, the CPAT reduces the number of windings required to implement a series-shunt compensation system. The preliminary design ratio values of the primary and secondary turns ($N_1$, $N_4$) are determined as in a typical transformer as a function of the required operating voltages, as shown in (3.11). With a pre-determined shunt converter voltage, the shunt winding turns ($N_2$) can be estimated using (3.11). In (3.12), the relationship should be maintained to determine the maximum primary, shunt, series and secondary winding current ($i_{1max}$, $i_{2max}$, $i_{3max}$, $i_{4max}$). With a pre-determined series converter current, the series winding turns ($N_3$) can be estimated using (3.12).

$$\frac{v_1}{N_1} = \frac{v_4}{N_4} = \frac{v_2}{N_2} \tag{3.11}$$

$$N_1 i_{1max} + N_2 i_{2max} = N_3 i_{3max} = N_4 i_{4max} \tag{3.12}$$

In a CPAT, the series voltage varies according to the design parameters as well as the voltage and the current across each winding. Using pre-determined design parameters, the equivalent magnetic circuit can be used to determine the resultant series voltage under various operating points for a selected number of turns. Neglecting the effect of core-reluctances and leakage reluctances, the maximum open-circuit voltage across the series winding can be expressed as follows:

$$v_{3max} = N_3 \left( \frac{v_1}{N_1} + \frac{v_4}{N_4} \right) = 2 v_1 \frac{N_3}{N_1} \tag{3.13}$$

### 3.4.2 Structures

A three-phase CPAT is comparable in structure to a three-phase series-shunt compensation system that consists of single-phase shell-type transformers and three-phase core-type transformers. Using the methodology discussed in the previous section to determine the core size reduction, three compensation scenarios were compared to a three-phase CPAT. The results of this comparison are tabulated in the following subsection.

In the first configuration, a three-phase CPAT was compared to a three-phase compensation system. The latter system consisted of three single-phase shell-type shunt transformers, series transformers and power transformers, with the power transformer situated between the compensation transformers (Fig. 3.7). Each transformer consisted of limb types $a_1$ and $c_1$ and yokes $b_1$. As in the single-phase methodology, it was assumed that limb type $a_1$ and yoke type $b_1$ were equal, whereas limb type $c_1$ was considered double the size of type $a_1$ due to its required power-handling capability. It was also assumed that the relationship between the core size of each power transformer and each compensation transformer was linear for all core elements.
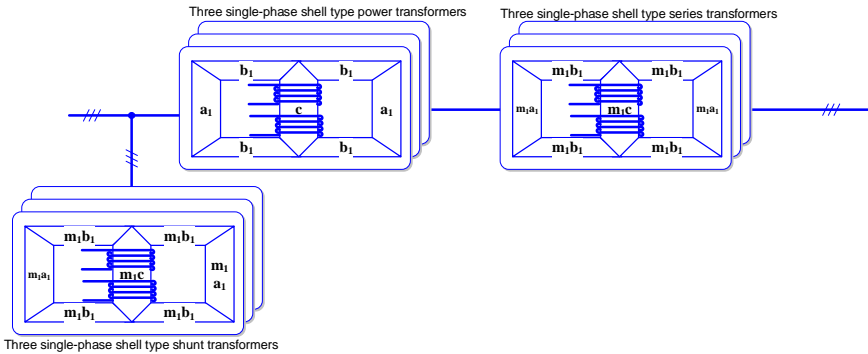
**Fig. 3.7.** Configuration of a three-phase compensation system using single-phase transformers.

The structure of a three-phase shell-type CPAT can be divided similarly into core limbs and yokes, as shown in Fig. 3.8. In a CPAT, limbs $a_2$ and yokes $b_2$ are considered equal, and double the size of a typical single-phase shell-type transformer ($a_2 = 2a_1$) due to their required power-handling capability. Series compensation limbs have the same core size as a typical compensation transformer with a core-size reduction factor $m_1$. Design of the common yokes between phases is based on the core material's capacity to operate without saturation. The common core factor $m_2$ would have a value between 1 and 2, which is equivalent to three single-phase CPATs stacked on top of each other ($m_2$=2) and three single-phase CPATs sharing a yoke that is equal in size to all other yokes ($m_2$=1).
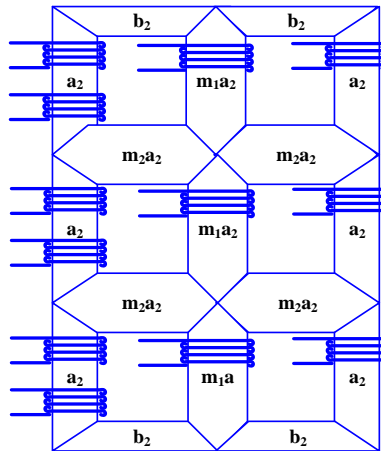


**Fig. 3.8.** Core limbs and yokes elements of a three-phase shell type CPAT.

In the second configuration, a three-phase CPAT is compared to a three-phase compensation system consisting of a three-phase shunt transformer, three-phase series transformer and three-single phase shell-type power transformers. The power transformer is situated between the two compensation transformers, as shown in Fig. 3.9. Since windings in a three-phase transformer are wound on each limb, each limb in a compensation transformer is assumed to be a factor of the power-handling limb $c_1$.
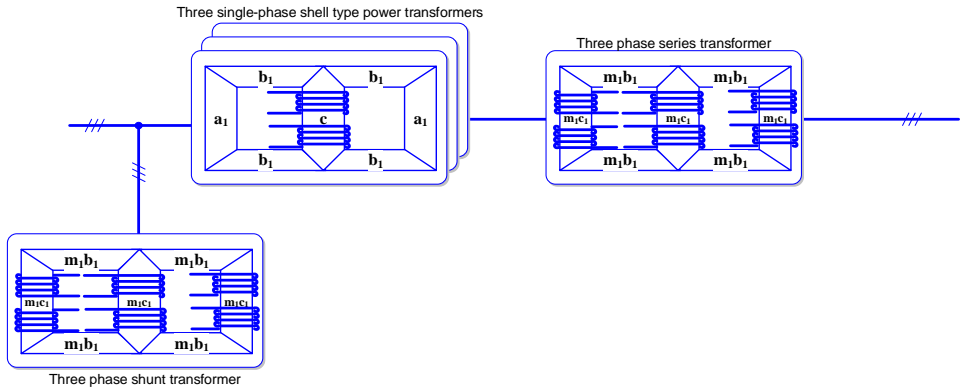
**Fig. 3.9.** Configuration of a three-phase compensation system using single-phase power transformers and three-phase compensation transformers.

In the final configuration, a three-phase CPAT is compared to three three-phase (Fig. 3.10). In this case, each limb in the power transformer is labelled $c_1$ since all limbs are equal and handle power delivery between primary and secondary limbs.
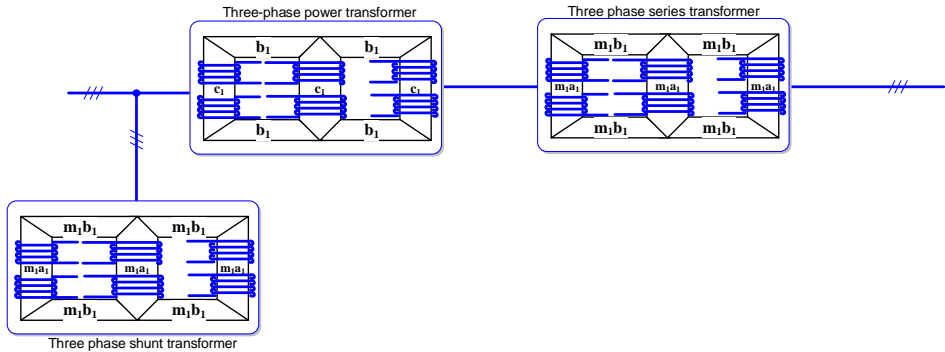


**Fig. 3.10.** Configuration of a three-phase compensation system using three-phase transformers.

### 3.4.3   Summary

Table 3.1 shows a summary of the comparisons for a three-phase CPAT, in terms of windings, tanks and core size reduction. A CPAT would reduce the number of windings required as compared to any other configuration. Regarding the number of tanks, the CPAT in Fig. 3.4 requires as many tanks as the typical three-phase compensation system shown in Fig. 3.10. However, the three-phase shell-type CPAT (Fig. 3.5) provides additional benefits in this case due to its monolithic structure. The core size of a three-phase CPAT, compared with the system shown in Fig. 3.10, is not beneficial, mainly due to the larger core yokes required for better coupling between primary and secondary limbs. However, if a CPAT is compared to the systems in Fig. 3.7 and Fig. 3.9, core-size reduction is possible under the constraints of $m_1$ and $m_2$.

**Table 3.1** Evaluation of CPAT vs. other transformer configurations.

| CPAT configuration | | Compensation configuration | | |
|---|---|---|---|---|
| | | **Fig. 3.7** | **Fig. 3.9** | **Fig. 3.10** |
| **Reduction in windings** | **Fig. 3.5** | Yes (33.3%) | | |
| | **Fig. 3.4** | | | |
| **Reduction in tanks** | **Fig. 3.5** | Yes (88.8%) | Yes (80%) | Yes (66%) |
| | **Fig. 3.4** | Yes (66.6%) | Yes (40%) | Equal |
| **Core size reduction** | **Fig. 3.5** ($m_2$=1) | Yes ($m_1$>9.5%) | Yes ($m_1$>28.6%) | No ($m_1$>128.5%) |
| | **Fig. 3.4** | Yes ($m_1$>28.6%) | Yes ($m_1$>85%) | No ($m_1$>185.7%) |

## 3.5    Modelling

### 3.5.1    Single-phase CPAT

If low-frequency responses are viewed as the main concern in FACTS applications, the conventional magnetic-circuit-based model can be adopted to obtain a topologically correct equivalent model. By discretizing the magnetic flux paths in the core (Fig. 3.1), an equivalent model (Fig. 3.11a) can be deduced. The layout in Fig. 3.11(a) shows $m$ number of limbs and $k$ winding types, with $k$=1 (primary), 2 (shunt), 3 (series), and 4 (secondary). The magnetic fluxes in this circuit are characterized as core linkage fluxes ($\Phi_{cm}$), winding fluxes ($\Phi_k$), leakage fluxes per winding ($\Phi_{Lk}$), and core leakage flux ($\Phi_0$). Core limbs and yokes are represented by non-linear reluctances $\Re_Y$ and $\Re_L$, with a value calculated based on the B-H characteristics of the core material. In addition, a non-linear reluctance is modelled as a controlled magneto-motive source in a closed-loop between input flux and output magneto-motive force ($F$), as shown in Fig. 3.11(b). This model would produce an opposing magneto-motive force based on the limb or yoke length ($l$), area ($A$) and the core B-H characteristics shown in Fig. 3.12.

Winding leakage reluctances ($\Re_k$) and core leakage reluctance ($\Re_0$) are represented by linear reluctances. Leakage reluctances are evaluated based on dimensions, as in (3.14), using the flux path length, mean area and relative permeability of air ($\mu_0$=4$\pi$10$^{-7}$). The flux generated by each winding is linked to a winding electric circuit, shown in Fig. 3.11(c), to model winding losses and core equivalent losses. For any applied winding voltage ($v_k$), the equivalent transformer winding current ($i_k$) depends on the winding resistance ($R_k$), equivalent core loss resistance ($R_c$) and the effective winding current ($i_{ek}$). The effective

current is calculated based on the effective magneto-motive force ($F_k$) of the winding and number of turns ($N_k$), as shown in Fig. 3.11(c). The winding flux in the magnetic circuit is deduced from the effective voltage ($v_{ek}$) in the winding electric circuit.

$$\Re_0, \Re_k = \frac{l}{4\pi 10^{-7} A} \tag{3.14}$$

To overcome algebraic loops due to the coupling between electric, magnetic and non-linear reluctance circuits, a one-simulation-step-time delay is applied. However, such an approach should be considered with a high sampling-rate to avoid numerical oscillations.



(a)

(b)



(c)
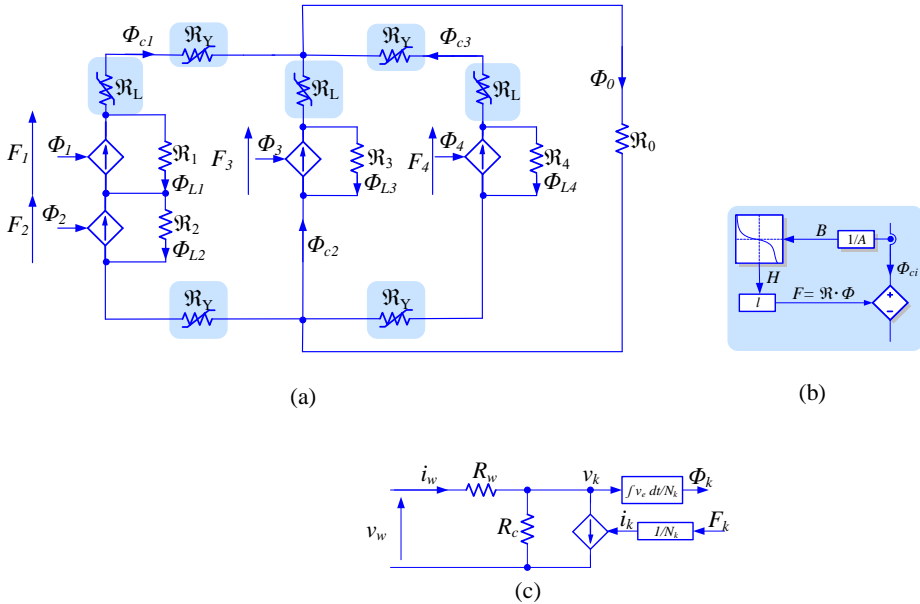
**Fig. 3.11.** Magnetic circuit model of a single-phase CPAT. (a) Core magnetic circuit, (b) non-linear reluctance model and (c) winding electric circuit model.
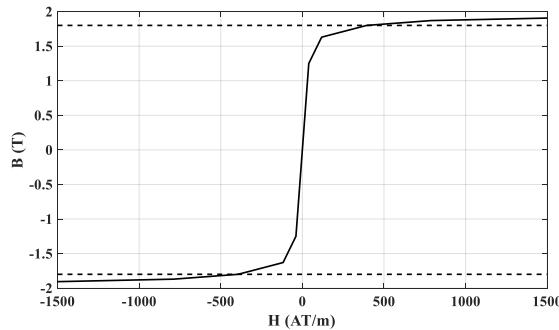


**Fig. 3.12.** BH characteristics of the core material with 1.8T nominal flux density at rated voltage.

A linear representation of the model can be derived through duality transformation of the magnetic circuit (Fig. 3.11a) to its equivalent electric circuit (Fig. 3.13). Non-linear core impedances are assumed to be constant and large enough to sustain perfect couplings between primary, shunt, series and secondary windings. Core magnetizing impedances and core loss resistances are represented by $L_{e1}$, $L_{e2}$ and $L_{e3}$ and $R_{e1}$, $R_{e2}$ and $R_{e3}$ respectively. In this model, the transformer leakage inductances and zero-sequence magnetizing inductance are represented by $L_k$ and $L_0$ respectively. The equivalent circuit (Fig. 3.13) is identical to the circuit of a three-phase transformer, apart from two windings on the centre and secondary limbs. The parameters of this circuit can be determined based on the typical transformer tests methodology [86] for low- and mid-frequency transient simulations. It is worth to mention that core impedances are typically large, due to the low equivalent core reluctance of each core limb and yoke. In turn, leakage impedances are significantly lower than core impedances. Therefore, in an ideal transformer scenario, the primary, shunt, series and secondary windings are perfectly coupled.
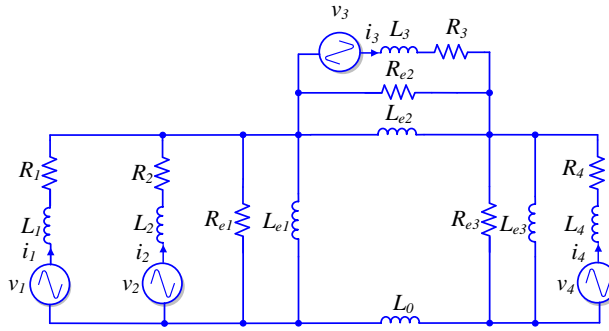


**Fig. 3.13.** Equivalent electric circuit of a single-phase CPAT.

### 3.5.2    Three-phase CPAT

In a three-phase system consisting of three single-phase CPATs, as shown in Fig. 3.4, the CPATs are not magnetically coupled to one another and the equivalent model would be a repetition of the single-phase model shown in Fig. 3.11. The three-phase shell-type CPAT shown in Fig. 3.5 stacks three single-phase CPATs on top of each other, such that each phase shares a common yoke with another phase. The equivalent magnetic circuit shown in Fig. 3.14 is represented by fluxes ($\Phi_{pk}$, $\Phi_{Lpk}$, $\Phi_{Ypm}$, $\Phi_{cpm}$), magnetomotive forces ($F_{pk}$), linear reluctances ($\Re_{pk}$, $\Re_0$), and non-linear reluctances ($\Re_{Y1}$, $\Re_{Y2}$); here, $p$ denotes the phase number, $k$ the winding number, and $m$ the limb or yoke number. According to this design, the common yokes ($\Re_{Y2}$) are initially assumed to be double the size of the outer yokes ($\Re_{Y1}$), such that the core structure is equal to three single-phase CPATs. The core flux paths are divided into common yoke fluxes ($\Phi_{Ypm}$) and limb fluxes ($\Phi_{cpm}$). The effect of the shared yokes can be better understood in the equivalent electric circuit (Fig. 3.15). In this figure, the shared yoke impedance can be observed between phase 1,2 ($R_{Y1}$, $L_{Y1}$, $R_{Y2}$, $L_{Y2}$) and between 2,3 ($R_{Y3}$, $L_{Y3}$, $R_{Y4}$, $L_{Y4}$). Each of the equivalent parameters $R_{e11}$, $L_{e11}$, $R_{e13}$, $L_{e13}$, $R_{e31}$, $L_{e31}$, $R_{e33}$ and $L_{e33}$ represent one limb and yoke. The parameters $R_{e12}$, $L_{e12}$, $R_{e22}$, $L_{e22}$, $R_{e32}$, $L_{e32}$, $R_{e21}$, $L_{e21}$, $R_{e23}$ and $L_{e23}$ each represent one limb.
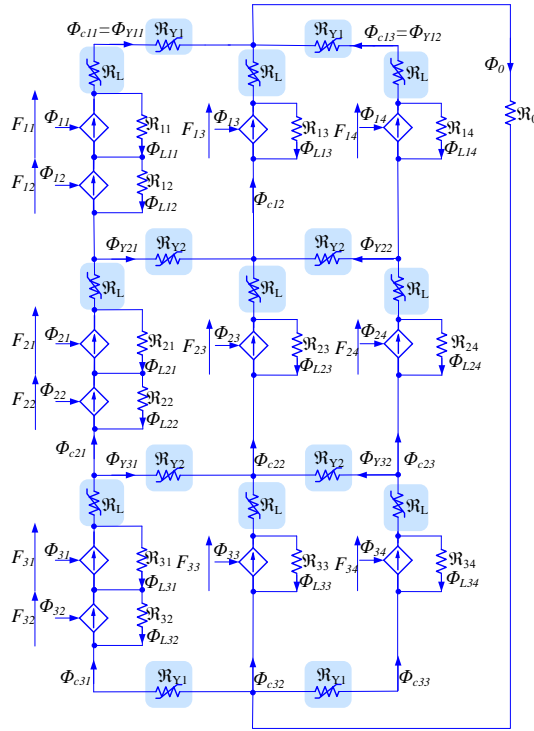
**Fig. 3.14.** Equivalent magnetic circuit of a three-phase shell type CPAT.
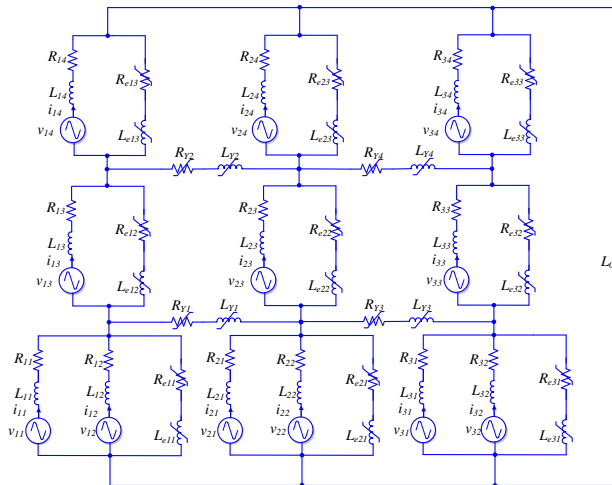


**Fig. 3.15.** Equivalent electric circuit of a three-phase shell type CPAT.

Due to the complexity of the circuits shown in Fig. 3.14 and Fig. 3.15, only the magnetic-circuit model is considered in this study. The circuits in Fig. 3.14 and Fig. 3.15 consists of 26 states, which is too complex to analyze. Therefore, this study presents analysis of the applicability and operational capability of the three-phase shell-type CPAT. Deep analysis of various operational states, transients and design considerations will be conducted in future research, as it will be discussed in Chapter 6.

## 3.6    Operation

As discussed in Section 3.2, the CPAT was investigated for its operation as an integrated single-phase UPQC and as an integrated three-phase UPFC. To assess these operations, the single-phase CPAT model shown in Fig. 3.11 was analysed to explore its ability to achieve harmonic compensation and power-flow control through shunt and series windings. Further analysis and confirmation through simulations and experimental prototypes are discussed in Chapters 4 and 5.

### 3.6.1    CPAT-UPQC

In the following analysis, the CPAT was viewed as if it was used in power quality enhancement for a distribution system application. Based on the electric circuit in Fig. 3.11(c), $F_k$ can be represented by (3.15) and limb fluxes $\Phi_{ck}$ are represented by (3.16). Both equations show that the winding voltage and the current affect both the flux and MMF. However, the effect depends on the design parameters for the core and windings. Considering that the winding voltage and current consist of $n$ harmonic components, as indicated in (3.17), the effects of windings on each other can be determined through basic magnetic-circuit analysis.

Using Ampere's law, the relationship between the primary limb MMF and the secondary limb MMF can be written as shown in (3.18). Assuming that the MMFs are mainly affected by currents, and these fluxes are mainly affected by voltages, the equations (3.18) shows that harmonics in the secondary current, primary voltage and secondary voltage yield to harmonics in the summation of the primary and shunt currents. Therefore, the shunt winding current can be properly regulated to make the primary grid current sinusoidal, independently of the harmonics in the secondary current or in the primary and secondary voltages. In this regard, the design of the magnetic circuit can include certain considerations to minimize the effect of the primary and secondary voltages in (3.18). Core reluctance can be minimized, and the equivalent core-loss resistance and winding leakage reluctance can be maximized.

$$F_e = N_k \left( i_k \left( 1 + \frac{R_k}{R_c} \right) - \frac{v_k}{R_c} \right) \tag{3.15}$$

$$\Phi_k = \frac{1}{N_k} \int (v_k - i_k R_k) dt - \frac{F_k}{\mathfrak{R}_k} \tag{3.16}$$

$$v_k, i_k = \sum_{h=1}^{h=n} I_h, V_h \sin(h\omega t + \theta_h) \tag{3.17}$$

$$F_1 + F_2 = F_4 + (\Phi_{c1} - \Phi_{c3})(\mathfrak{R}_L + 2\mathfrak{R}_Y) \tag{3.18}$$

Based on Gauss's law, the equation (3.19) is derived to show the effect of the central limb on the magnetic circuit. As noted from this equation, the summation of the primary and secondary fluxes in the transformer is influenced by the central limb flux and MMF. Therefore, the central limb flux can be properly regulated to induce those voltage components that could cancel out the effect of primary limb flux on the secondary limb flux. If this is successfully performed, it would be possible to achieve sinusoidal voltage waveforms at the secondary side, independently of the voltage distortion at the primary side. As (3.19) shows, the central limb magnetic performance depends directly on the value of the core leakage reluctance ($\mathfrak{R}_0$). Thus, a large core leakage reluctance would allow the central limb to provide the required compensation flux with minimal control limitations.

$$\Phi_{c1} + \Phi_{c2} + \Phi_{c3} = \Phi_0 = \frac{F_3 - \Phi_3 \mathfrak{R}_L}{\mathfrak{R}_0} \tag{3.19}$$

### 3.6.2 CPAT-UPFC

By analysing a single-phase CPAT in power-flow applications, the other phases can be considered as a repetition. In this analysis, it is assumed that the single-phase CPAT shown in Fig. 3.11 is connected to a stiff grid on primary and secondary windings; that is, $v_1$ and $v_4$ are constant. Hence, neglecting the effect of winding and core-loss resistance, $\Phi_1$ and $\Phi_4$ would also be constant. The values of $F_1$, $F_2$ and $F_4$ terms vary depending on the current in their respective windings. With a fixed flux through the core between the primary and secondary limbs, the flux $\Phi_3$ would be responsible for changing the magnetomotive force of the central limb. This produces changes in the primary and secondary magneto-motive forces. The following analysis clarifies this state of operation of a CPAT.

Using Gauss's and Ampere's laws, the relationship in (3.20) can be derived from the equivalent magnetic circuit shown in Fig. 3.11. Based on (3.20), the effective current in the secondary winding ($i_{e4}$) is coupled to the flux in the primary ($\Phi_1$), secondary ($\Phi_4$) and series ($\Phi_3$) windings, as well as the magnetomotive force in the primary ($F_1$) and series ($F_3$) windings. Assuming an ideal transformer, the effect of the core reluctances can be considered minimal, depending on the core material used and assuming that the core is working in the linear B-H region. Therefore, neglecting the effect of core reluctances, the magnetomotive forces would be equal, such that $F_1 + F_2 \approx F_3 \approx F_4$. Under this assumption, the current in the secondary winding ($i_4$) would depend on $\Phi_1$, $\Phi_2$, $\Phi_3$ and $F_2$, as shown in (3.21). Because $\Phi_1$ and $\Phi_4$ are constants, $i_4$ would be affected by $\Phi_3$ and $F_2$, which are equivalent to series winding voltage ($v_3$) and shunt winding current ($i_2$). In conclusion, the required $v_3$ to regulate $i_4$ depends mainly on the leakage reluctances.

$$F_4 = N_4 i_{e4} = \frac{\mathfrak{R}_4\big(\Phi_4(2\mathfrak{R}_Y\mathfrak{R}_0\mathfrak{R}_1\mathfrak{R}_3 + \mathfrak{R}_L\mathfrak{R}_0\mathfrak{R}_1\mathfrak{R}_3 + \mathfrak{R}_1\mathfrak{R}_3)\big)}{\mathfrak{R}_1\mathfrak{R}_3(2\mathfrak{R}_Y\mathfrak{R}_0 + \mathfrak{R}_L\mathfrak{R}_0 + \mathfrak{R}_0\mathfrak{R}_4 + 1)}$$
$$+ \frac{\mathfrak{R}_4(\Phi_1\mathfrak{R}_1\mathfrak{R}_3 - F_1\mathfrak{R}_3 + \Phi_3\mathfrak{R}_1\mathfrak{R}_3 - F_3\mathfrak{R}_1)}{\mathfrak{R}_1\mathfrak{R}_3(2\mathfrak{R}_Y\mathfrak{R}_0 + \mathfrak{R}_L\mathfrak{R}_0 + \mathfrak{R}_0\mathfrak{R}_4 + 1)} \tag{3.20}$$

$$F_4 \approx N_4 i_4 \approx \frac{\Phi_4 + \Phi_1 + \Phi_3 + \dfrac{F_2}{\mathfrak{R}_1}}{\mathfrak{R}_0 + \dfrac{1}{\mathfrak{R}_1} + \dfrac{1}{\mathfrak{R}_3} + \dfrac{1}{\mathfrak{R}_4}} \tag{3.21}$$

Similarly, the magnetomotive force in the primary winding ($F_1$) can be represented as in (3.22). Using the previous assumption, based on neglecting core reluctances, the equation results in the ideal transformer state where $F_1 + F_2 \approx F_4$. This entails that the current in the primary winding ($i_1$) depends on the current supplied through the shunt winding ($i_2$) as well as on the current in the secondary winding ($i_4$). Therefore, the shunt winding can provide harmonic and fundamental current components eliminating their requirement from the primary winding.

$$F_1 = N_1 i_{e1}$$
$$= \frac{(2\mathfrak{R}_Y + \mathfrak{R}_L)\mathfrak{R}_1\mathfrak{R}_4(\Phi_1 - \Phi_4) - F_2\mathfrak{R}_1\mathfrak{R}_4 + F_4\big(\mathfrak{R}_1\mathfrak{R}_4 - \mathfrak{R}_1(2\mathfrak{R}_Y + \mathfrak{R}_L)\big)}{\mathfrak{R}_1\mathfrak{R}_4 + \mathfrak{R}_4(2\mathfrak{R}_Y + \mathfrak{R}_L)} \tag{3.22}$$

# Single-Phase CPAT-UPQC

*I*n this chapter, a UPQC application, based on using a CPAT, is investigated *considering scenario where the grid voltage is distorted and non-linear loads are connected. In this case, currents and voltages in the auxiliary windings are actively controlled through power converters, although they could also be drawn using another active or passive technique. In this chapter, it will be shown that it is possible to regulate the magnetic fluxes and magnetomotive forces in the transformer core, by regulating currents and voltages in the auxiliary windings. This feature permits controlling the current and voltage in the primary and secondary windings, respectively.*

## 4.1    Configuration

The use of CPAT in a single-phase UPQC application (CPAT-UPQC) results in the configuration shown in the previous Chapter 3, to be more precise in Fig. 3.3. This configuration can be implemented using a three-phase converter and a filter, as shown in Fig. 4.1. The objective of the presented UPQC is to maintain a sinusoidal voltage waveform at the load side when a distorted source voltage is supplied. Another objective is to achieve a sinusoidal current waveform at the source side, with a unity power factor, when a non-linear load is connected at the secondary side.

As Fig. 4.1 shows, the leg *a* of the converter is connected to the series compensation winding through an LC filter. This leg will be responsible of controlling the voltage across the capacitor in order to provide the necessary series compensation to achieve a sinusoidal voltage at the secondary side of the transformer. On the other hand, the leg *b* of the converter is connected to the shunt compensation winding through an LCL filter. This leg controls the filter output current to provide shunt compensation and hence to achieve sinusoidal currents at the primary side of the transformer. The design of the series filter inductor ($L_a$), the shunt filter inductors ($L_{b1}$ and $L_{b2}$), the series capacitor ($C_a$) and the shunt capacitor ($C_b$) are all

based on the required control bandwidth and the switching frequency of the converter. Passive damping of the LC and LCL resonance is achieved by means of using the damping resistors $R_{ca}$ and $R_{cb}$. Finally, leg $c$ of the converter act as the current return leg for both, shunt and the series windings. Having this common leg for both compensation outputs presents some control challenges, due to the coupling between the legs. Considering the strategies proposed in the literature, this study uses a strategy based on 3-leg UPQC SVM due to its simplicity and effectiveness [97]. The gate signals $G\_a$, $G\_b$ and $G\_c$ depicted in Fig. 4.1, are used to control the converter switches.
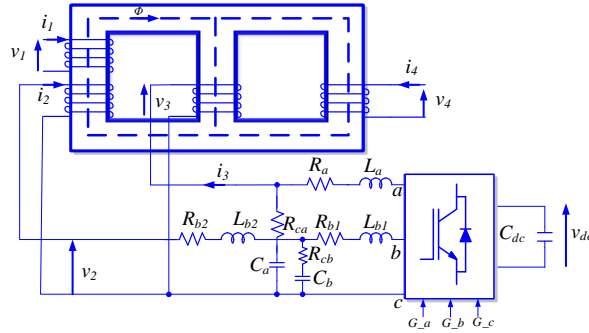


**Fig. 4.1.** Configuration of a CPAT-UPQC.

According to (3.15), if a sinusoidal grid voltage is connected to the primary winding and a non-linear load is connected to the secondary winding, the primary limb MMF ($F_1+F_2$) will consist of the same harmonics as $F_3$. Further harmonics will be induced due to the non-linearity of the core reluctance. The injection of a shunt compensation current ($i_{sh}$) permits adjusting the required MMF from the primary winding, with the primary current ($i_{prim}$) being conditioned accordingly. Moreover, $i_{sh}$ will have a component at the fundamental frequency to control the DC bus voltage ($v_{dc}$) and to compensate the reactive power required by the primary winding. The harmonic content in the grid and load voltage will increase the harmonics level in $F_1 + F_2$ due to the effect of $\Phi_1$ and $\Phi_4$, as stated in (3.16).

According to (3.18), if the core leakage flux is set to the minimum, thanks to an optimal design, the secondary flux ($\Phi_4$) can regulated if the series flux ($\Phi_3$) is be properly controlled– that is, controlling the central limb winding voltage ($v_{ser}$). Therefore, as $v_{prim}$ consists of harmonic components, they can be cancelled out in the secondary winding voltage by injecting specific harmonic voltages through the central limb. The magnitude of the fundamental frequency of $v_{sec}$ can be controlled by adding a fundamental-frequency voltage component to the series winding voltage. This will permit also compensating voltage swells and sags.

The non-linear reluctances of the core vary according to the hysteresis-loop characteristics of the core material. The non-linearity shown in Fig. 3.12, based on magnetic field intensity ($H$) and magnetic field density ($B$), can be classified into a saturation region and a nonlinear region. When a CPAT is used as a regular transformer, with shunt and series winding controllers disabled, the CPAT operates as a typical single-phase core-type

transformer. As the flux in the core due to the primary winding voltage is constant, the generated MMF will reflect the magnetizing current harmonics. In this case, the core non-linearity will draw current harmonics in the primary current due to the change in reluctance during each cycle, as shown in Fig. 4.2. Although the magnitude of such distorted magnetizing currents is insignificant at nominal operating conditions, a shunt winding controller can be tuned to compensate for the MMF originating from the currents. This would cancel their effect on the primary current. Moreover, if the CPAT reaches the saturation region – for example, during the transformer connection (which may result in known inrush currents), the shunt winding MMF can be controlled to compensate the inrush current components. This feature reduces the impact of such transient currents on the grid. Thus, the effect of non-linear core reluctances can be handled by means performing an appropriate control of CPAT auxiliary windings.
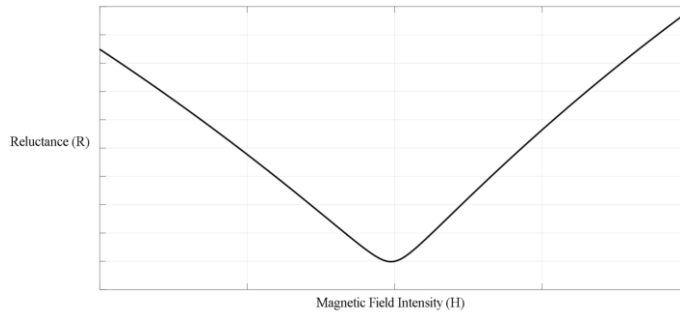


**Fig. 4.2.** Non-linear characteristics of core-reluctance.

## 4.2    Control

The control architecture is presented in Fig. 4.3 and Fig. 4.4 As it can be seen in these figures, it consists of two controllers, namely the shunt and series compensation controllers. The series compensation controller (Fig. 4.3) consists of two parts; the magnitude of the secondary voltage $V_{sec}$ is kept constant at the reference value $V_{sec}^*$ by a PI controller. The resulting command voltage is multiplied by the secondary voltage-synchronizing signal $sin(\omega t)_{sec}$ , giving rise, as a result, an in-phase compensation of the secondary voltage magnitude. The secondary voltage harmonics by a cascaded block of resonant (R) controllers, each tuned at one required compensating frequency $n\omega$, where $n$ represents the harmonic order. In this case, in order to cancel them all the secondary voltage harmonics references $v_{sec\_h}^*$ are set to zero. Therefore, each controller generates a command voltage at a selected frequency, which would attenuate the error The R controllers are implemented as their high gains at selected frequencies and the lack of phase shift or gain at other frequencies are advantageous features in this case [97].

The resulting sum of command voltages from the PI and R controllers yields the required injected voltage $v_{ser}$. This term represents the output voltage from leg $a$ with respect to leg $c$ in the single-phase set-up shown in Fig. 4.1.
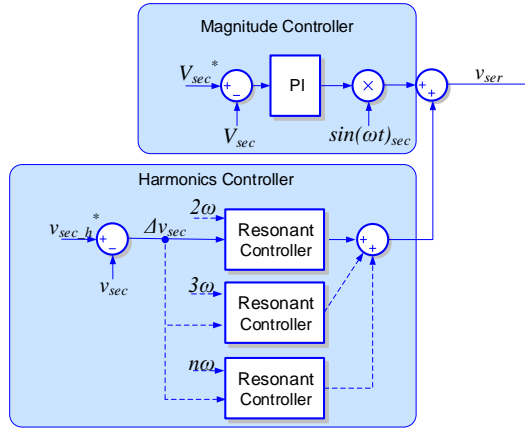
**Fig. 4.3.** Series compensation control loop of single-phase CPAT-UPQC.
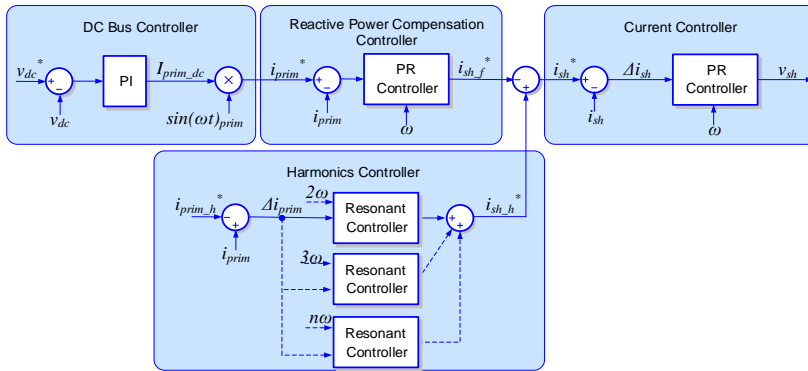


**Fig. 4.4.** Shunt compensation control loop for single-phase CPAT-UPQC.

The shunt compensation controller in Fig. 4.4 consists of four blocks. Two controllers regulate the fundamental component of the primary current. The third one is used for compensating harmonic components, meanwhile the last one is a shunt-winding current controller that achieves the required reference current from the previous controllers. The DC bus voltage controller maintains a constant reference voltage $v_{dc}^*$ across the converter capacitor, absorbing active power from the primary winding of the transformer. The PI controller placed at the beginning of the chain determines the required capacitor charging current, $I_{prim\_dc}$. The $I_{prim\_dc}$ is synchronized with the fundamental primary voltage $sin(\omega t)_{prim}$ to acquire the reference primary current $i_{prim}^*$. The error that results from subtracting the measured primary current $i_{prim}$ from the reference value, $i_{prim}^*$, constitutes the input of a proportional resonant (PR) controller, tuned at the fundamental frequency, which provides the required fundamental shunt compensation current $i_{sh\_f}^*$. The reference current keeps a constant DC bus voltage and zero-reactive power from the primary winding, damping also the primary current during transients. The primary harmonic currents are compensated through R controllers with a reference $i_{prim\_h}^*$ which is set to zero. This yields the required

shunt compensation harmonic currents, $i_{sh\_h}{}^*$. The overall compensation current $i_{sh}{}^*$ is controlled through a PR controller to obtain the required converter shunt output voltage, $v_{sh}$.

Primary frequency ($\omega$), synchronizing signal ($sin(\omega t)_{prim}$), secondary voltage magnitude ($V_{sec}$), and secondary voltage synchronizing signal ($sin(\omega t)_{sec}$) are all obtained through a DSOGI-FLL.

## 4.3    Simulation Results

The configuration shown in Fig. 4.1, with the parameters shown in Table 4.1, was simulated to examine the operation of CPAT under various scenarios. To investigate the effectiveness of series harmonic compensation, the primary voltage was generated through a combination of harmonic components 3, 5, 7 and 9, with proportions of 25%, 12.5%, 6.25% and 3.13% of the fundamental component, respectively. The Shunt harmonics compensation was investigated by connecting a non-linear load (shown in Fig. 4.5) at the terminals of the secondary winding. This allowed the withdrawal of non-linear, active and reactive currents in the harmonic spectrum, consisting of $3^{rd}$, $5^{th}$, $7^{th}$ and $9^{th}$ fundamental components having the proportions of 23%, 6.34%, 1.56% and 0.85% respectively. The secondary voltage-magnitude control was tested by applying voltage disruption during operation. Finally, the primary current transient damping was investigated by suddenly applying a voltage to the primary winding to observe the inrush current effect, with and without compensation.

**Table 4.1.** Simulation Parameters.

| Parameter | Value |
|---|---|
| Simulation step time | 1μsec |
| Transformer rated power | 50kW |
| Turns ratio | 1:1 |
| Average length of core limbs | 0.45 m |
| Average length of yoke sections | 0.2 m |
| Core area | 0.012 m$^2$ |
| System voltage | 220 V |
| Converter rated power | 5 kW |
| Switching frequency | 10 kHz |
| Dead band | 3μsec |

| $R_a, L_a$ | 15 mΩ, 1.5 mH |
|------------|---------------|
| $R_{ca}, C_a$ | 2 Ω, 40 µF |
| $R_{b1}, L_{b1}$ | 60 mΩ, 6 mH |
| $R_{b2}, L_{b2}$ | 20 mΩ, 2 mH |
| $R_{cb}, C_b$ | 4.7 Ω, 5 µF |
| $C_{dc}$ | 5 mF |
| $R_{sec}, L_{sec}$ | 1 Ω, 100mH |
| $R_{sec\_l}, L_{sec\_l}$ | 3 Ω, 3.5mH |
| $R_l, C_{sec\_l}$ | 5 Ω, 1.1 µF |



**Fig. 4.5.** Non-linear load connected at the secondary winding.

### 4.3.1   Harmonics Compensation, Voltage Regulation and Reactive Power Compensation

During a primary voltage sag of 50%, illustrated in Fig. 4.6, the secondary voltage magnitude controller increases the fundamental frequency component of the injected series voltage ($v_{ser}$) to compensate for this drop. The secondary voltage harmonic content changes as the transformer is loaded. This is typically due to the inductive action of the transformer under load acting as a filter to reduce the harmonic contents of the secondary voltage. However, this process yields a voltage drop in the load voltage, and the presence of a magnitude controller is essential. Through the transformer's design, such a drop can be minimized by considering low core-leakage impedance, which yields a higher reluctance path of yokes and end limbs.
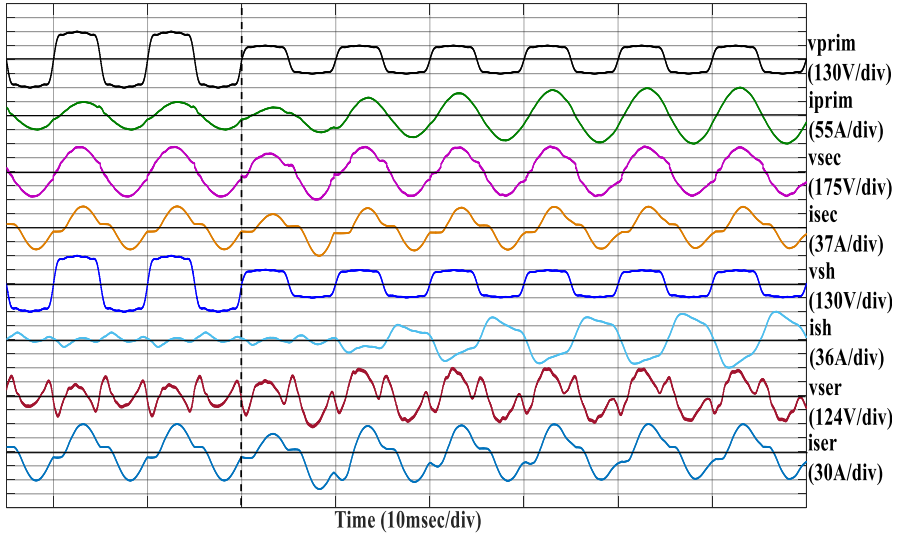
**Fig. 4.6.** Voltage and current waveforms during 50% primary voltage sag.

The effect of the sag on the power exchanged between the converter and the grid is shown in Fig. 4.7 and Fig. 4.8. The shunt leg of the converter absorbs more active power to supply the series leg to supply the difference in voltage.
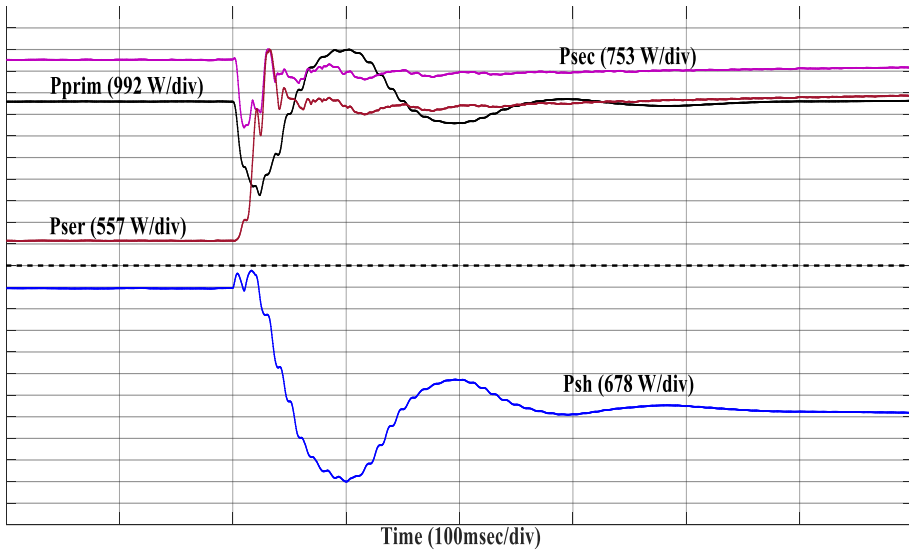


**Fig. 4.7.** Active Power variation during a 50% primary voltage sag.
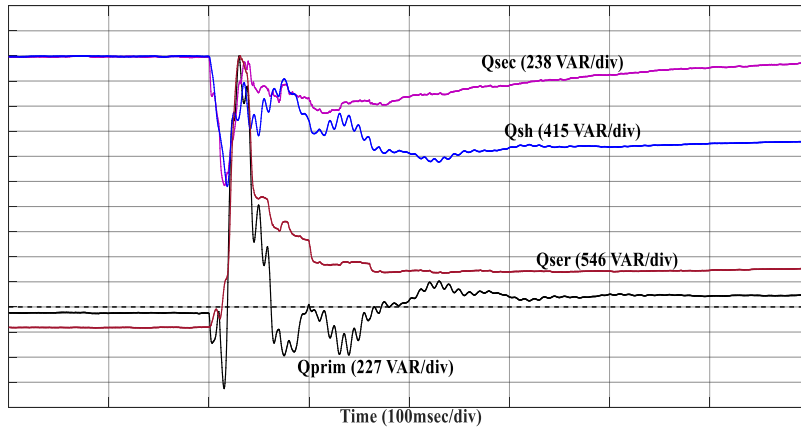
**Fig. 4.8.** Reactive Power variation during a 50% primary voltage sag.

This pattern can also be observed in the DC bus voltage and current (Fig. 4.9). As the series leg demands more power, the DC bus voltage decreases until the shunt controller provides sufficient power to the DC bus.
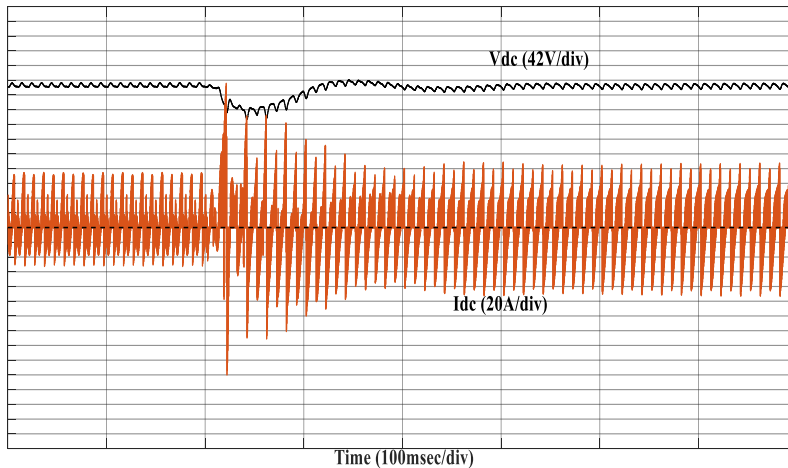


**Fig. 4.9.** Converter DC voltage and current during 50% primary voltage sag.

Enabling the shunt harmonics controller results in the injected current, shown in Fig. 4.10, which includes harmonic components required by the load. The series harmonics controller injects harmonic voltages into the series winding, as illustrated inFig. 4.11, to attenuate the secondary voltage harmonics.
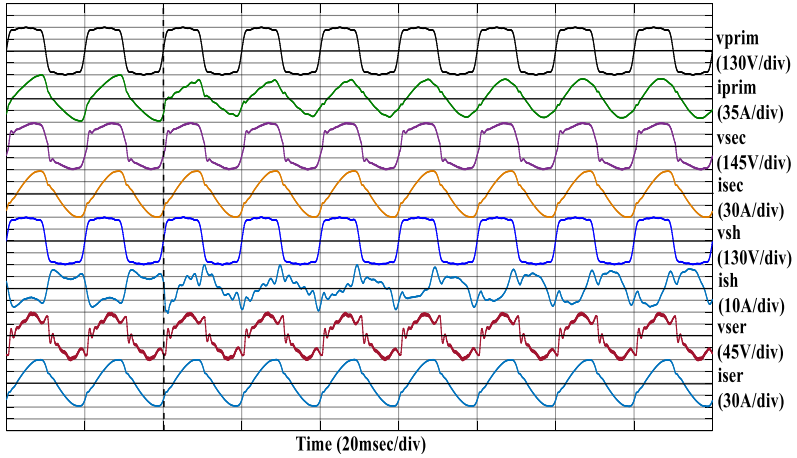
**Fig. 4.10.** Voltage and current waveforms with shunt harmonics compensation.
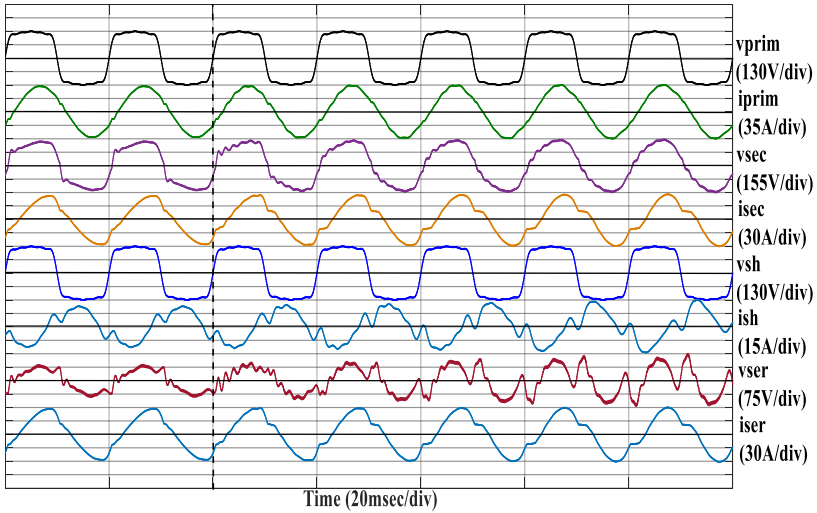


**Fig. 4.11.** Voltage and current waveforms with series harmonic compensation.

The resulting harmonic components present in the primary current (Fig. 4.12 (a)) are significantly reduced relative to the secondary current (Fig. 4.12 (b)). Moreover, the effect of the series winding harmonics compensation controller is evident in the secondary voltage, shown in Fig. 4.13(b), relative to the primary voltage harmonics (Fig. 4.13 (a)).

(a)                                                                    (b)
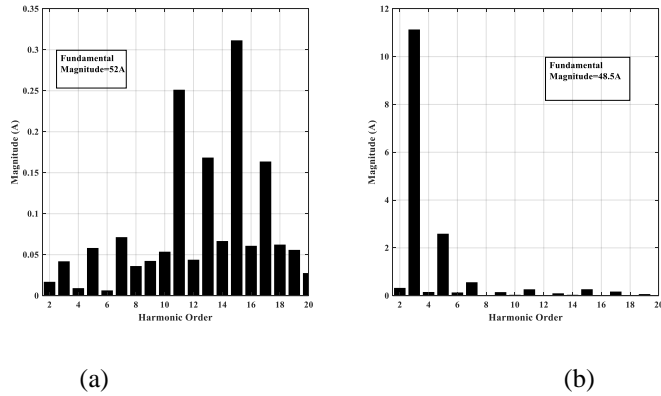
**Fig. 4.12.** Harmonic spectrum of (a)primary current and (b) secondary current.



(a)                                                                    (b)
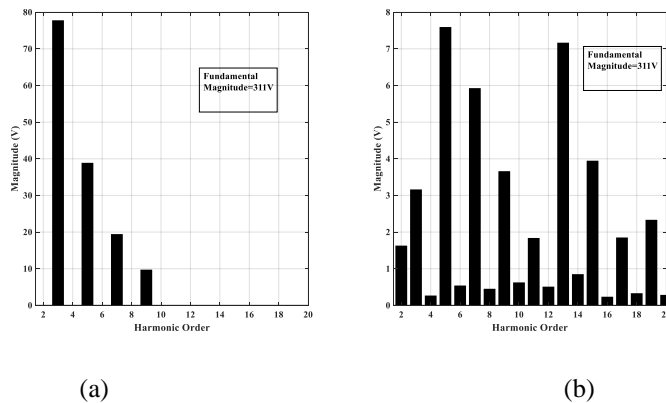
**Fig. 4.13.** Harmonic spectrum of (a) primary voltage and (b) secondary voltage.

The magnitude of the current components injected through the shunt converter (Fig. 4.14(b)) are larger than the required components in the secondary current (Fig. 4.12(b)). This difference arises because the shunt converter also compensates for magnetizing current harmonics required by the transformer.

The series harmonics compensator compensates not only for harmonic voltages present in the primary, but also for harmonic voltages induced by the non-linear current being absorbed by the load and passing through the transformer equivalent reluctance, as demonstrated in (3.19). This process can be observed through the series injected voltage spectrum in Fig. 4.14(a) compared to Fig. 4.13(a). Moreover, controller parameters and filters affect the bandwidth for which compensation is possible, and the inverter output voltage and current harmonics also affect the resulting compensation. The series current spectrum shown in Fig. 4.15(a) is identical to that of the secondary current in Fig. 4.12(b), since both circuits are constructed in series.

(a)                                    (b)
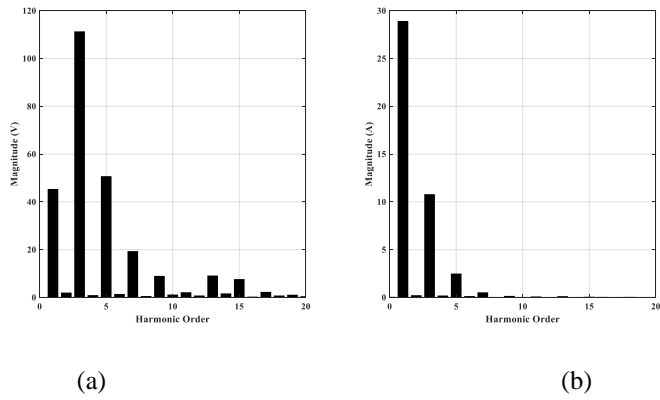
**Fig. 4.14.** Harmonic spectrum of (a)series voltage and (b) shunt current.



(a)                                    (b)
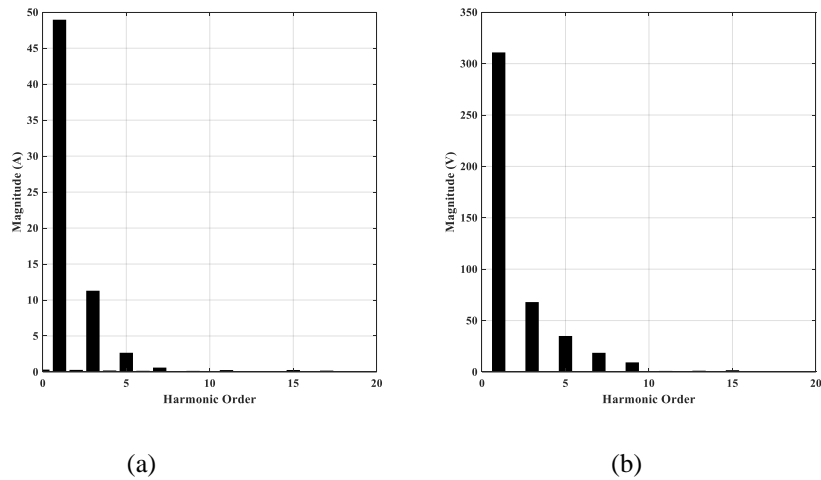
**Fig. 4.15.** Harmonic spectrum of (a)series current and (b) shunt voltage.

To enable the reactive power compensator, a shunt reactive current was injected into the transformer to eliminate the requirement of reactive power from the primary side (Fig. 4.16). The reactive power required by the transformer depends on the transformer's design and equivalent impedance.
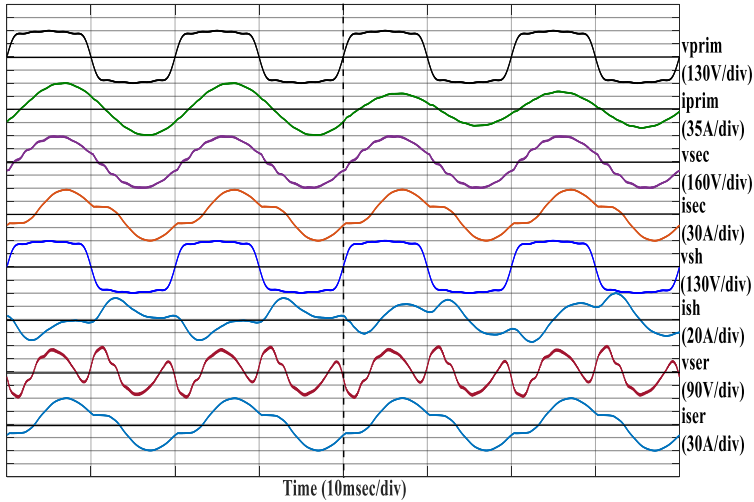
**Fig. 4.16.** Voltage and current waveforms with reactive power compensation.

### 4.3.2    Inrush Current Mitigation

The reactive power compensation controller presented in Fig. 4.4 can achieve damping of the primary current during transients. Therefore, during transformer excitation, the required inrush current can be supplied through the shunt winding to the transformer, thus reducing its impact on the source grid. The inrush current through the transformer when the rated primary voltage was applied with no load is shown in Fig. 4.17. The magnitude, harmonics and decay time of the primary current indicate the substantial impact of the inrush current on the grid.
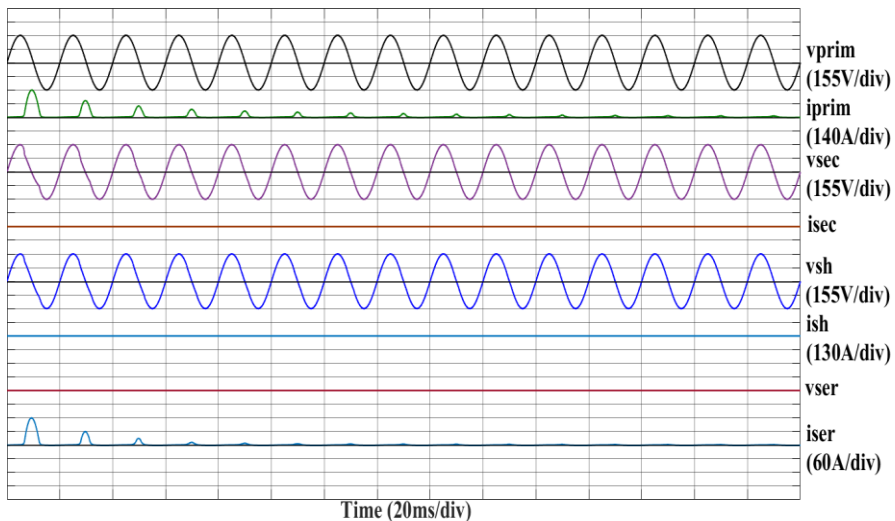


**Fig. 4.17.** Voltage and current waveforms during inrush transient without compensation.

Enabling shunt compensation controllers would dampen the primary current magnitude during such transients. This is achieved through the reactive power compensation controller, which acts directly on the primary current magnitude at fundamental frequency. The reference primary current at start-up is zero, as the DC bus is fully charged and thus the reactive power compensation controller would maintain zero primary current at energization. Moreover, primary current harmonics are mitigated through the primary current harmonics controller. This is shown in Fig. 4.18, where the primary current magnitude and harmonics are significantly minimized. However, the transformer still absorbs the same inrush current to energize through the primary and shunt windings.
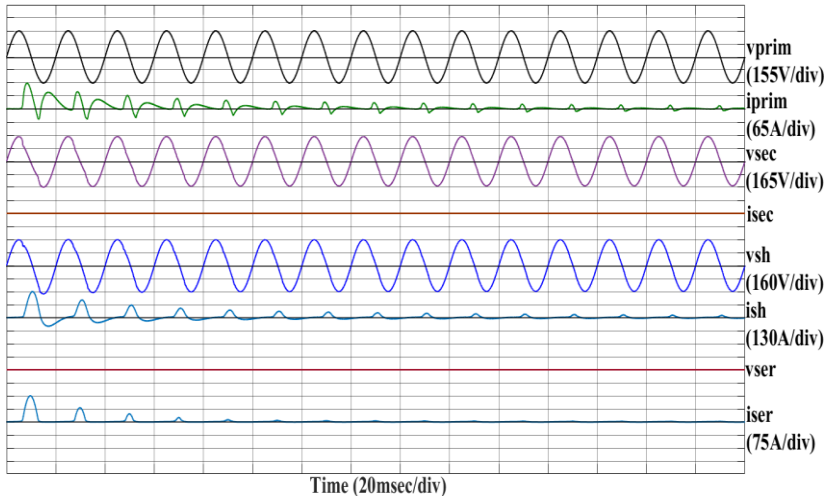


**Fig. 4.18.** Voltage and current waveforms during inrush transient with compensation.

Due to the strong current passing through shunt winding in this compensation strategy, the simulation presented here is based on operating the converter at extreme conditions. That is, the current and applied voltage to the filter operate above the nominally rated values and below the absolute maximum values. Moreover, the series winding may be shorted at start-up, to avoid connection of the filter circuit to the series winding acting as a load. During this operation, DC bus control is disabled to avoid absorbing charging current at start-up through the shunt winding yielding a higher inrush current. Thus, this operation requires a pre-charged DC bus, which discharges during the inrush mitigation, as shown in Fig. 4.19 and Fig. 4.20. Another issue that is not addressed in the presented controller is the decaying DC-offset (Fig. 4.17 and Fig. 4.18), as the inrush current tends to a steady-state.
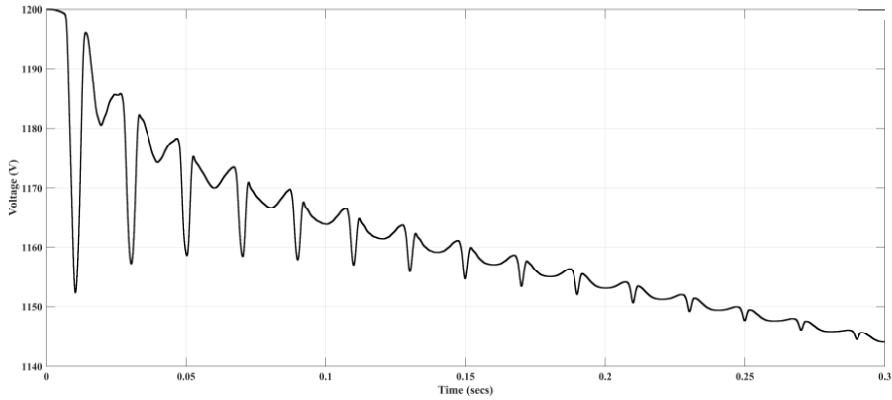
**Fig. 4.19.** DC bus voltage during inrush mitigation operation.
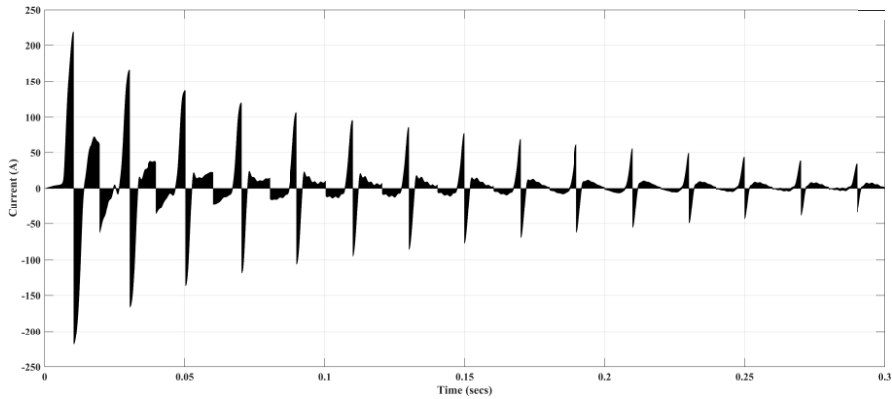


**Fig. 4.20.** DC current during inrush mitigation operation.

A harmonic analysis of the inrush current is shown in Fig. 4.21. This diagram illustrates the capacity of the shunt controller to mitigate fundamental and harmonic components throughout the inrush current cycles. In turn, this mitigates the peak current required from the grid during each cycle, as shown in Fig. 4.22. The performance of this mitigation relies on the controller and converter bandwidth. The average over 15 cycles showed a 51.5% reduction in the inrush current peak magnitude with the utilized set-up.
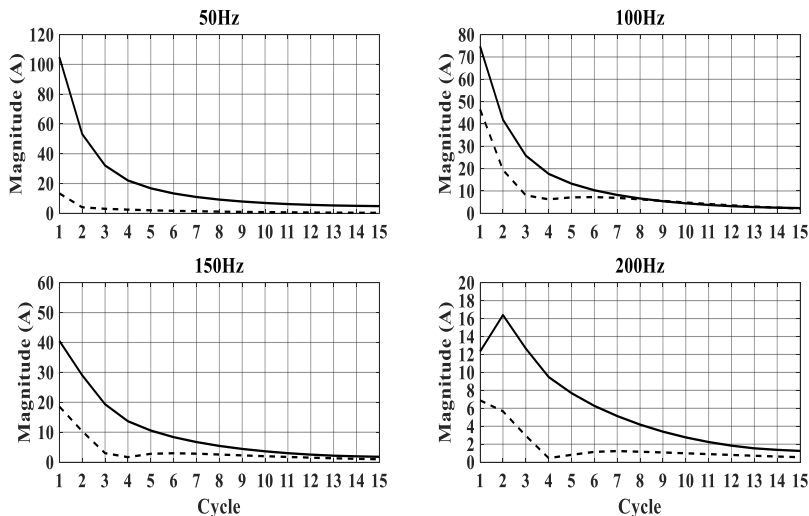
**Fig. 4.21.** Harmonic components of primary current during inrush transient without compensation (solid line) and with compensation (dashed line).
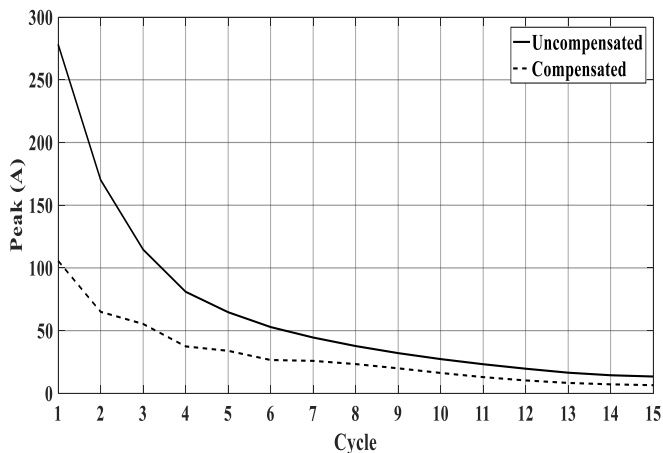


**Fig. 4.22.** Peak magnitude of primary current during inrush transient.

## 4.4   Experimental Results

The hardware set-up illustrated in Fig. 4.23 was implemented as shown in Fig. 4.24. The model consisted of a 50-kW three-phase core-type transformer, of which four windings were used for primary, secondary, shunt compensation and series compensation. Primary voltage and compensating voltages were provided through a 21-kW (7 kW/phase) three-

phase power amplifier, to examine the effect of injecting voltage into the series and shunt winding. The three phases of the amplifier *U*, *V* and *W* were used.

Phase *U* emulates primary voltage through the reference $v_{prim}^{\phantom{prim}*}$, phase *V* injects a controlled shunt compensating current through the reference $v_{sh}^{\phantom{sh}*}$, and phase *W* applies series compensating voltage through the reference $v_{ser}^{\phantom{ser}*}$. The $v_{prim}^{\phantom{prim}*}$ is generated by OPAL-RT independently of the control algorithm, with a defined harmonic spectrum. Control of the amplifier is achieved through an OPAL-RT real-time simulator, which includes the entire control structure for shunt and series compensation (Fig. 4.3 and Fig. 4.4). The controller emulates the DC bus voltage by measuring the output current from the amplifier phases *iV* and *iW*, which represent shunt and series compensation currents respectively. Data points of the results waveform have been captured for plotting and analysis.
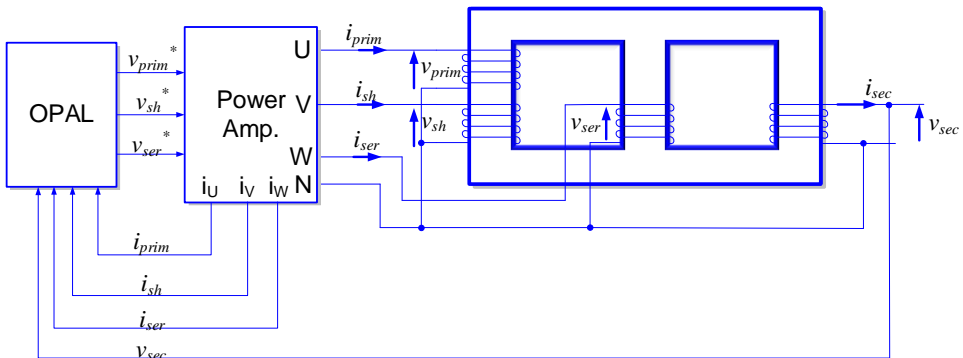


**Fig. 4.23.** Single-phase CPAT-UPQC experimental set-up diagram.
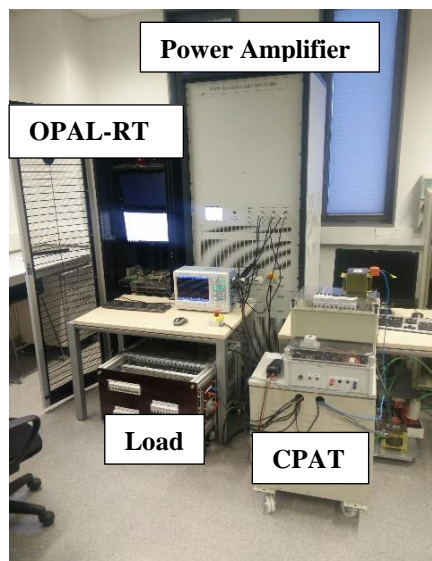


**Fig. 4.24.** Single-phase CPAT-UPQC experimental set-up layout.

### 4.4.1 Harmonics Compensation, Voltage Regulation and Reactive Power Compensation

To investigate the effectiveness of the series compensation controller, a sustained 30% voltage sag was applied to the primary winding, as shown in Fig. 4.25, at the instant indicated by the vertical line. With a reference of 195 V, the series controller was observed injecting an increased fundamental component to compensate for the voltage sag. The resulting voltage recovery during the sag was similar to the typical response of a dynamic voltage regulator.
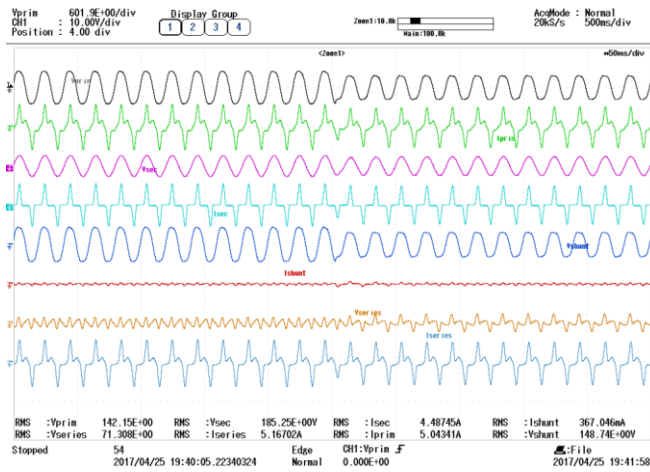


(a)
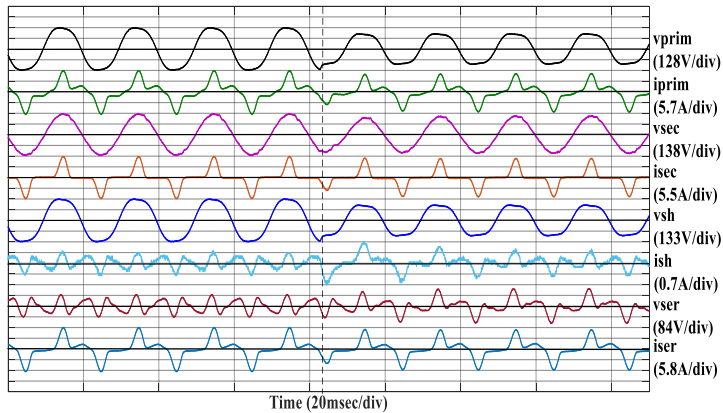


(b)

**Fig. 4.25.** Experimental waveforms during a 30% voltage sag (a) scope capture and (b) replot with scales.

Harmonic compensation was performed with a non-linear load connected at 200 V (operating voltage). The series harmonic compensation controller's performance is shown in Fig. 4.26 and was enabled at the instant indicated by the vertical line. Fig. 4.26 illustrates the transformation of the secondary voltage from a harmonic-rich voltage to a sinusoidal voltage. As mentioned earlier, harmonic components present in the secondary voltage arise from primary voltage harmonics and load current harmonics. Fig. 4.27 illustrates the moment when a sinusoidal voltage was applied to the primary, while the harmonics controller of the series winding was disabled and shunt winding was enabled. Enabling the shunt harmonics controller at the instant indicated by the vertical line resulted in attenuation of the primary current harmonics. However, secondary voltage consisted of harmonic components induced by the secondary current as in (3.18).
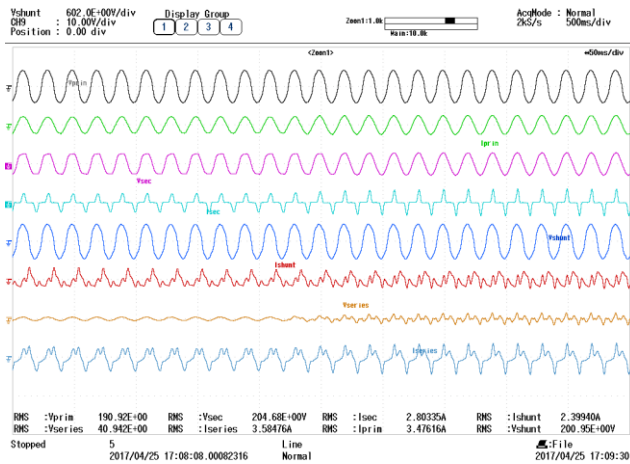


(a)
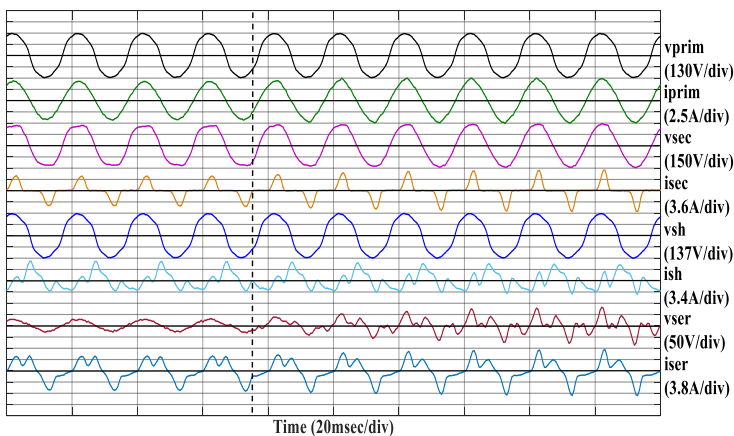


(b)

**Fig. 4.26.** Experimental waveforms with shunt-series harmonics compensation (a)scope capture and (b) replot with scales.
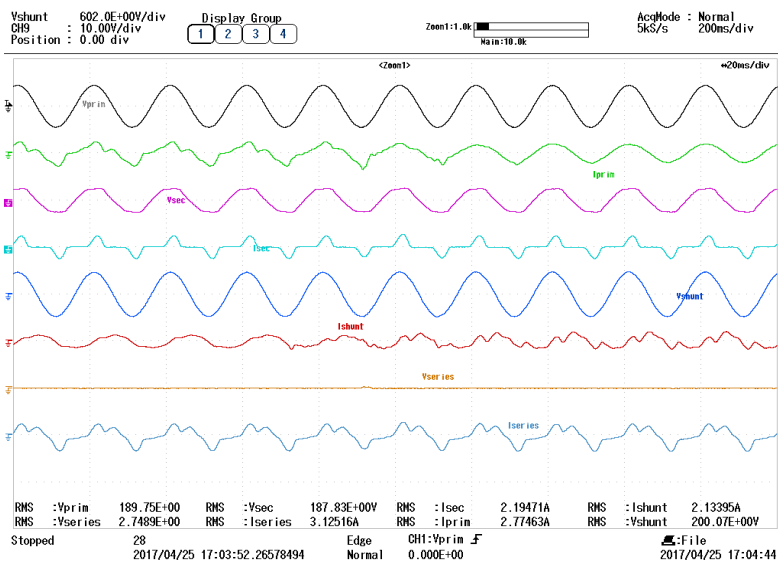
(a)
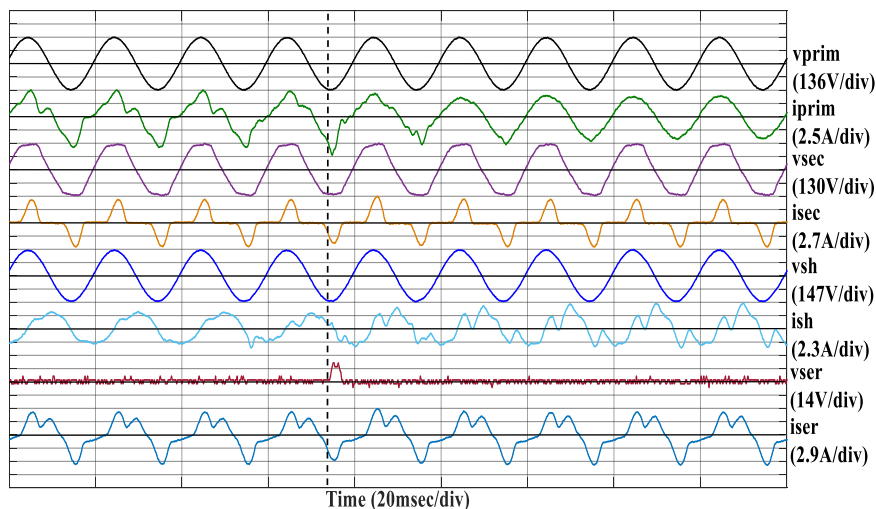


(b)

**Fig. 4.27.** Experimental voltage and current waveforms with shunt harmonic compensation (a)scope capture and (b)replot with scales.

Reactive power compensation through the shunt controller was observed through the phase shift of the primary current with respect to the primary voltage, shown in Fig. 4.28. The shunt controller injected reactive current to the shunt winding, eliminating the required reactive power from the primary side for feeding the load and transformer (Fig. 4.29). As

shown in Fig. 4.30, active power was supplied through the primary winding and absorbed through the shunt winding to maintain a constant DC bus during this operation.
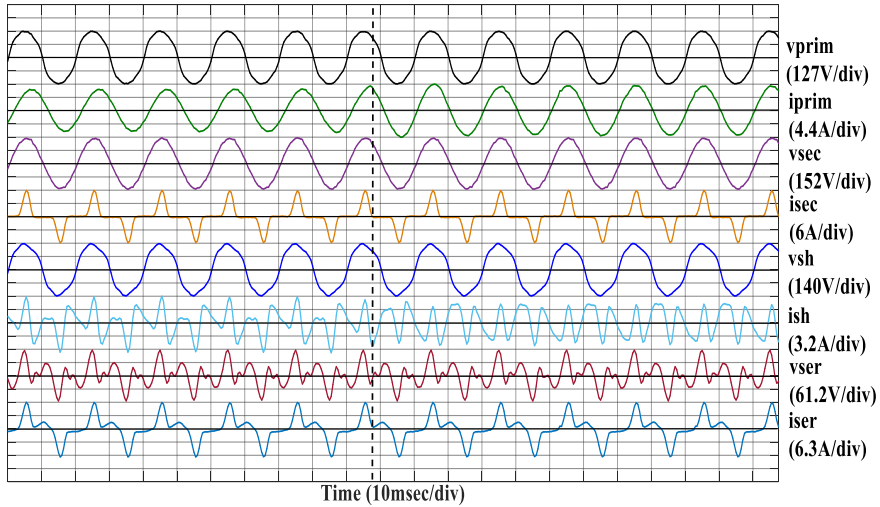


**Fig. 4.28.** Experimental voltage and current waveforms with reactive power compensation.
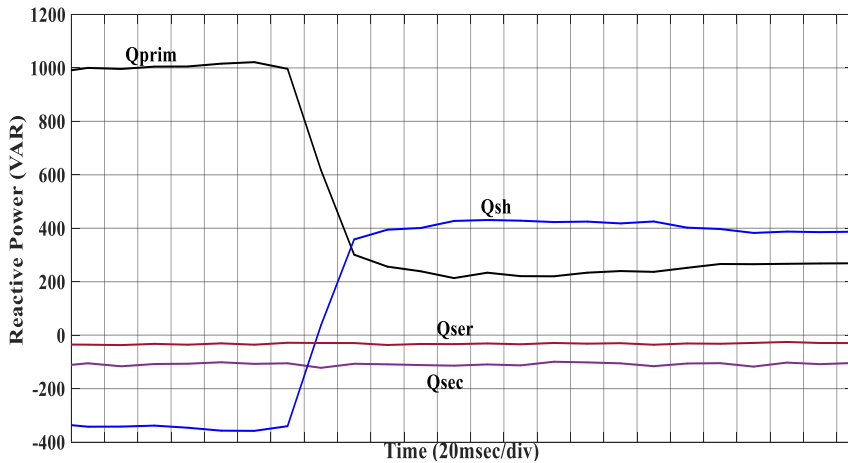


**Fig. 4.29.** Experimental reactive power variation during reactive power controller activation.
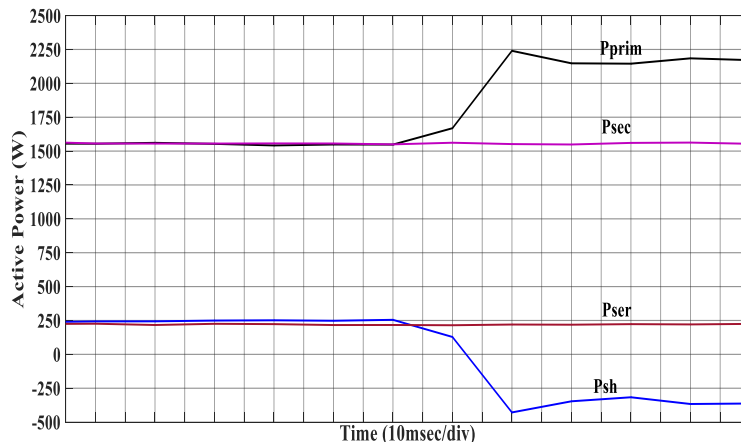
**Fig. 4.30.** Experimental active Power variation during reactive power controller activation.

### 4.4.2 Inrush Current Mitigation

The effects of damping the inrush current at the grid side using the shunt controller was experimentally investigated. In this case a 60% of the rated transformer voltage was applied the primary winding having no-loads connected. The results depicted in Fig. 4.31 evidence the appearance of a peak current, the harmonic contents and the transient decay. All this phenomena where seen in the simulation results discussed earlier. Once the shunt controller is enabled there is a substantial reduction in the peak current magnitude and in the harmonic content of the inrush current, as it is shown in Fig. 4.32.
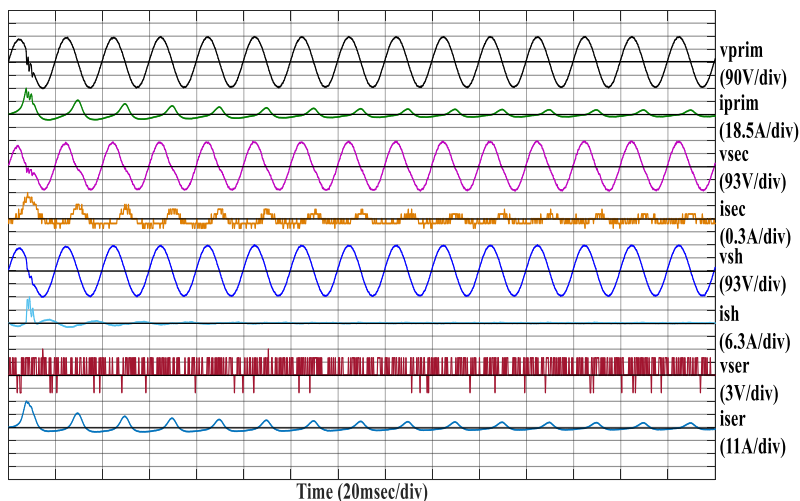


**Fig. 4.31.** Experimental primary inrush current without shunt compensation.
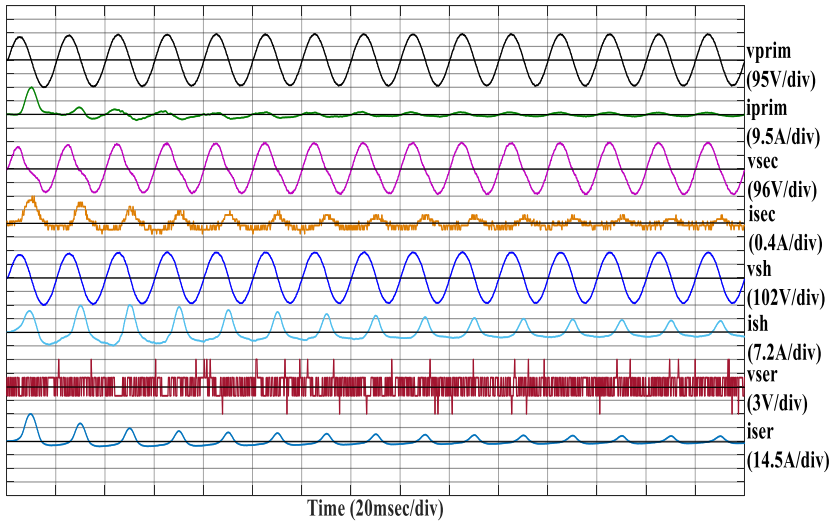
**Fig. 4.32.** Experimental primary inrush current with shunt compensation.

Further analysis of the resulting primary current waveform before and after compensation is illustrated in Fig. 4.33. A significant reduction in the harmonic components of the primary current was observed, which eventually resulted in a reduced peak grid current (Fig. 4.34). An average over 15 cycles shows a reduction of 22.3% in the inrush current from the primary winding.
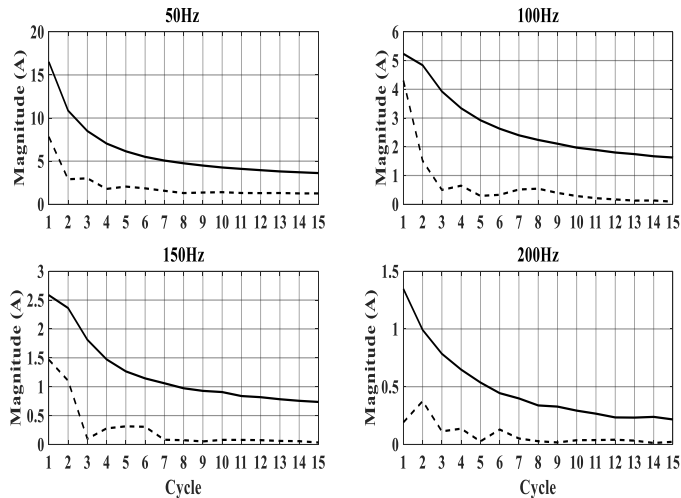


**Fig. 4.33.** Experimental harmonic components of primary current during inrush transient without compensation (solid line) and with compensation (dashed line).
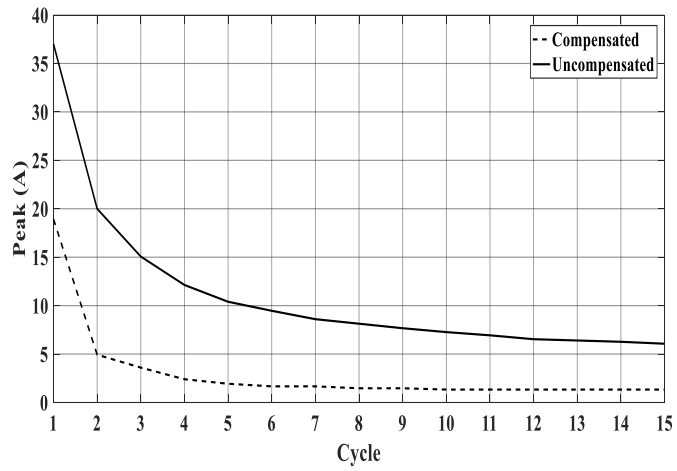
**Fig. 4.34.** Experimental peak magnitude of primary current during inrush transient.

# Three-Phase CPAT-UPFC

*T*his chapter presents the simulation and experimental analysis of two three-phase CPAT configurations. One configuration uses three single-phase CPATs meanwhile the other ones uses a shell-type three-phase CPAT. Both CPAT structures were evaluated in simulation, considering a UPFC application as well as the elimination of transformer magnetizing current harmonics from the grid. In this chapter, a control architecture for the shunt and series converters of the CPAT-UPFC is proposed to provide the required services. The CPAT-UPFC was tested through simulations and experiments considering a power-flow control application between two stiff grids. The CPAT-UPFC was simulated as a substation transformer in a 5-bus power system under power-flow control and load perturbation in the power system. The acquired real-time simulation and experimental results prove the capability of a CPAT-UPFC to provide power flow control, reactive power compensation, voltage regulation and harmonics elimination.

## 5.1   Configurations

The configuration in Fig. 3.4 was implemented using the topology illustrated in Fig. 5.1. A three-phase back-to-back converter was connected to the shunt and series windings of the CPAT. As in a typical UPFC, the shunt converter operated as a current controlled voltage source inverter (CCVSI) equipped with an LCL filter. The filter parameters $L_{1sh}$, $C_{sh}$ and $L_{2sh}$ were selected based on the required attenuation of switching frequency harmonics and resonance frequency. The damping of the filter's resonance was achieved thanks to the shunt damping resistance ($R_{sh}$). The converter was connected in a three-phase 4-wire topology to facilitate the capacity to inject triplen harmonic current in the shunt windings. The magnetizing harmonic currents required by the transformer were evident. Therefore, injecting such harmonic current components through the shunt winding would prevent their appearance at the grid side. The shunt converter controller maintains a constant DC bus voltage ($v_{dc1}$, $v_{dc2}$) over each DC bus capacitor ($C_{dc}$) and controls the shunt converter current

($i_{p2sh}$). The primary voltage ($v_{p1}$) and current ($i_{p1}$) were measured to synchronize the shunt converter voltage ($v_{p2}$) with the $v_{p1}$ and to provide the required services to $i_{p1}$. The output PWM signals of the shunt converter controller drove the converter switches of the shunt converter to control the shunt current according to the required reference.
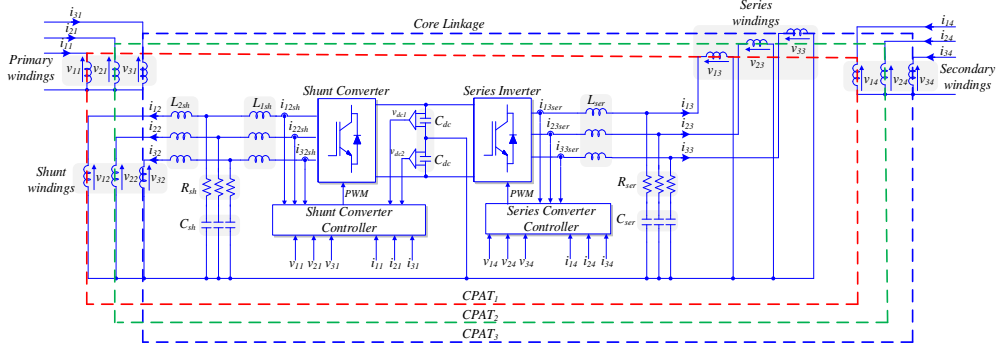


**Fig. 5.1.** Back-to-back converter topology for the three-phase CPAT.

The series inverter operated as a voltage source inverter, equipped with an LC filter to attenuate switching frequency harmonics of the output voltage ($v_{p3}$). Similarly, the filter parameters $L_{ser}$, $C_{ser}$ and $R_{ser}$ were selected based on the required attenuation of switching frequency harmonics and resonance damping. The secondary voltage ($v_{p4}$) and current ($i_{p4}$) were measured to control the series voltage ($v_{p3}$) according to the required services provided to $i_{p4}$. The output PWM signals from the series converter controller drove the series inverter to achieve the required reference series voltage. As shown in Fig. 5.1, each phase of the primary, shunt, series and secondary winding were linked in a common CPAT core, resulting in a three-phase CPAT configuration.

An average model of both converters, accompanied by the linear model of the CPAT, are shown in Fig. 3.15. This system can be utilized to investigate the performance of a CPAT in low- to mid-frequency transients. The average model neglects the effect of the switching frequency harmonics by using a linearly controlled voltage source, as shown in Fig. 5.2. Because harmonics are not considered in this model, a three-phase three-wire converter configuration was used. The common DC bus was emulated at each model sample instant ($v_{dc}$) using the measured shunt converter power ($P_2$) and series converter power ($P_3$) as demonstrated in (5.1).

$$v_{dc1} = v_{dc2} = -\frac{1}{2} \int \frac{P_2 + P_3}{C_{dc} v_{dc}} dt \qquad (5.1)$$
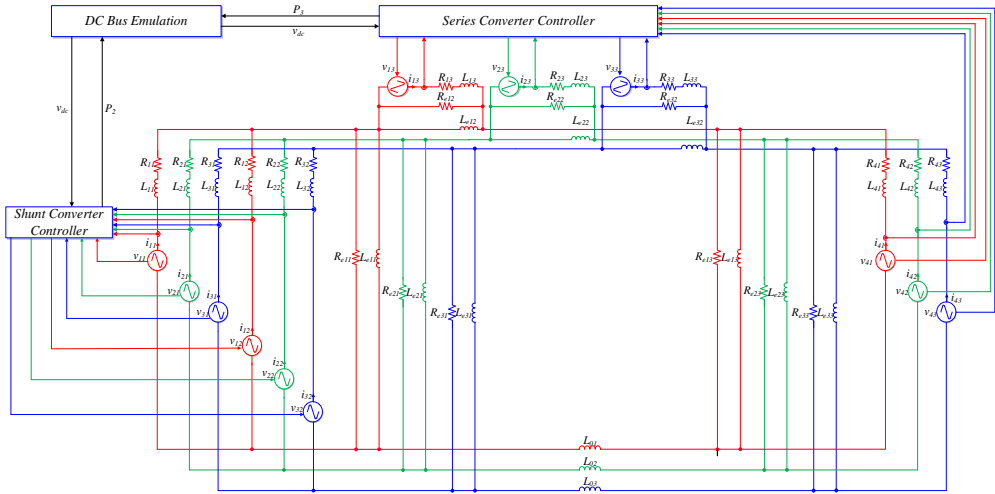
**Fig. 5.2.** Average model of the three-phase CPAT and back-to-back converter.

## 5.2 Control

The control architecture for the previously analysed objectives is presented in Fig. 5.3(a) and Fig. 5.3(b) respectively. As discussed earlier, the objectives of the shunt converter controller are as follows: to maintain a constant DC bus voltage based on the reference DC bus voltage ($V_{dc}^*$), to regulate reactive power through the primary based on the reference reactive power ($Q_1^*$), and to eliminate harmonic components present in the primary current. The measured values for these objectives are $v_{p1}$, $i_{p1}$, $i_{p2sh}$, $v_{dc1}$ and $v_{dc2}$. The series converter controller simultaneously controls the active and reactive power flow through the secondary winding of the CPAT, based on the reference active ($P_4^*$) and reactive ($Q_4^*$) power. Moreover, $Q_{4*}$ can be set through a controller that regulates a load bus voltage ($V_{load}$). The measured variables for these control objectives are $v_{p4}$, $i_{p4}$ and $v_{load}$. Both $i_{p2sh}$ and series converter current ($i_{p3ser}$) are also used for over-current protection in each converter.

Measurements from each architecture were sampled through a sample and hold block (Fig. 5.3) to obtain the $n$ sample value of each measured variable. The synchronization system uses the measured voltages to determine their equivalent frequency ($\omega$), synchronizing signals ($sin(\omega t)$, $cos(\omega t)$), magnitude ($V$) and synchronous reference-frame components ($v_\alpha$, $v_\beta$). These signals, along with the measured variables and reference variables, were passed to the equivalent controller, which determined the required modulation of the converter ($M$). Finally, the PWM module determined the equivalent switching state of each switch ($g$) to achieve the required control objectives.
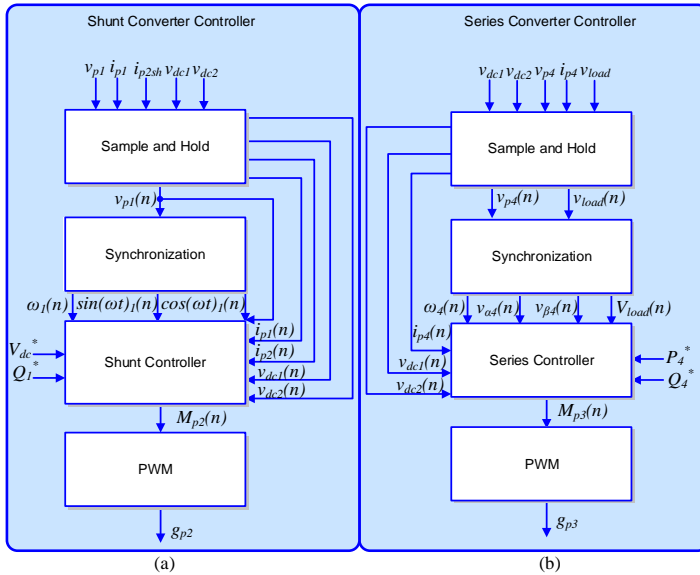
**Fig. 5.3.** Control architectures of (a) Shunt Converter Controller and (b) Series Converter Controller.

### 5.2.1    Shunt Controller

The shunt controller block, shown in Fig. 5.4, received the signals from the synchronization block and sampled variables to determine the required shunt current delivered through the converter.
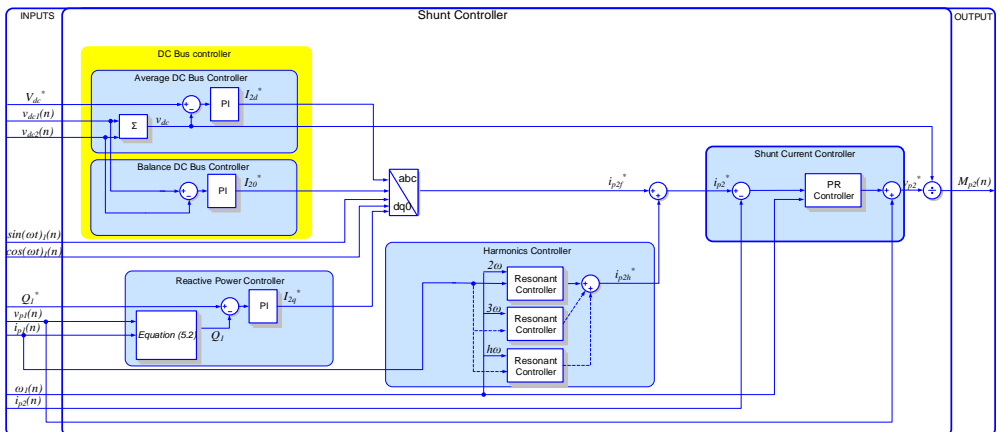


**Fig. 5.4.** Shunt Controller block structure.

The shunt controller block consisted of four sub-controllers: DC bus controller, reactive power controller, harmonics controller and a shunt current controller. The DC bus compensation stage maintained the DC bus voltage at a constant level through two PI

controllers for maintaining a constant total DC bus voltage and a balanced voltage across the split capacitors. The controllers determined the active ($I_{2d}^*$) and zero sequence ($I_{20}^*$) components of the shunt winding current. The reactive component ($I_{2q}^*$) was determined through the reactive power controller, which consisted of a PI controller that determined the required reactive current component ($I_{2q}^*$) to achieve the reference reactive power ($Q_1^*$) through the primary winding. Feedback reactive power through the primary winding is calculated through (5.2).

$$Q_1 = \frac{1}{\sqrt{3}} \begin{bmatrix} v_{11} & v_{21} & v_{31} \end{bmatrix} \begin{bmatrix} 0 & -1 & 1 \\ 1 & 0 & -1 \\ -1 & 1 & 0 \end{bmatrix} \begin{bmatrix} i_{11} \\ i_{21} \\ i_{31} \end{bmatrix} \tag{5.2}$$

In the harmonics compensation stage, the active, reactive and zero sequence components of the reference shunt current were transformed into their equivalent fundamental phase current values ($i_{p2f}^*$). The harmonics controller measured the primary current ($i_{p1}$), and through cascaded resonant controllers tuned to $h$ harmonic orders, the reference harmonic shunt current ($i_{p2h}^*$) was determined. The calculated $i_{p2h}^*$ injected through the shunt winding compensated for the harmonic currents required from the primary winding; thus, only fundamental component current flowed through the primary. The resultant shunt reference currents ($i_{p2}^*$) were controlled through the shunt current controller, consisting of a proportional resonant (PR) controller tuned to the fundamental frequency. The measured and controlled current could be set to $i_{p2sh}$ or $i_{p2}$ according to performance requirements. The resultant reference shunt voltage ($v_{p2}^*$) is divided by the DC bus voltage to achieve the required shunt converter modulation index ($M_{p2}$).

### 5.2.2 Series Controller

The series controller shown in Fig. 5.5 consists of three stages: a reference reactive power calculation, a secondary current calculation and a secondary current controller.
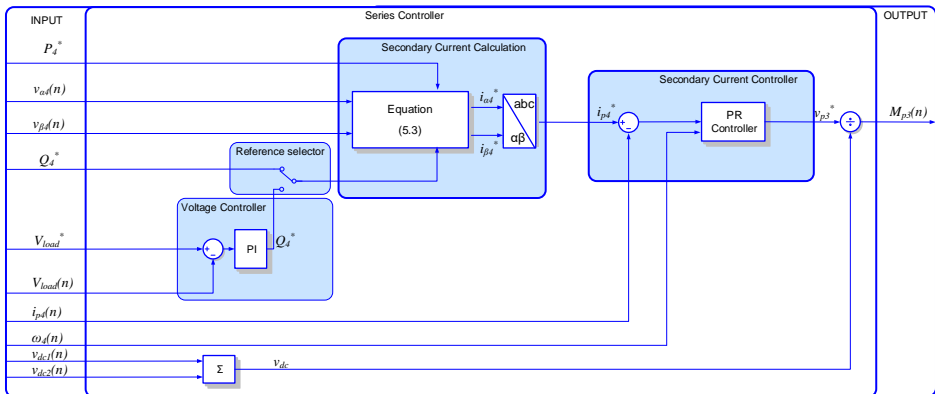


**Fig. 5.5.** Series Controller block structure.

The reference reactive power ($Q_4{}^*$) is set either manually or through a secondary voltage controller that determines the required reactive power to maintain the reference load voltage ($V_{load}{}^*$). The secondary current calculation determines the equivalent stationary reference-frame secondary current ($i_{\alpha4}$, $i_{\beta4}$), based on the reference active and reactive power ($P_4{}^*$, $Q_4{}^*$) using the stationary reference-frame secondary voltage ($v_{\alpha4}$, $v_{\beta4}$). Equation (5.3) summarises the calculations.

$$[i_{\alpha4} \quad i_{\beta4}] = \frac{1}{v_{\alpha4}{}^2 + v_{\beta4}{}^2}[P_4{}^* \quad Q_4{}^*]\begin{bmatrix} v_{\alpha4} & -v_{\beta4} \\ v_{\beta4} & v_{\alpha4} \end{bmatrix} \tag{5.3}$$

Using the secondary synchronizing signals ($sin(\omega t)_4$, $cos(\omega t)_4$), $i_{\alpha4}$ and $i_{\beta4}$ are transformed to their equivalent three-phase quantities ($i_{p4}{}^*$). A PR controller tuned to the fundamental frequency ($\omega_4$) controls the secondary current ($i_{p4}$) to match the reference $i_{p4}{}^*$. The resultant reference series voltage ($v_{p3}{}^*$) is divided by the DC bus voltage ($v_{dc}$) to determine the modulation index of the series converter ($M_{p4}$).

## 5.3    Simulation Results

Using the modelling approach discussed in Chapter 3, the CPAT configurations in Fig. 3.4 and Fig. 3.5 were modelled based on the parameters presented in Table 5.1. The transformer model consists of number of turns $N$, limb length $l_L$, yoke length $l_Y$ and limb area $A$. Common core yokes between phases in Fig. 3.5 were considered double the area of other yokes ($m_2$=2). All core material follow a flux density ($B$) and flux intensity ($H$) relationship shown in Fig. 3.12.

The three-phase CPAT was tested considering a stiff grid connection condition and as a substation transformer in a 5-bus power system. In the stiff grid scenario, the primary and secondary winding were connected to a common stiff grid as shown in Fig. 5.6. In this condition, there is no power flow between the primary and secondary since both are excited by an equal voltage. Therefore, only the magnetizing current of the CPAT would be divided between both windings to excite the core. A magnitude and sweep test was further preformed on the configuration in Fig. 3.5. Three-phase shell type CPAT for UPFC applications. to investigate the operation of the three-phase shell-type CPAT as well.
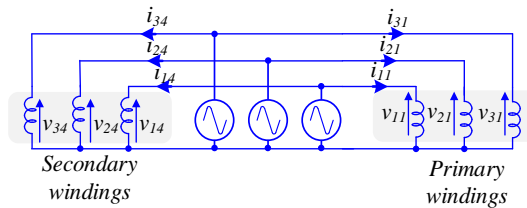


**Fig. 5.6.** Stiff grid connection to primary and secondary windings.

**Table 5.1.** CPAT and Converters Parameters.

| Parameter | Value |
|---|---|
| Grid voltage/phase | 220V |
| $v_{p1}$, $v_{p2}$, $v_{p3}$, $v_{p4}$ | 240V, 240V, 480V, 240V |
| $i_{p1}$, $i_{p2}$, $i_{p3}$, $i_{p4}$ | 70A, 7.2A, 7.2A, 70A |
| $R_{pk}$, $R_c$ | 0.02 p.u., 0.02p.u. |
| $l_L$, $l_Y$ | 0.51m, 0.3m |
| $A$ | 0.0156 m$^2$ |
| $N_{p1}$, $N_{p2}$, $N_{p3}$, $N_{p4}$ | 50, 50, 100, 50 |
| $V_{dc}$ | 700V |
| Sampling Frequency, Switching Frequency | 10kHz |
| $C_{dc}$ | 20mF |
| $L_{1sh}$, $L_{2sh}$, $L_{ser}$ | 6mH, 2mH, 7mH |
| $R_{sh}$, $R_{ser}$ | 4.7Ω, 2.35 Ω |
| $C_{sh}$, $C_{ser}$ | 5µF, 10µF |

To investigate the operation of a three-phase CPAT in a power system, the CPAT was used in a 5-bus power system study case, as the one shown in Fig. 5.7. The study case set-up consisted of two machines, G1 and G2, rated 1000MVA and 1200MVA, respectively. The CPAT was placed between the generator bus (B1) and the transmission bus (B3) to replace a 1000MVA step-up transformer for the 50km transmission line to the load bus (B5). The CPAT was modelled according to the configuration shown in Fig. 5.2 with the equivalent parameters presented in Table 5.2.
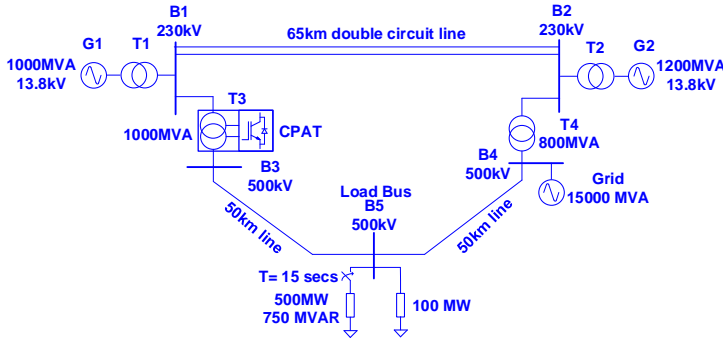
**Fig. 5.7.** Single-line diagram of 5-bus power system case study with a three-phase CPAT model.

**Table 5.2.** Parameters of the Average CPAT and Converter Model.

| Parameter | Value |
|---|---|
| Simulation step-time | 0.1µsec |
| Rated Power/CPAT | 333MVA |
| $v_{p1}$, $v_{p2}$, $v_{p3}$, $v_{p4}$ | 138.5kV, 138.5kV, 138.5kV,288.6kV |
| $R_{pk}$, $R_{epm}$ | 0.002 p.u., 500 p.u. |
| $L_{pk}$, $L_{epm}$, $L_0$ | 0.002 p.u., 500 p.u., 0.003 p.u. |
| $v_{dc1}$, $v_{dc2}$ | 250kV |
| Control sampling frequency | 10kHz |

In this system, the series winding of the CPAT-UPFC was utilized to control active power through the 50km transmission line and regulate the load bus voltage ($V_{load}$). Due to the fact that the CPAT-UPFC was not connected at the load bus, a 100msec delay in the measured load bus voltage was considered to account for communication delay [98]. The CPAT also regulated reactive power absorbed between B1 and B3 through its shunt winding. A 500MW,750MVAR load was suddenly connected on bus B5 at T=15secs to investigate the effectiveness of a CPAT to regulate the load bus voltage as well as the power flow through the system.

### 5.3.1    Three single-phase CPATs stiff-grid connection

The primary and secondary were excited with the same voltage, as shown in Fig. 5.6, while the shunt and series converters injected zero current and voltage respectively. The primary current consisted mainly of 3rd, 5th and 7th-order harmonics, as shown in Fig. 5.8(a). Because there was no power flow between the primary and secondary in this scenario, the primary current consisted mainly of fundamental CPAT magnetizing current and DC bus

regulation current. The shunt harmonics controller tuned to these frequencies eliminated these components from the primary current waveform, as shown in Fig. 5.8(b). Uncompensated higher-order harmonics were not a concern because these harmonic currents would not be magnified, as the primary current increased beyond the magnetizing current and yet would remain below standards. The shunt reactive power controller, set with a reference of 0 VAR, was enabled so that the shunt converter supplied the reactive power required by the CPAT, as shown in Fig. 5.9.
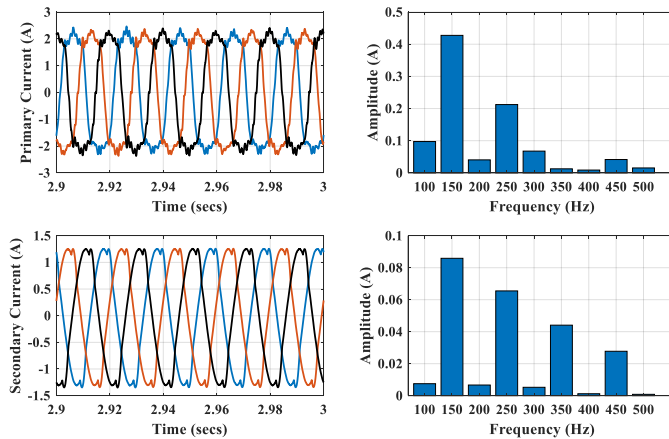


(a)
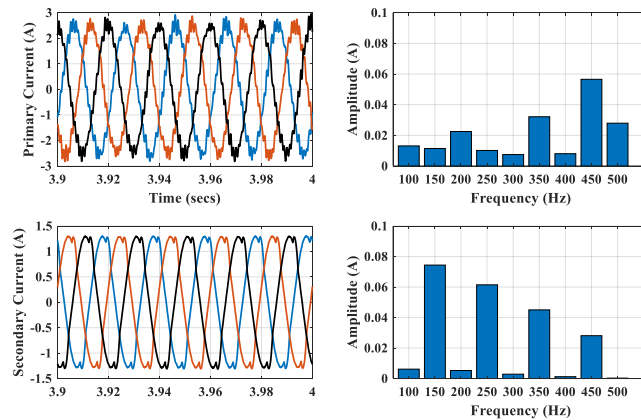


(b)

**Fig. 5.8.** Primary and secondary current waveform and harmonics spectrum. (a) without harmonics compensation and (b) with harmonics compensation.
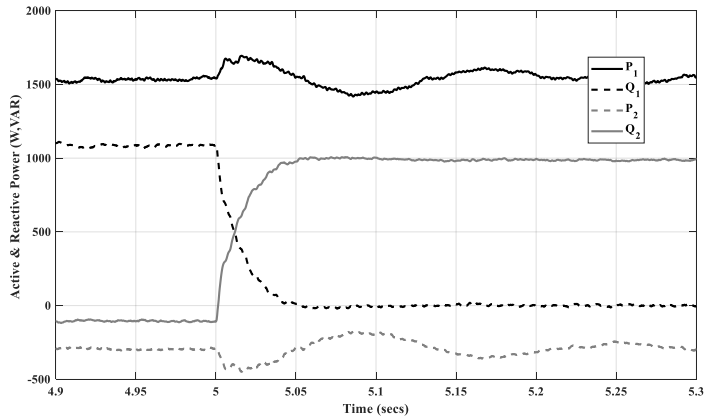
**Fig. 5.9.** Active and reactive power through the primary and shunt winding with enabled Reactive Power Controller.

The secondary current controller was enabled, with a reference of 5 kW and 0 kVAR between the primary and secondary (Figure 5.10). The series converter supplied reactive power to the series winding to alter the equivalent impedance between the primary and secondary windings. The power injected to the grid by the secondary winding was received by the primary winding as illustrated in Fig. 5.11. The DC bus controller maintained a constant DC bus voltage throughout the operation, as illustrated in Fig. 5.12. The resultant primary and secondary current waveform from this reference is shown in Fig. 5.13. The diagram illustrates the effectiveness of the harmonics controller in attenuating the primary current harmonics at the tuned frequencies throughout the operation.
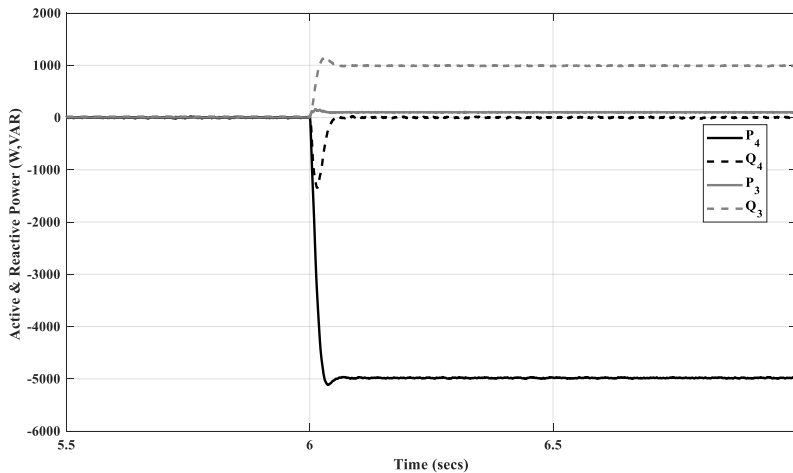


**Fig. 5.10.** Active and reactive power through the secondary and series winding during activation of the Secondary Current Controller.
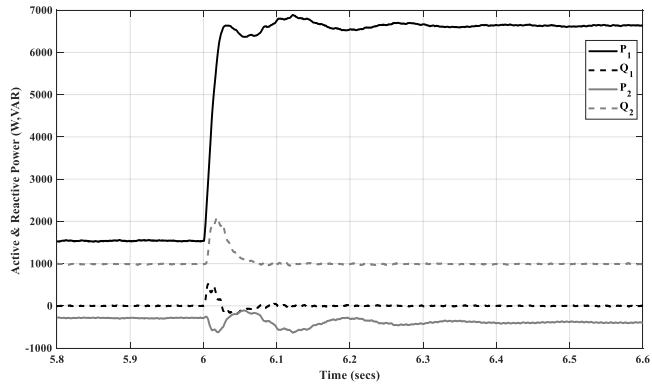
**Fig. 5.11.** Active and reactive power through the primary and shunt windings during step change in reference output power.
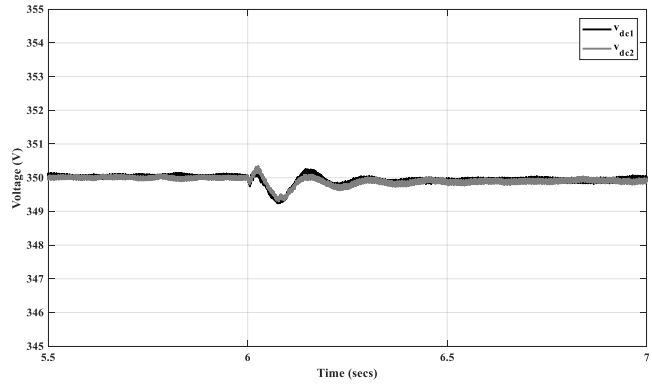


**Fig. 5.12.** DC bus voltage during change in reference output power.
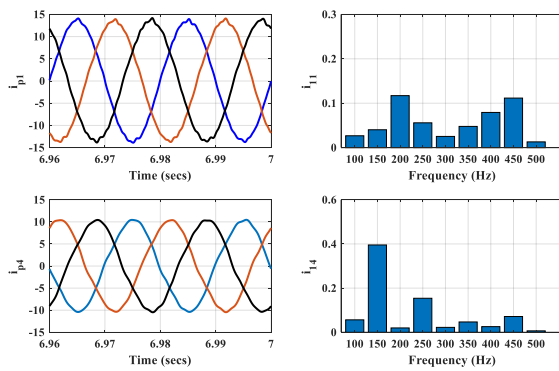


**Fig. 5.13.** Primary and secondary current waveform and harmonics spectrum with all controllers enabled.

### 5.3.2    Three-phase shell-type CPAT sweep test

Considering a common voltage at the primary and secondary windings of the CPAT in Fig. 5.6, a magnitude and angle sweep test was performed on the series winding with a maximum voltage of 480V/phase. The result illustrated in Fig. 5.14 shows the ability of the CPAT to control the active and reactive power flow between primary and secondary according to the applied series voltage. Under such test conditions, the series winding supplies reactive power to vary the impedance between the primary and secondary, thus varying the power flow between them. The contour shown in Fig. 5.14, illustrates the maximum permissible power flow control that can be maintained with the selected series converter in Table 5.2. Based on the utilized model and converter, up to 23% of the maximum power can be controlled using the selected series converter. The relationship between the maximum power flow control that can be achieved with the utilized CPAT and series converter power is shown in Fig. 5.15.
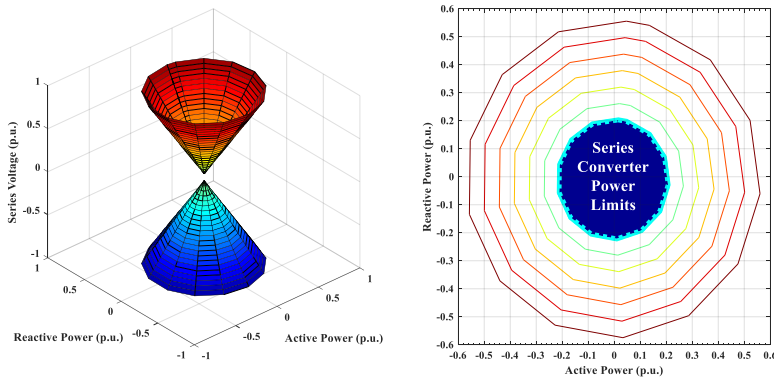


**Fig. 5.14.** Sweep test of three-phase shell type CPAT and its equivalent contour showing operation limits.
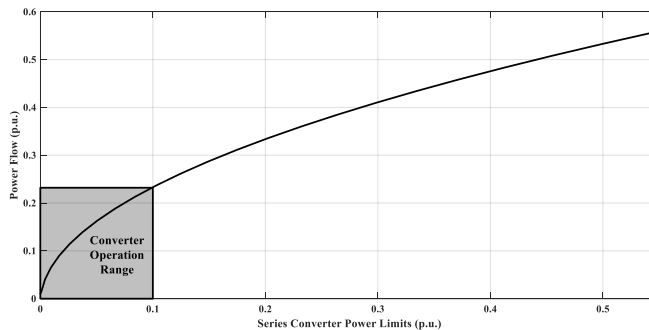


**Fig. 5.15.** Relationship between series converter power limit and maximum power flow.

To investigate the effect of the common limb in a three-phase shell type CPAT, the common yokes are assumed to be 1.3 times the size of other yokes ($m_2$=1.3). A comparison

of harmonic contents between three single-phase CPATs and three-phase shell type CPAT is shown in Fig. 5.16. The results illustrate the similarity between both configurations results, and the effectiveness of the shunt converter in eliminating the tuned harmonic components.
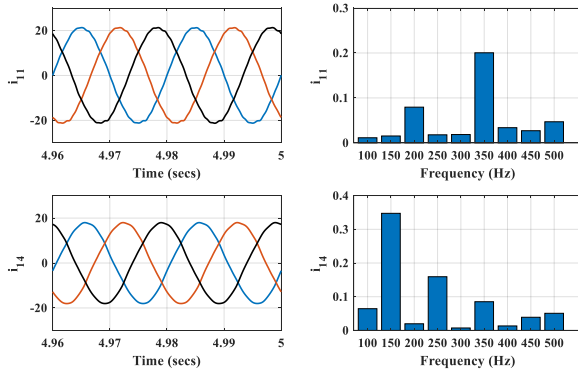


(a)
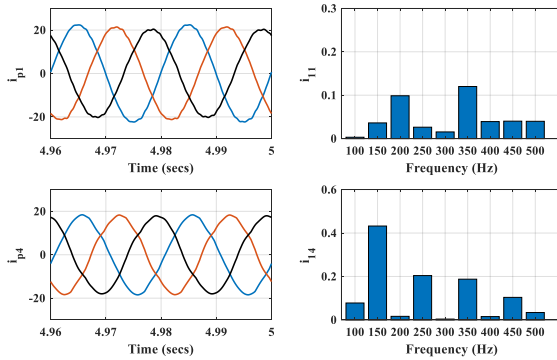


(b)

**Fig. 5.16.** Harmonic spectrum of primary and secondary current with compensation. (a) Three-single phase CPATs and (b) Three-phase shell type CPAT.

### 5.3.3    Three-single phase CPATs in 5-bus power system

This analysis examined the operation of the CPAT-UPFC system, with and without compensation, under a sudden load connection in the power system (Fig. 5.7). All power references were set to the nominal power-flow values before load connection with $P_4^*$=330MW, $Q_4^*$=-30MVAR, $Q_1^*$=-25MVAR, $V_{load}$=500kV and $v_{dc}^*$=500kV. Once these references were set, the behaviour of the system was compared to a system without a CPAT-

UPFC controller (i.e. both shunt and series converters disabled). Fig. 5.17 illustrates the effect of load connection at T = 15 secs on the power-system sources. The CPAT displayed significant damping on G1 (Fig. 5.17(a)), shifting the oscillations to G2 (Fig. 5.17(c)) and to the grid (Fig. 5.17(e)). Moreover, reactive power requirements were reduced, as shown in Fig. 5.17(b), Fig. 5.17(d) and Fig. 5.17(f), because the CPAT mainly supplied reactive power to compensate for the load.
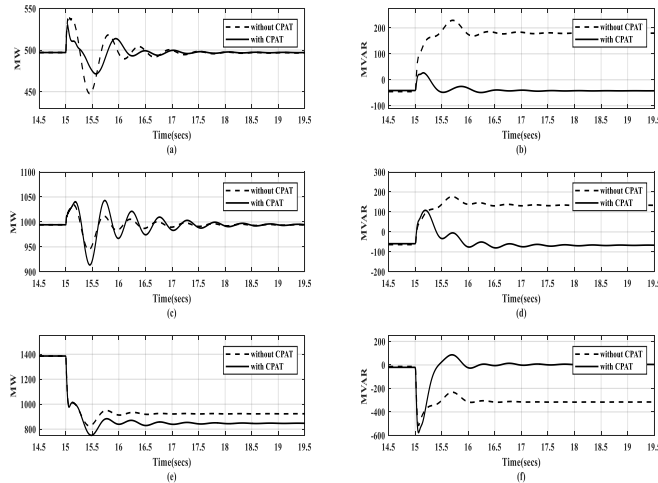


**Fig. 5.17.** Output active and reactive power through grid sources during load connection (a-b) G1, (c-d) G2 and (e-f) grid.

The CPAT was controlled considering constant references. Fig. 5.18 shows the output active and reactive power through different grid sources. The reactive power flowing through the transformer primary winding, shown in Fig. 5.18 (b), was significantly reduced because the shunt converter (Fig. 5.18(f)) supplied such power. In addition, the shunt converter supplied the increased reactive power demand at the load bus, as shown in Fig. 5.18 (d). Primary and secondary active power damping, shown in Fig. 5.18(a) and Fig. 5.18 (c), were achieved through the series converter controller. The damping effect was evident in the series converter action (Fig. 5.18(g)) as it absorbed active power to maintain a constant secondary current at the load connection instant. The shunt winding supplied this power to the primary, as shown in Fig. 5.18(e). Later, the series converter supplied the steady-state required active and reactive power to maintain the required secondary power reference, as shown in Fig. 5.18(g–h).
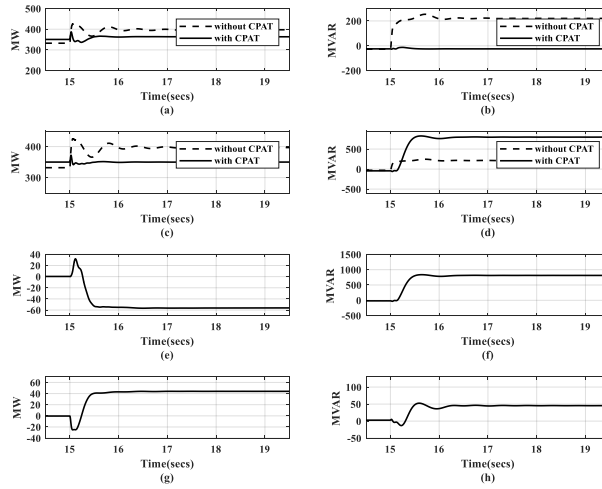
**Fig. 5.18.** Output active and reactive power through the CPAT during load connection (a-b) primary, (c-d) secondary, (e-f) shunt and (g-h) series.

The regulation effect on the load bus voltage and DC bus voltage during load connection is shown in Fig. 5.19. The communication delay affected the damping of the load voltage oscillation. However, the voltage drop of 5% at the load bus was compensated for through the CPAT, as shown in Fig. 5.19(a). The tuning effect of the voltage controller on the response with a communication delay was not investigated in this study.

The DC bus voltage increased during the load connection, as shown in Fig. 5.19(b), because the series converter absorbed active power (Fig. 5.18(g)). Fig. 5.19(b) shows the DC bus recharging to maintain a constant voltage when the shunt converter absorbed active power and injected reactive power to the grid, as presented in Fig. 5.18(e–f).
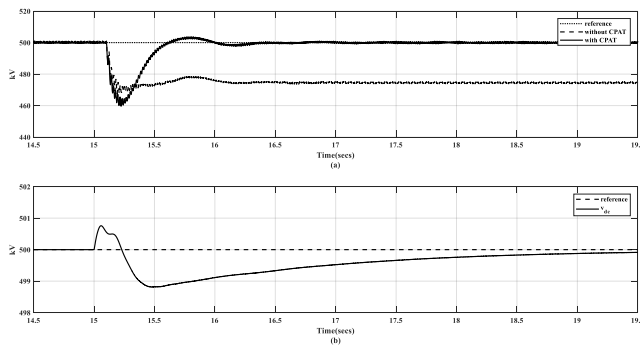


**Fig. 5.19.** Voltage profile during load connection (a) load bus and (b) DC bus voltage.

## 5.4    Experimental Results

The laboratory set-up shown in Fig. 5.20 consisted of three multi-winding three-phase transformers and two 5-kW back-to-back converters, connected according to the configuration in Fig. 5.1. All transformer parameters are presented in Table 5.1. The primary and secondary windings were connected according to the configuration shown in Fig. 5.6. Each converter was controlled through a DS1103 controller board, with a sampling and switching frequency of 10kHz. In order to investigate the improvement in the stability of the 5-bus power system when using a CPAT, a real-time simulation of the system using OPAL-RT was performed.
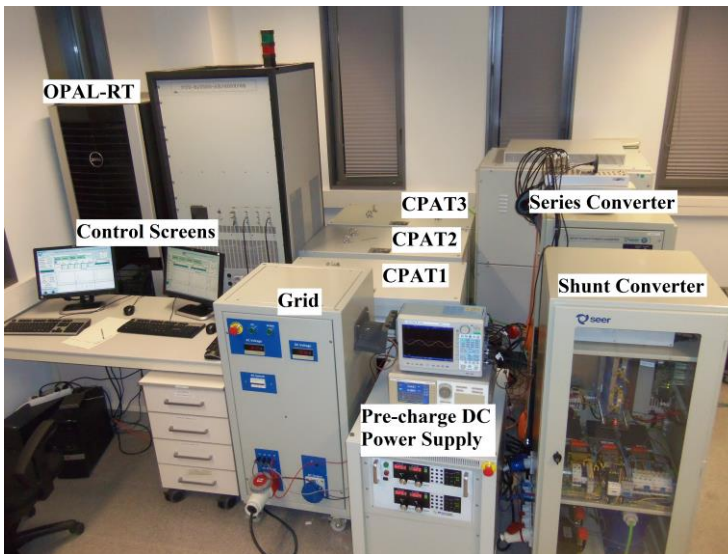


**Fig. 5.20.** Laboratory setup layout of the three-phase CPAT-UPFC.

### 5.4.1    Three single-phase CPAT stiff-grid connection

The set-up was initiated with the DC bus controller enabled, to maintain a constant DC bus for the set-up operation. During this state, the harmonic spectrum of the primary current consisted mainly of $3^{rd}$ and $5^{th}$-order harmonics, of 55% and 18% magnitude respectively, as shown in Fig. 5.21(a). The $2^{nd}$ and $7^{th}$-order harmonics represented 2% of the magnetizing current. With the harmonics controller tuned to $3^{rd}$, $5^{th}$ and $7^{th}$-order frequencies, the harmonics present in the primary current were mitigated, with each component reduced by more than 95% (Fig. 5.21(b)).
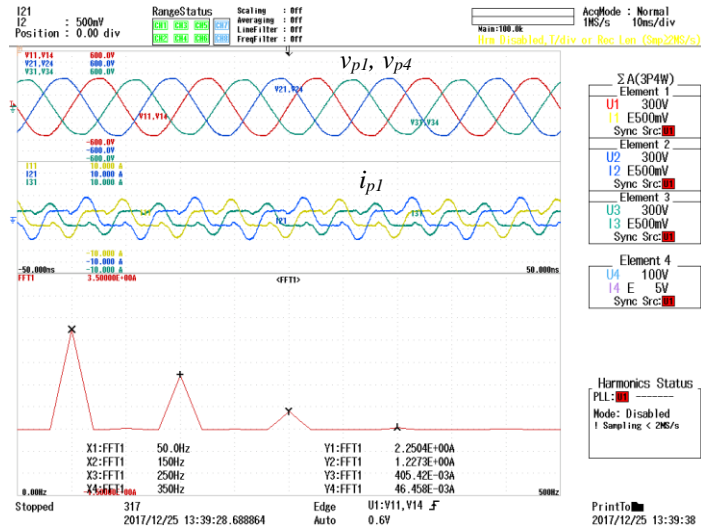
(a)
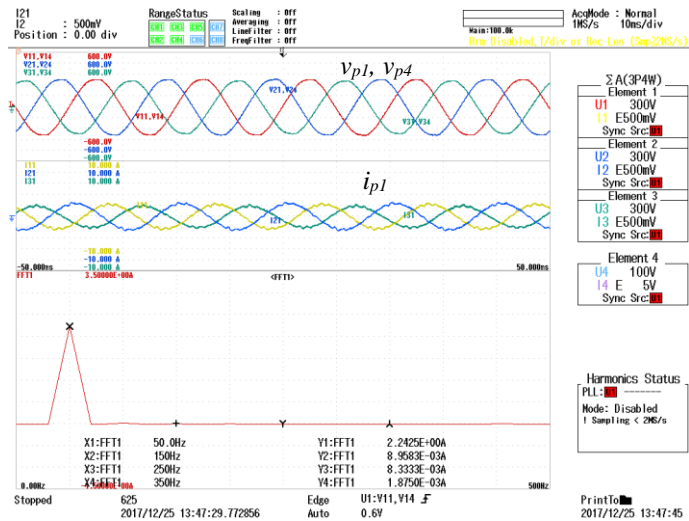


(b)

**Fig. 5.21.** Experimental primary current waveform and harmonics spectrum. (a) without harmonics compensation and (b) with harmonics compensation.

The reactive power compensation controller was set to decrease the reactive power through the primary to zero, as shown in Fig. 5.22. At that instant, the shunt winding current increased, as shown in Fig. 5.22(a), so that the 1.8 kVAR required from the primary (Fig. 5.22(b)) was supplied through the shunt converter. The 1.8 kVAR represented the CPAT

magnetizing power. At steady-state, the shunt converter supplied the reactive power required by the CPAT and secondary winding.
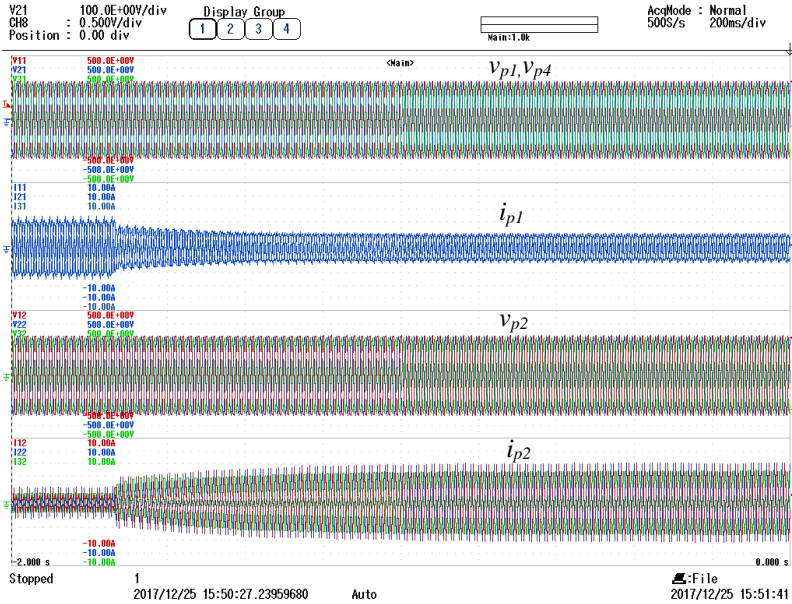


(a)
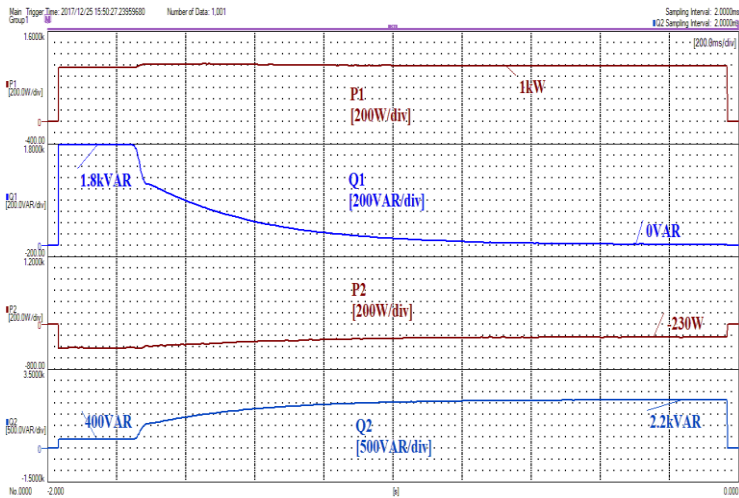


(b)

**Fig. 5.22.** Experimental results of shunt converter operation with Reactive Power Compensator controller set to 0kVAR. (a) voltage and current waveforms, (b) active, reactive power through the primary and shunt windings.

The series converter was set with a minus-5kW reference for secondary power, so that an extra 5 kW would be absorbed from the primary to the secondary and fed to the grid. Activation of the secondary current controller with the pre-set reference resulted in an increase in the secondary current, shown in Fig. 5.23(a), corresponding to the required output power (Fig. 5.23(b)).
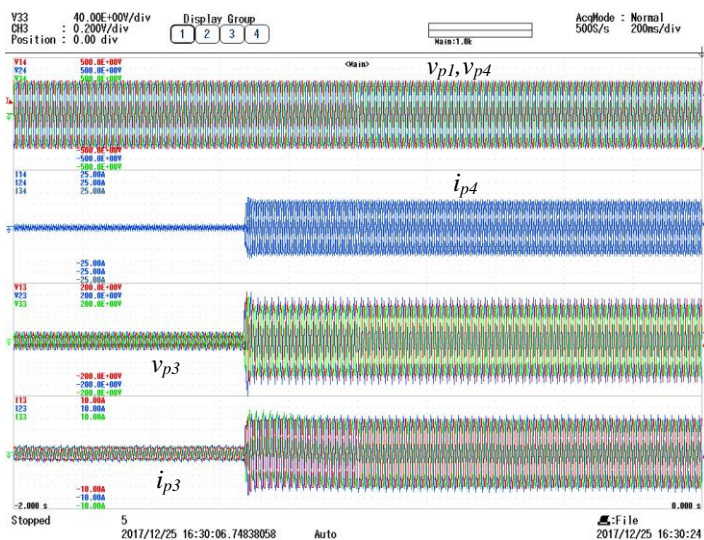


(a)
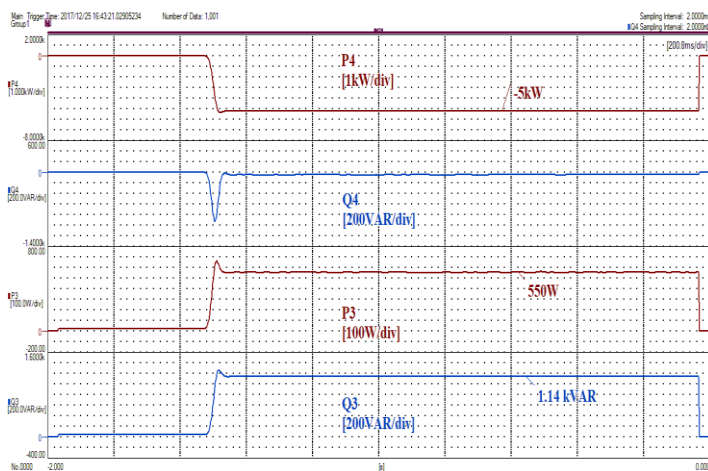


(b)

**Fig. 5.23.** Experimental results of series converter operation with Secondary Current Controller set to -5kW. (a) voltage and current waveforms, (b) active, reactive power through the secondary and series windings.

The series converter supplied mainly reactive power, using approximately 25% of the rated converter power, to change the power flow in the transformer by 10% of its rated power. At the same instant, the primary current increased (Fig. 5.24(a)) to supply the required active power by the secondary winding and transformer core (Fig. 5.24(b)).
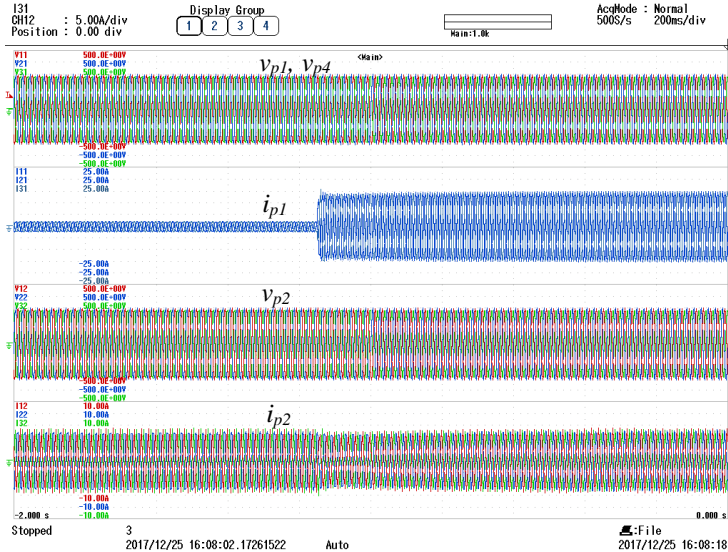


(a)
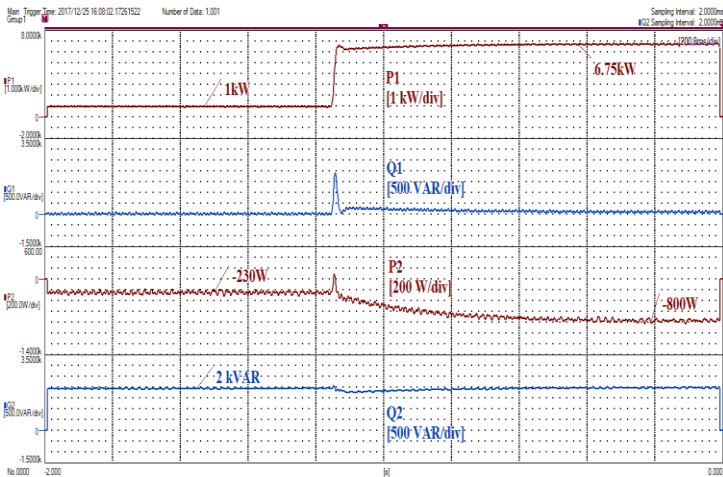


(b)

**Fig. 5.24.** Experimental results of primary and shunt winding power during activation of Secondary Current Controller set to -5kW. (a) voltage and current waveforms, (b) active, reactive power through the primary and shunt windings.

Moreover, the shunt converter absorbed an extra 570 W to maintain a constant DC bus voltage while supplying the series converter with its required active power. Fig. 5.25 illustrates this scenario, where the DC bus voltage increased to the nominal value after activation of the secondary current controller.
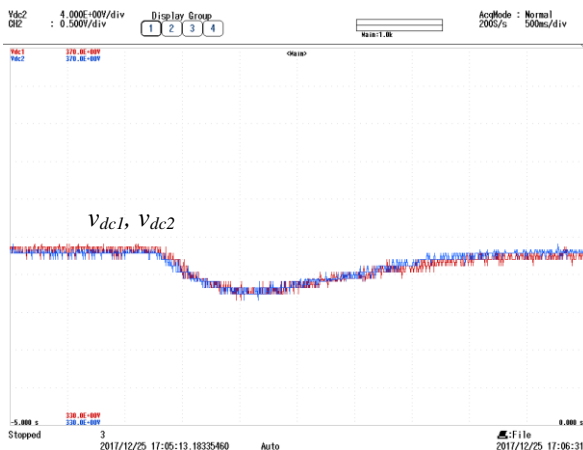


**Fig. 5.25.** DC bus voltage during activation of the Secondary Current Controller with DC Bus voltage controller enabled.

### 5.4.2    Three-single phase CPATs in a 5-bus power system

Using the OPAL-RT, a real-time simulation of the 5-bus power system was performed to investigate the stability of the power system with the CPAT in operation. The effect of the CPAT on G1, G2 and the grid during the connection of the 500 MW and 750 MVAR shown in Fig. 5.26(a), validated the simulation results in Fig. 5.17. Similar reductions were observed for G1 active and reactive power oscillations and for G2 reactive power. Fig. 5.27(b) illustrates the reduced primary and secondary winding oscillations and the regulation of power by the shunt and series controllers. Similarly, the real-time simulation results of the load bus voltage and DC bus voltage, shown in Fig. 5.18, match with the results presented in Section 5.3.3. These results together validate the functionality of the CPAT in a power system.
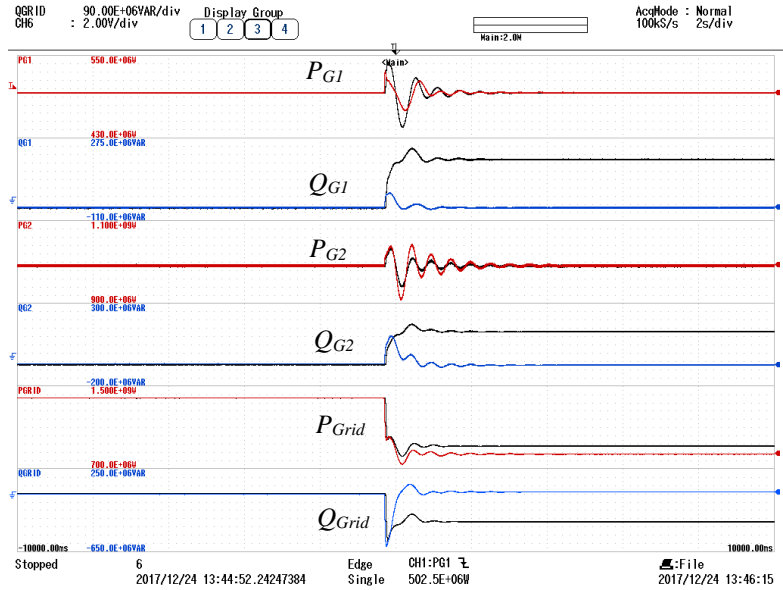
(a)
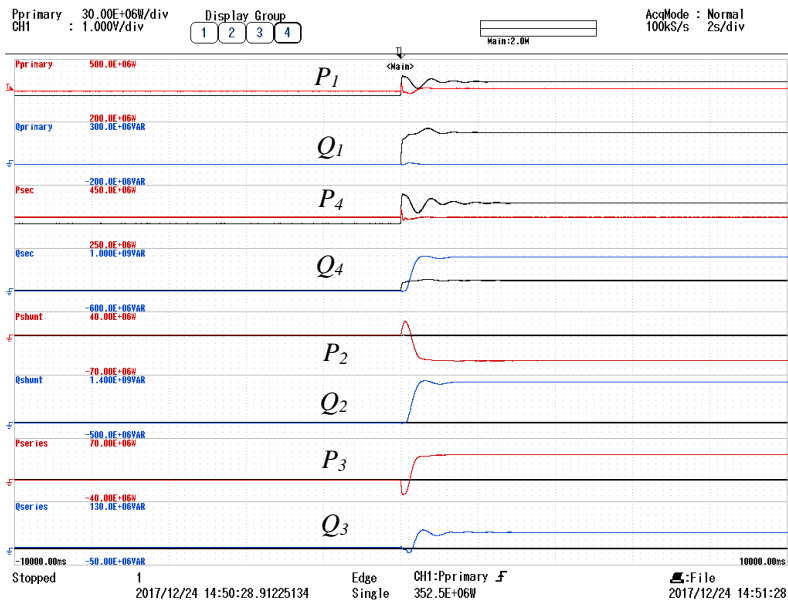


(b)

**Fig. 5.26.** Real-time simulation of the active and reactive power through the 5-bus power system without CPAT controllers enabled (black lines) and with CPAT controllers enabled. (a) Grid sources and (b) CPAT windings.
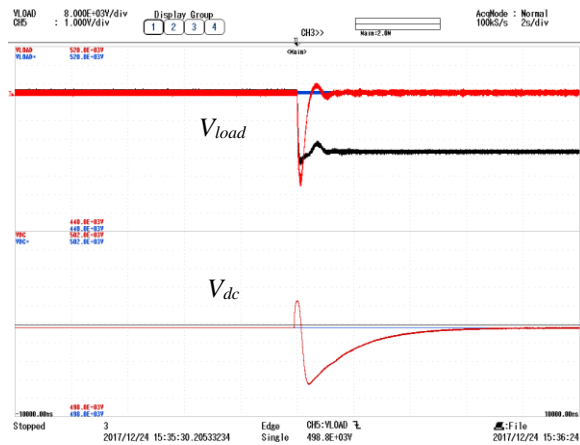
**Fig. 5.27.** Real-time simulation of the load voltage and DC bus voltage during load connection without CPAT controllers activated (black line) and with CPAT controllers enabled.

# Conclusion and Future Work

## 6.1 Conclusion

The work presented in this PhD dissertation was devoted to the introduction, description, analysis and validation of the CPAT which has shown the ability to combine series and shunt power conditioning in a single transformer, giving rise to a system that goes beyond the state of the art and is able to provide promising functionalities.

In addition to the technical feasibility of the CPAT, the effectiveness of the proposed device in terms of cost and size reduction was proven through the decrease in the equivalent core-size, number of windings and supplementary manufacturing requirements when compared to multiple transformer compensation approach.

In this PhD a single-phase CPAT has been presented and analyzed in terms of operation and design considerations. Moreover, the possibility for extension to three-phase and multi-phase CPAT shows the expandability of the proposed transformer. Simulation and experimental results of the CPAT-UPQC show the ability of the transformer to achieve compensation of primary current harmonics and reactive power. Moreover, the CPAT is able to provide secondary voltage regulation and harmonics compensation under severe operating conditions. Based on the analysis and results presented, in terms of integration of power converters in transformers, the CPAT shows a competitive and cost-effective solution. In addition to these features, the shunt compensation system is able to provide inrush current mitigation during energization of the transformer, reducing the effect of inrush current on the source grid.

A three-phase CPAT has also been proposed in two possible configurations. Both configurations were modeled and analyzed based on their equivalent magnetic circuit

showing that both configurations operate identically. Moreover, core structure of the three-phase shell type transformer has been compared to several shunt-series compensation configurations to investigate the limitations and benefits of a three-phase CPAT. The analysis shows that the three-phase CPAT can be mostly beneficial when utilized instead of a compensation system consisting of multiple three-phase transformers. In addition, the CPAT requires a reduced number of windings as well as supporting structure and protection equipment.

In order to validate the performance of the CPAT in applications linked to electrical networks support, linear and non-linear modeling approaches of a CPAT has been presented and investigated under stiff-grid operation and in a 5-bus power system model. Finally, simulation and experimental analysis of a power flow control application shows the applicability of a three-phase CPAT to effectively achieve shunt and series services to the grid through fractional power converters.

The analysis in Chapter 4 and Chapter 5 have considered the magnetic circuit of the transformers presented in Chapter 3 to realize the interaction between different windings in the core of a CPAT. Such simulations have represented the state of operation under low equivalent series and shunt impedance of the transformer core. Furthermore, the experimental transformer was rated at 2.1kV at each limb to account for a regular three-phase transformer design with a low core reluctance.

These simulations and experiments have shown the operation of a CPAT for low frequency disturbances to voltage and current waveform of the grid and load respectively. Such disturbances have been attenuated in a single-phase system through simulations of a switching converter and experiments using a linear amplifier in Chapter 4. Moreover, the proposed three-phase systems have been tested in Chapter 5 through simulations and experiments of a switching converter and through simulation of a linear converter in a 5-bus power system.

## 6.2   Future Work

As discussed in the previous Chapters and concluded in the previous section, the CPAT has been considered for low frequency performance. Moreover, cost comparison in terms of iron to copper requirements of the proposed configurations has not been evaluated. Since in principle the CPAT presents an integrated FACTS solution, it is necessary to realize the break-even point of such a structure as compared to modern compensation solutions. This can be achieved through the realization of manufacturing requirements while taking into consideration the principle assumptions presented in this thesis which includes low equivalent transformer core reluctance and increased coupling between windings.

Further applications, configurations and theories may be investigated using the CPAT which include and limited to:

- Direct converter connection to auxiliary windings (excluding a filter). Considering the CPAT's auxiliary windings form an equivalent series inductor. This integrated

filtering may be interesting to resolve filter size and cost of an off-the-shelf converter.

- Utilization of the generalized CPAT structure presented in Chapter 3 to create a cascaded connection between several converters. Such an approach aids the formation of an isolated multilevel output voltage waveform through a single transformer. This resolves the un-isolated connection of multilevel converters which require an isolated transformer per converter for safe operation.

- Utilization of energy storage within the DC bus of the back-to-back configuration in a CPAT may be investigated to realize the impact of a distribution or transmission CPAT on the power system. In such a study, optimal allocation of compensation devices can be assessed based on the available transformer stations. Hence this would provide the flexibility of upgrading a substation transformer rather than installing a compensation system.

- The CPAT may be economically assessed based on the principle that it allows the manufacturer to salvage an installed distribution transformer and reuse the core materials. A typical compensation system is formed by manufacturing and installing it. However, a CPAT can upgrade an existing transformer by reusing its core materials to build the new CPAT.

- A reliability comparison between a CPAT and a power electronics-based transformer may reveal the difference between depending on a single integrated transformer rather than power electronics modules. Moreover, it should be noted that the CPAT enables interconnection between primary and secondary areas even if the power electronics module is faulty. This is not the case with power electronics-based transformers.

- Other control techniques and configurations can be investigated for inrush current mitigation. This includes per-charging the CPAT before grid connection through its auxiliary windings using an energy source.

# References

[1]    "Commission regulation (EU) No 548/2014 implementing Directive 2009/125/EC of the European Parliament and of the Council with regard to small, medium and large power transformers," 2014.

[2]    Siemens, "New EU requirements for transformers: Ecodesign Directive from the European Commission," 2015. [Online]. Available: http://m.energy.siemens.com/US/pool/hq/power-transmission/Transformers/inserts/insert_new-eu-requirements-for-transformers_ecodesign-directive_EN.pdf.

[3]    Blumsack, M. Sahraei-Ardakani and S. A., "Transfer Capability Improvement Through Market-Based Operation of Series FACTS Devices," *IEEE Trans. Power Syst.,* vol. 31, no. 5, pp. 3702-3714, Sept. 2016.

[4]    Y. Liu, S. Yang, X. Wang, D. Gunasekaran, U. Karki and F. Peng, "Application of Transformer-Less UPFC for Interconnecting Two Synchronous AC Grids With Large Phase Difference," *IEEE Trans. Power Electron.,* vol. 31, no. 9, pp. 6092-6103, Sept. 2016.

[5]    F. Z. Peng, Y. Liu, S. Yang, S. Zhang, D. Gunasekaran and U. Karki, "Transformer-Less Unified Power-Flow Controller Using the Cascade Multilevel Inverter," *IEEE Trans. Power Electron.,* vol. 31, no. 8, pp. 5461-5472, Aug. 2016.

[6]    S. Yang, Y. Liu, X. Wang, D. Gunasekaran, U. Karki and F. Peng, "Modulation and Control of Transformerless UPFC," *IEEE Trans. Power Electron.,* vol. 31, no. 2, pp. 1050-1063, Feb. 2016.

[7]     E. McMurray, "Power converter circuits having a high frequency link". USA Patent US3517300, 23 Jun. 1970.

[8]     M. Liserre, G. Buticchi, M. Andresen, G. De Carne, L. Costa and Z. Zou, "The Smart Transformer: Impact on the Electric Grid and Technology Challenges," *IEEE Ind. Electroc. Mag.,* vol. 10, no. 2, p. 46–58, Jun. 2016.

[9]     M. Liserre, M. Andresen, M. Costa and G. Buticchi, "Power Routing in Modular Smart Transformers: Active Thermal Control Through Uneven Loading of Cells," *IEEE Ind. Electron. Mag.,* vol. 10, no. 3, p. 43–53, Sept. 2016.

[10]    L. Ferreira Costa, G. De Carne, G. Buticchi and M. Liserre, "The Smart Transformer: A solid-state transformer tailored to provide ancillary services to the distribution grid," *IEEE Power Electron. Mag.,* vol. 4, no. 2, pp. 56-67, Jun. 2017.

[11]    D. Wang, J. Tian, C. Mao, J. Lu, Y. Duan, J. Qiu and H. Cai, "A 10-kV/400-V 500-kVA Electronic Power Transformer," *IEEE Trans. Ind. Electron.,* vol. 63, no. 11, pp. 6653-6663, Nov. 2016.

[12]    T. Vandoorn, J. D. M. De Kooning, B. Meersman, J. Guerrero and L. Vandevelde, "Voltage-Based Control of a Smart Transformer in a Microgrid," *IEEE Trans. Ind. Electron.,* vol. 60, no. 4, pp. 1291-1305, Apr. 2013.

[13]    M. Andresen, K. Ma, G. De Carne, G. Buticchi, F. Blaabjerg and M. Liserre, "Thermal Stress Analysis of Medium-Voltage Converters for Smart Transformers," *IEEE Trans. Power Electron.,* vol. 32, no. 6, pp. 4753-4765, Jun. 2017.

[14]    E. Ronan, S. Sudhoff, S. Glover and D. Galloway, "A power electronic-based distribution transformer," *IEEE Trans. Power Del.,* vol. 17, no. 2, p. 537–543, Apr. 2002.

[15]    D. Li, Q. Chen, Z. Jia and C. Zhang, "A high-power active filtering system with fundamental magnetic flux compensation," *IEEE Trans. Power Del.,* vol. 21, no. 2, p. 823–830, Apr. 2006.

[16]    P. Thiwanka Bandara and Wijekoon, "Power Quality Control". Europe Patent EP20130192880, 21 May 2014.

[17]    C. Wang, X. Yin, Z. Zhang and M. Wen, "A Novel Compensation Technology of Static Synchronous Compensator Integrated With Distribution Transformer," *IEEE Trans. Power Del.,* vol. 28, no. 2, p. 1032–1039, Apr. 2013.

[18]     V. Valdivia, J. Pleite, P. Zumel and C. Gonzalez, "Improving design of integrated magnetics for power electronics converters," *IEEE Electron. Lett.,* vol. 44, no. 11, p. 693–694, May 2008.

[19]     A. Dimitrovski, Z. Li and B. Ozpineci, "Magnetic Amplifier-Based Power-Flow Controller," *IEEE Trans. Power Del.,* vol. 30, no. 4, p. 1708–1714, Aug. 2015.

[20]     "Multiphase Power Converters Having Shared Magnetic Core Sections". USA Patent US20130083575, 4 Apr. 2013.

[21]     G. Gohil, L. Bede, R. Teodorescu, T. Kerekes and F. Blaabjerg, "Optimized Integrated Harmonic Filter Inductor for Dual-Converter-Fed Open-End Transformer Topology," *IEEE Trans. Power Electron.,* vol. 32, no. 3, p. 1818–1831, Mar. 2017.

[22]     M. Tian, J. Yin and Y. Liu, "Magnetic Integration Technology in Controllable Reactor of Transformer Type Constituted by Various Magnetic Materials," *IEEE Trans. Appl. Supercond.,* vol. 24, no. 5, pp. 1-5, Oct. 2014.

[23]     D. Das, R. P. Kandula, J. A. Muñoz, D. Divan, R. G. Harley and J. E. Schatz, "An Integrated Controllable Network Transformer—Hybrid Active Filter System," *IEEE Trans. Ind. Appl.,* vol. 51, no. 2, p. 1692–1701, Mar.–Apr. 2015.

[24]     J. Pleite, V. Valdivia, P. Zumel and C. Gonzalez, "Transformer and Series Inductance Integration for Harmonic Filtering in PWM Inverters Based in a Simple Design Procedure," *IEEE International Symposium on Industrial Electronics,* pp. 1201-1206, Jun. 2007.

[25]     B. Ambati and V. Khadkikar, "Variable Frequency Transformer Configuration for Decoupled Active-Reactive Powers Transfer Control," *IEEE Trans. on Energy Convers.,* vol. 31, no. 3, pp. 906-914, Sept. 2016.

[26]     V. Valdivia, J. Pleite, P. Zumel, C. Gonzalez and A. Roldan, "Three phase LCL filter and transformer with integrated magnetics for grid connected converters," *34th Annual Conference of IEEE Industrial Electronics,* pp. 1027-1032, Nov. 2008.

[27]     R. M. Hutchison and D. J. Corrigall, "Shunt coil controlled transformer". USA Patent US5187428, 16 Feb. 1993.

[28]     K. Sen and M. L. Sen, "Introducing the family of "Sen" transformers: a set of power flow controlling transformers," *IEEE Trans. Power Del.,* vol. 18, no. 1, pp. 149-157, Jan. 2003.

[29]     Y. Lee, L.-P. Wong and D. Cheng, "Simulation and design of integrated magnetics for power converters," *IEEE Trans. Mag.,* vol. 39, no. 2, pp. 1008-1018, Mar. 2003.

[30]     K. Sen and M. L. Sen, "Comparison of the "Sen" transformer with the unified power flow controller," *IEEE Trans. Power Del.,* vol. 18, no. 4, pp. 1523-1533, Oct. 2003.

[31]     J. Yuan, L. Chen and B. Chen, "The improved Sen transformer — A new effective approach to power transmission control," in *Energy Conversion Congress and Exposition*, Pittsburgh, PA, 2014.

[32]     A. Gole, J. Martinez-Velasco and K. J. F., "Modeling and Analysis of System Transients Using Digital Programs," *IEEE PES Special Publication,* no. TP-133-0, Jan. 1999.

[33]     X. Chen and P. Neudorfer, "Digital model for transient studies of a three phase five-legged transformer," *IEE Proceedings Generation, Transmission and Distribution,* vol. 139, no. 4, p. 351–358, Jul. 1992.

[34]     M. Magalhães de Oliveira, Power Electronics for Mitigation of Voltage Sags and Improved Control of AC Power Systems, Stockholm, Sweden: Doctoral Dissertation in Electrical Power Engineering, Royal Institute of Technology, 2000.

[35]     S. Amara and H. Hsan, "Power system stability improvement by FACTS devices: A comparison between STATCOM, SSSC and UPFC," in *First International Conference on Renewable Energies and Vehicular Technology (REVET)*, Tunisia, 2012.

[36]     D. Divan and H. Johal, "Distributed FACTS - A New Concept for Realizing Grid Power Flow Control," in *IEEE 36th Conference on Power Electronics Specialists*, Recife, Brazil, Jun. 2005.

[37]     A. Edris, "FACTS technology development: an update," *IEEE Power Engineering Review,* vol. 20, no. 3, pp. 4-9, Mar 2000.

[38]     M. Rahimi, M. Fotuhi-Firuzabad and A. Karimi, "Short term voltage-based risk assessment by incorporating reactive power adequacy," *Ain Shams Engineering Journal,* vol. 7, no. 1, pp. 131-141, 2015.

[39]     A. Kumar and G. Priya, "Power system stability enhancement using FACTS controllers," *International Conference on Emerging Trends in Electrical Engineering and Energy Management (ICETEEEM),* pp. 84-87, Dec. 2012.

[40]   C. R. F. Esquivel, Steady State Modelling and Analysis of Flexible AC Transmission Systems, Glasgow, Scotland: Doctoral Dissertation in Electronics and Electrical Engineering,University of Glasgow, 1997.

[41]   K. Padiyar, FACTS controllers in power transmission and distribution, New Delhi, India: New Age International Publishers, 2007.

[42]   X. Zhang, C. Rehtanz and B. Pal, Flexible AC Transmission Systems: Modelling and Control, Verlag Berlin Heidelberg: Springer, 2012.

[43]   A. Kumar, "Comparison of IPFC and GUPFC for congestion management in deregulated electricity markets," in *9th International Conference on Industrial and Information Systems (ICIIS)*, Gwalior, India, Dec. 2014.

[44]   T. Prakash and N. Nair, "Voltage Sag Mitigation in Multi-Line Transmission System Using GUPFC," *International Journal of Electrical and Power Engineering,* vol. 1, no. 5, pp. 517-523, 2007.

[45]   Z. Yuan, S. de Haan, J. Ferreira and D. Cvoric, "A FACTS Device: Distributed Power-Flow Controller (DPFC)," *IEEE Trans. Power Electron.,* vol. 25, no. 10, pp. 2564-2572, Oct. 2010.

[46]   G. Laszlo, C. D. Schauder and K. Sen, "Static synchronous series compensator: a solid-state approach to the series compensation of transmission lines," *IEEE Trans. Power Electron.,* vol. 12, no. 1, pp. 406-417, Jan. 1997.

[47]   L. Gyugyi, "A unified power flow control concept for Flexible AC transmission Systems," in *Proceedings of IEEE International Conference on AC and DC Power Transmission*, London, UK, 1991.

[48]   B. Renz, A. Keri and A. Mehraban, "AEP unified power flow controller performance," *IEEE Trans. Power Del.,* vol. 14, no. 4, pp. 1374-1381, Oct.1999.

[49]   Y. Pal, A. Swarup and B. Singh, "A Review of Compensating Type Custom Power Devices for Power Quality Improvement," in *Joint International Conference on Power System Technology (POWERCON) and IEEE Power India Conference*, New Delhi, India, 2008.

[50]   K. Çatay BAYINDIR, Modeling of Custom Power Devices, Adana, Turkey: Doctoral Dissertation in Electrical and Electronics Engineering, UNIVERSITY OF ÇUKUROVA, Institute of Natural and Applied Science, 2006.

[51]   A. Ghosh and G. Ledwich, POWER QUALITY ENHANCEMENT USING CUSTOM POWER DEVICES, New York: Springer US, 2002.

[52]    L. Palav, Modelling of Custom Power Devices on an Electromagnetic Transients Program, Manitoba, Canada: Master Thesis in Electrical and Computer Engineering, The University of Manitoba Winnipeg, 1998.

[53]    N. Hingorani, "Introducing custom power," *IEEE Spectrum,* vol. 32, no. 6, Jun. 1995.

[54]    S. Singh, "Flexible AC Transmission Systems (FACTS) controllers: an overview," *International Journal of Energy Technology and Policy,* vol. 4, no. 3, pp. 236-254, 2006.

[55]    M. Marei, E. El-Saadany and M. Salama, "Flexible distributed generation: (FDG)," *IEEE Power Engineering Society Summer Meeting,* vol. 1, no. 1, pp. 49-53 , July 2002.

[56]    J. Bloemink and T. Green, "Benefits of Distribution-Level Power Electronics for Supporting Distributed Generation Growth," *IEEE Trans. Pow. Del.,* vol. 28, no. 2, pp. 911-919, April 2013.

[57]    A. Cetin and M. Ermis, "VSC-Based D-STATCOM With Selective Harmonic Elimination," *IEEE Trans. Ind. App.,* vol. 45, no. 3, pp. 1000-1015, Jun. 2009.

[58]    M. El-Habrouk, M. Darwish and P. Mehta, "Active power filters: a review," *IEEE Proceeding on Electrical Power Applications,* vol. 147, no. 5, pp. 403-413, Sep. 2000.

[59]    P. A. Desale, V. J. Dhawale and R. M. Bandgar, "Brief Review Paper on the Custom Power Devices for Power Quality Improvement," *International Journal of Electronic and Electrical Engineering,* vol. 7, no. 7, pp. 723-733, 2014.

[60]    V. Khadkikar, "Enhancing Electric Power Quality Using UPQC: A Comprehensive Overview," *IEEE Trans. Pow. Electron.,* vol. 27, no. 5, pp. 2284-2297, 2012.

[61]    A. Teke, L. Saribulut and M. Tumay, "A Novel Reference Signal Generation Method for Power-Quality Improvement of Unified Power-Quality Conditioner," *IEEE Trans. Power Del.,* vol. 26, no. 4, pp. 2205-2214, Oct. 2011.

[62]    C. Sao, P. Lehn, M. Iravani and J. Martinez, "A benchmark system for digital time-domain simulation of a pulse-width-modulated D-STATCOM," *IEEE Trans. Power Del.,* vol. 17, no. 4, pp. 1113-1120, 2002.

[63]    M. Mishra, A. Ghosh and A. Joshi, "Operation of a DSTATCOM in voltage control mode," *IEEE Trans. Power Del.,* vol. 18, no. 1, pp. 258 - 264, 2003.

[64]    K. Sen, "SSSC-static synchronous series compensator: theory, modeling, and application," *IEEE Trans. Power Del.,* vol. 13, no. 1, pp. 241-246, Jan. 1998.

[65]    L. Yun Wei, D. Vilathgamuwa, F. Blaabjerg and L. Poh Chiang, "A Robust Control Scheme for Medium-Voltage-Level DVR Implementation," *IEEE Trans. Ind. Electron.,* vol. 54, no. 4, pp. 2249-2261, Aug. 2007.

[66]    K. Shuhong, Y. Zhongdong, S. Renzhong and S. Weidong, "A Survey on the Principle and Control of Dynamic Voltage Restorer," in *International Conference on Energy and Environment Technology*, Guilin, China, 2009.

[67]    M. Newman, D. Holmes, J. Nielsen and F. Blaabjerg, "A dynamic voltage restorer (DVR) with selective harmonic compensation at medium voltage level," *IEEE Trans. Ind. App.,* vol. 41, no. 6, pp. 1744-1753, Nov. 2005.

[68]    R. Strzelecki and G. Benysek, "Power flow in typical series-parallel hybrid filters topologies," in *IEEE Conference on Power Quality and Supply Reliability*, P rnu, Estonia, 2008.

[69]    H. Fujita and H. Akagi, "The unified power quality conditioner: The integration of series and shunt-active filters," *IEEE Trans. Power Electron.,* vol. 13, no. 2, p. 315–322, Mar. 1998.

[70]    F. Peng, G. Ott and D. Adams, "Harmonic and reactive power compensation based on the generalized instantaneous reactive power theory for three-phase four-wire systems," *IEEE Trans. Power Electron.,* vol. 13, no. 6, p. 1174–1181, Nov. 1998.

[71]    S. Bhattacharya and D. Divan, "Synchronous frame based controller implementation for a hybrid series active filter system," in *30th Ind. Appl. Soc. Annu. Meet.*, Orlando, FL, USA,, Oct. 1995.

[72]    M. Kesler and E. Ozdemir, "A novel control method for unified power quality conditioner (UPQC) under non-ideal mains voltage and unbalanced load conditions," in *Conf. Proc. Appl. Power Electron.*, Palm Springs, CA, USA, Feb. 2010.

[73]    S. Kouro, M. Malinowski, K. Gopakumar, J. Pou, L. Franquelo, W. Bin, J. Rodriguez, M. Perez and J. Leon, "Recent Advances and Industrial Applications of Multilevel Converters," *IEEE Trans. Ind. Electron.,* vol. 57, no. 8, pp. 2553-2580, Aug. 2010.

[74]     L. Franquelo, J. Rodriguez, J. Leon, S. Kouro, R. Portillo and M. Prats, "The age of multilevel converters arrives," *IEEE Ind. Electon. Mag.,* vol. 2, no. 2, pp. 28-39, Jun. 2008.

[75]     D. Soto and T. Green, "A comparison of high-power converter topologies for the implementation of FACTS controllers," *IEEE Trans. Ind. Electron.,* vol. 49, no. 5, pp. 1072-1080, Oct. 2002.

[76]     Y. Long, X. Xiao, Y. Xu, Y. Baolai, Y. Xu and J. Hao, "MMC-UPQC: Application of Modular Multilevel Converter on Unified Power Quality Conditioner," in *IEEE Power and Energy Society General Meeting (PESGM)*, Vancouver, BC, Canada, 2013.

[77]     B. Andersen, L. Xu and K. Wong, "Topologies for VSC transmission," in *Seventh International Conference on AC-DC Power Transmission*, London,UK, Nov. 2001.

[78]     Y. Kolhatkar and S. Das, "Experimental investigation of a single-phase UPQC with minimum VA loading," *IEEE Trans. Power Del.,* vol. 22, no. 1, p. 371–380, Jan. 2007.

[79]     "A line voltage regulator/conditioner for harmonic-sensitive load isolation," in *Proc. Ind. Appl. Soc. Annu. Meet. Conf.*, San Diego, CA, USA, 1989.

[80]     A. Nasiri and A. Emadi, "Different topologies for single-phase unified power quality conditioners," in *38th Int. Appl. Soc. Annu. Meet. Ind. Appl. Conf.*, Salt Lake City, UT, USA, 2003.

[81]     M. Khoor and M. Machmoum, "A novel single-phase reduced parts on-line UPS with power quality conditioning capability," in *Proc. Power Electron. Spec. Conf.*, Orlando, FL, USA, 2007.

[82]     V. Khadkikar and A. Chandra, "UPQC-S: A novel concept of simultaneous voltage sag/swell and load reactive power compensations utilizing series inverter of UPQC," *IEEE Trans. Power Electron.,* vol. 26, no. 9, p. 2414–2425, Sep. 2011.

[83]     V. Khadkikar, A. Chandra and B. Singh, "Digital signal processor implementation and performance evaluation of split capacitor, four-leg and three H-bridge-based three-phase four-wire shunt active filters," *IET Power Electron.,* vol. 4, no. 4, p. 463–470, Apr. 2011.

[84]     S. Zhang, X. Lu, Y. Liu, B. Ge and F. Z. Peng, "Nine IGBTs based UPFC topology and control for renewable power integration," in *Twenty-Eighth Annual IEEE Conference and Exposition (APEC) in Applied Power Electronics*, Long Beach, CA, USA, 2013.

[85]     J. H. Harlow, Electric Power Transformer Engineering-The Electric Power Engineering Series, Boca Raton,FL: CRC Press, 2014.

[86]     J. Martinez, R. Walling, B. Mork, J. Martin-Arnedo and D. Durbak, "Parameter determination for modeling system transients-Part III: Transformers," *IEEE Trans. Power Del.,* vol. 20, no. 3, pp. 2051-2062, Jul. 2005.

[87]     M. J. Heathcote, The J&P Transformer Book 12th Edition, Burlington, MA: Newnes, 1998.

[88]     J. Martinez and B. Mork, "Transformer modeling for low- and mid-frequency transients - a review," *IEEE Trans. Power Del.,* vol. 20, no. 2, pp. 1625-1632, Apr. 2005.

[89]     F. de Leon and A. Semlyen, "Complete transformer model for electromagnetic transients," *IEEE Trans. Power Del.,* vol. 9, no. 1, p. 231–239, Jan. 1994.

[90]     A. Gole, J. Martinez-Velasco and K. A. J. F., "Modeling and Analysis of System Transients Using Digital Programs," *IEEE PES Special Publication,* Jan. 1999.

[91]     "Guidelines for Representation of Network Elements when calculating Transients," CIGRE Working Group 02(SC33), 1990.

[92]     V. Brandwajn and H. W. Dommel, "Matrix representation of three-phase n-winding transformers for steady-state and transient studies," *IEEE Trans. Power App. Syst.,* Vols. PAS-101, no. 6, p. 1369–1378, Jun. 1982.

[93]     H. Dommel, Electromagnetic Transients Program Manual (EMTP Theory Book), Portland, OR: Bonneville Power Administration, 1986.

[94]     M. Elleuch and M. Poloujadoff, "A contribution to the modeling of three phase transformers using reluctances," *IEEE Trans. Magn.,* vol. 32, no. 2, p. 335–343, Mar. 1996.

[95]     X. Chen and P. Neudorfer, "Digital model for transient studies of a threephase five-legged transformer," *IEE Proceedings Generation, Transmission and Distribution,* vol. 139, no. 4, p. 351–358, Jul. 1992.

[96]     G. Slemon, "Equivalent circuits for transformers and machines including non-linear effects," *Proceedings of the Institution of Electrical Engineers,* vol. 100, no. 1, p. 129 – 143, Jul. 1953.

[97]     R. Teodorescu, M. Liserre and P. Rodríguez, Grid Converters for Photovoltaic and Wind Power Systems, United Kingdom: Wiley, 2011.

[98]     E. Rakhshani and P. Rodriguez, "Inertia Emulation in AC/DC Interconnected Power Systems Using Derivative Technique Considering Frequency Measurement Effects," *IEEE Trans. Power Syst.,* vol. 32, no. 5, pp. 3338-3351, Sept. 2017.

[99]     P. Meli´ın, J. Espinoza, J. Mu˜noz, C. Baier and E. Espinosa, "Decoupled control of a unified power quality conditioner based on a current source topology for fast AC mains disturbance compensation," in *IEEE Int. Conf. Ind. Technol.*, Vi a del Mar, Chile, Mar. 2010.

[100]    Y. Lu, G. Xiao, X. Wang, F. Blaabjerg and D. Lu, "Control Strategy for Single-Phase Transformerless Three-Leg Unified Power Quality Conditioner Based on Space Vector Modulation," *IEEE Trans. Power Electron.,* vol. 31, no. 4, pp. 2840-2849, Apr. 2016.
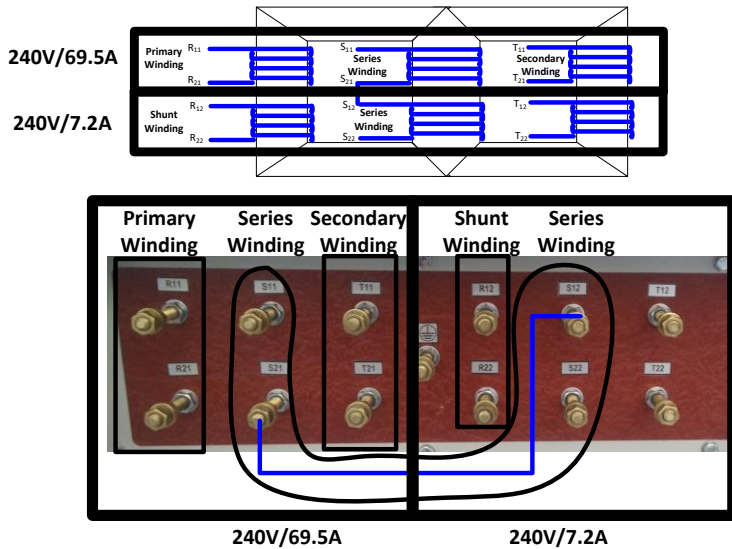
# Laboratory Experimental Setup
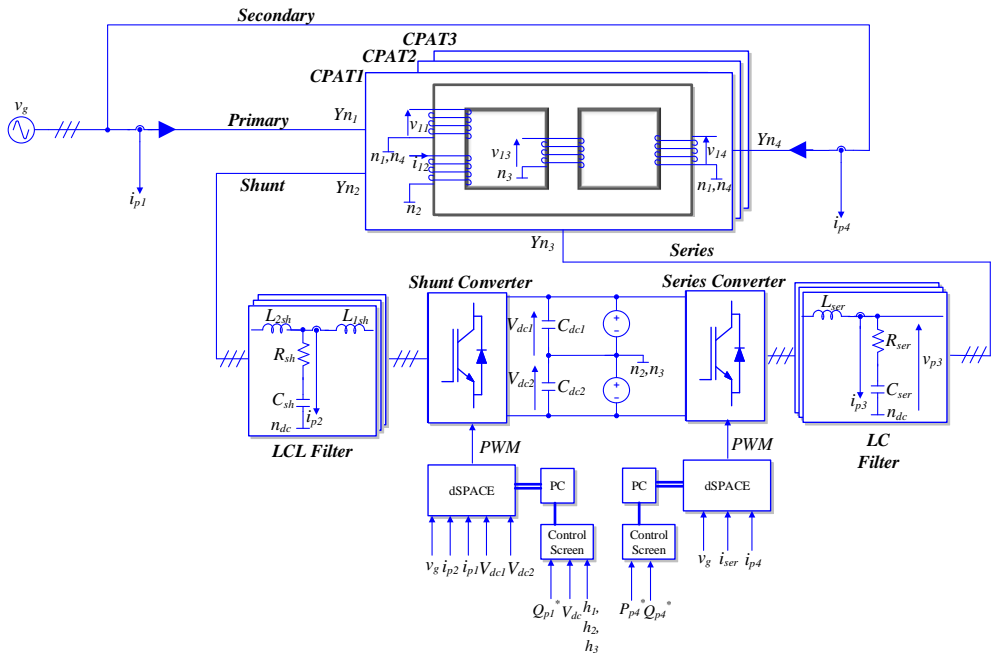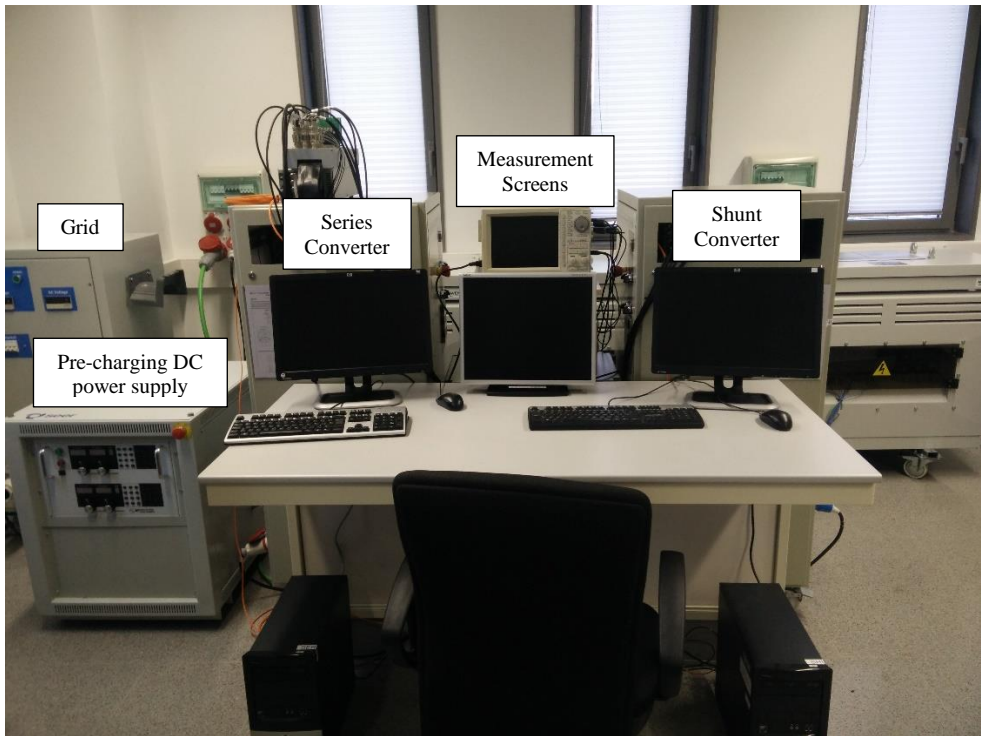


**A. 1.** Laboratory setup connection diagram
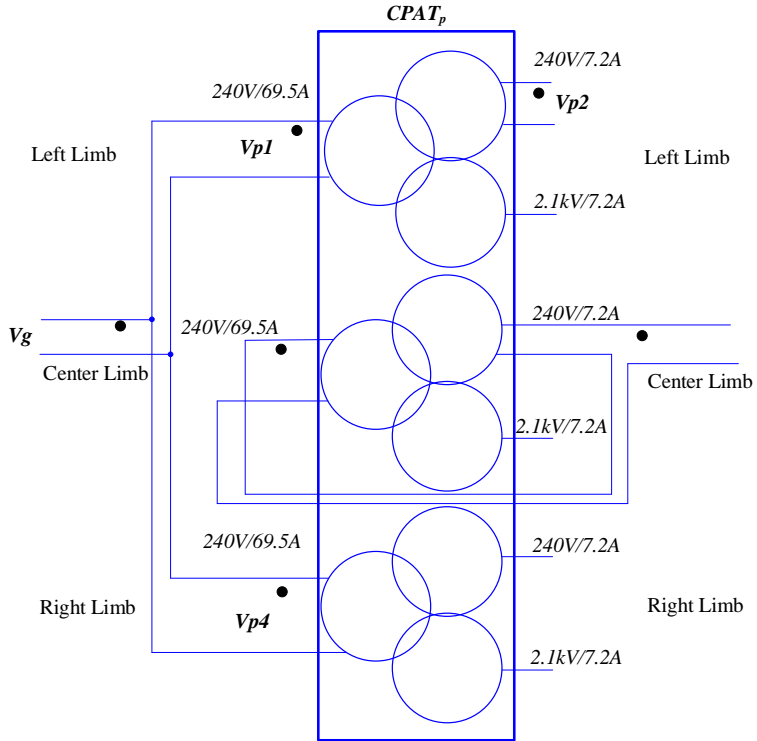
**A.2.** Connection diagram of each CPAT.



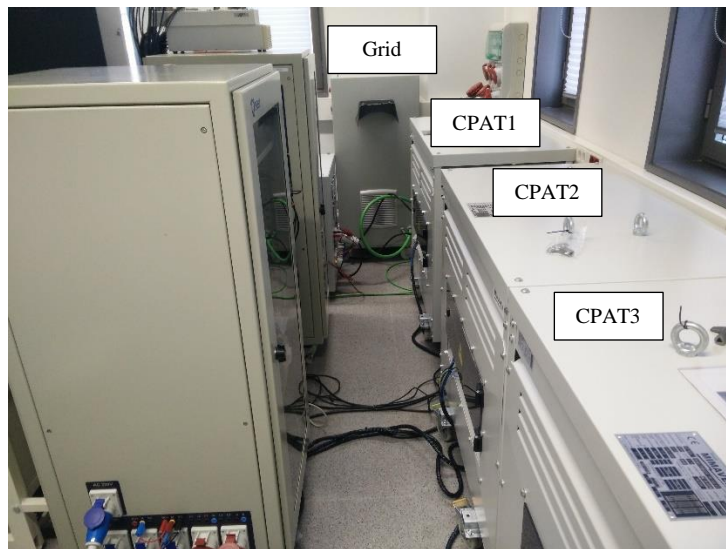**A. 3.** Transformer terminal windings connection.

**A. 4.** Experimental setup layout.



**A. 5.** Experimental setup transformers arrangement